# Chapter 1 Introduction and Review

## *1.1 Spatial Variability in Agricultural Fields and Precision Agriculture*

> Sustainable agriculture is considered the most viable means of meeting future food needs for the world's increasing population through its goal of delicately balancing crop productivity, profitability, natural resource utilization, sustainability of the soil-plant-water environment and environmental impacts. Precision agriculture is a proposed approach for achieving sustainable agriculture. (Corwin & Plant, 2005:1)

According to Lowenberg-DeBoer and Erickson (2000) precision agriculture is the means by which site-specific crop management is achieved. However, the treatment of individual paddocks as the basic unit of uniform management ignores the spatial variability of the soil properties. Hedley (2004) defines precision agriculture as the management of crops and/or soils at scales less than a whole field. However, directly sampling the soil at a scale suitable to recognise sub-paddock variability is prohibitively time consuming and costly. The efficiency of remote sensing has bridged this gap, by allowing either interpolation between the dispersed calibrating direct sample sites or through stratification of the sampling, by identifying zones of local significant variability.

The wine grape (*Vitis Vinifera* sp.) industry is characterised by spatially- and temporally- intensive management. The significant cost of inputs (i.e. soil conditioning, foliar treatments, irrigation); the need to manage individual vines (pruning, shoot thinning, leaf plucking, fruit thinning); and the effect of both vine-to-vine variability of fruit characteristics (overall wine quality) and yield (and hence, gross margin) has seen this agricultural sector embrace precision viticulture (Proffitt et al 2006). Moreover, grapevine productivity (yield and quality) is highly responsive to soil conditions. The monitoring of the soil in viticulture at the standard soil-sampling grid of 75 m (Bramley 2001a) fails to localise the soil variations with sufficient precision. Mobile, global positioning system based, geophysical soil mapping methods are potentially cost-effective solutions to the problem of delineating soil variation zones within agricultural fields/vineyards. For example, Bramley (2001a) concludes that, in combination with detailed grape yield

maps, a soil electrical conductivity map may assist in forecasting yields and identifying vineyard zones for different management strategies.

Until recently, a major setback to precision agriculture has been the unrealistic expectation that the main remote sensing tool used be satellite imagery. In particular, imagery can only give the real-time status of the plants. It cannot directly sense changing soil properties which may affect the plants in the future. To mitigate this shortcoming, precision agriculture has recruited ground-based geophysical mapping of sub-surface conditions (at the required sub-decametre resolution).

## 1.2 Geophysical Techniques in Agriculture

> The application of geophysical methods to agriculture will eventually become a well-recognised sub-discipline of geophysics. (Allred, Daniels & Ehsani 2008:14).

A variety of complementary, ground-based, geophysical techniques are currently available to the agricultural sector. Soil electrical resistivity (multi-electrode ER) and electromagnetic induction (EMI) are the most widely used geophysical techniques in agriculture, and along with dGPS-equipped harvester yield monitoring, are considered essential to the process of precision agriculture (Proffitt et al. 2006:45).

> Geophysical techniques currently used in agricultural research include electrical resistivity (ER), Time Domain Reflectometry (TDR), ground penetrating radar (GPS), capacitance probes (CPs), radar scatterometery or active microwaves (AM), passive microwaves (OM), electromagnetic inductions (EMI), neutron thermalisation, nuclear magnetic resonance (NMR) gamma ray attenuation, and near surface seismic …(Allred, Daniels & Ehsani 2008:17).

Some of these current and potential techniques (relevant to agriculture) are briefly described in this section. In addition, these techniques can be deployed on a variety of single- and multi-sensor platforms, including down-hole and tomographical configurations. Combinations of these geophysical techniques and deployments promise to yield the richest levels of information to support precision agricultural management (Allred, Daniels & Ehsani 2008).

### 1.2.1 Gamma Ray Spectroscopy (GRS)

The natural decay of radioactive elements in the underlying soil produces gamma rays with specific energies, equivalent to electromagnetic wavelengths, depending on the isotopes decaying. The energies detected are then diagnostic of different soil parent material and the soil forming process. The surveying technique is non-intrusive and is usually done from the air. However, at the resolution required for vineyards, a ground-level survey is preferred (Proffitt, Bramley, Lamb & Winter 2006:56). The detected total gamma radiation count can be separated into three basic energy levels (associated with the radioactive elements potassium, $^{40}K$, thorium, $^{232}Th$ and uranium $^{238}U$). The levels of these detected constituents can then be used to infer a variety of soil properties such as: texture, pH, electrical conductivity (Hazell n.d) and clay content (van Egmond, Loonstra & Limburg n.d.). van Egmond, Loonstra & Limburg (n.d) explain the application of the GRS based soil maps to precision agriculture and conclude GRS has a complementary role and would normally be used in conjunction with other techniques. It is a broad mapping tool (a typical pixel size of 50 m is quoted by Hazell (n.d.). However, it can be larger, or smaller, depending on elevation / line spacing. Some lightweight ground based systems are becoming practical.

As Proffitt, Bramley, Lamb & Winter (2006:56-57) note, however, the limitations of this technique include:

1. It is not equally applicable in all situations (i.e. geologies);
2. It is affected by rain and time of day;
3. It requires technical calibration to a number of ground sites as well as 'fingerprinting' of parent material;
4. It mainly senses just the top 15 cm of soil.

### 1.2.2 Time Domain Reflectometry (TDR)

In TDR, a multi-pronged metal probe is pushed into the soil and a voltage pulse is sent down the probe. The soil between the probes acts as the medium of a wave-guide. The pulse travel-time and the reflected pulse amplitude are processed to give volumetric water content and bulk electrical conductivity. However, while

this technique is capable of unattended data collection, it is a stationary instrument, not suited to efficient, detailed mapping (Corwin & Lesch 2005).

### 1.2.3 Ground Penetrating Radar (GPR)

GPR is the transmission of a radio frequency pulse into the ground and the detection and processing of the reflected signal. The reflections occur at boundaries of material with different dielectric. Travel times are related to the medium's dielectric which can be used to deduce soil moisture content. Different frequency equipment can give different information. For example, Hubbard et. al. (n.d.) discuss the use of a 900 MHz GPR travel-time application in a vineyard that yielded a very accurate water content measurement in the top 15 cm of soil at very high resolution. At the other end of the frequency spectrum these authors used a 100 MHZ GPR system (in dielectric contrast reflection mode) to identify sub-surface water channels between 1.0 and 1.5 m below the surface. While the instrument is capable of very high resolution (0.25 m x 25 m) it is not universally applicable to all situations and has speed-over-ground, and ground roughness limitations. The instrumentation remains relatively expensive and still requires a high degree of operation and interpretation skill. However, it is probably the second most well used group of geophysical technologies applicable to agriculture, after electromagnetic induction.

### 1.2.4 Magnetometry

Magnetometry, the imaging of the subsurface distribution of magnetic material, can be rapidly achieved with passive magnetic sensors. There are several types of magnetometers: proton precession, optically pumped, and fluxgates. These sensors all measure the earth's natural magnetic field and its variations (anomalies) that provide insight into subsurface location of magnetic marker materials. Allred, Daniels and Ehsani (2008:151-152) describe how the cultural disturbance of the naturally occurring magnetic minerals during installation of a previous drainage system was successfully mapped in an agriculturally related environmental issue. The same investigation also directly detected old steel water pipes. In addition, mapping of near surface magnetic geological features can be used to infer aspects of ground water flow/drainage. As can be seen from these specialised applications,

this technique is not a routine agricultural tool, but can be utilised for specific applications.

### 1.2.5 Seismic Methods

Seismic methods are initiated by the mechanical energising of the earth (via vibration, explosion, impact or acoustic means) and result in elastic waves being transmitted, reflected or refracted through ground. The analyses of the timing and amplitude of these received waves (via geophones) is routinely performed to infer sub-surface properties of the earth. Refraction and surface wave transmission are the most readily applicable to shallow applications such as depth to bedrock, soil stiffness, soil moisture content, soil porosity and compaction. However, while this method has a wide range of methodologies and applications they will be more widely applied to agriculture in the future (Allred, Daniels & Ehsani 2008:160-161).

### 1.2.6 Self-Potential

Self-Potential is the simplest geophysical technique, requiring just electrodes, electric-cables, and a voltmeter. The voltmeter is connected to the electrodes via the cable and the measured voltage is used to map sub-surface electric potentials. This technique detects the spontaneous potentials arising from electrochemical actions between minerals and solutions (Sharma 1976:261). This method can be used to detect leaks in dam walls, water-, effluent- or nutrient-storage ponds. In addition, the technique may be useful in detecting converging or diverging ground water flows, water table depression, salinity and clay distribution patterns (Allred, Daniels & Ehsani 2008:155). However, it does not have a routine use in agricultural applications.

### 1.2.7 Electrical Resistivity (Multi-electrode ER)

In Multi-electrode ER, four electrodes are inserted into the ground and current injected into one pair while the voltage difference is measured across the other pair. This gives a bulk electrical conductivity but is relatively slow. However, Veris Technologies (Salina, Kansas, USA: http://www.veristech.com) have developed a mobile ER system that uses tractor-towed rotating disks for the electrodes (Corwin

& Lesch, 2005). This technique disturbs the top few decimetres of soil and has limited effectiveness over stony ground. In either the stationary or mobile configuration, the ER technique's primary limitation is the electrical contact with the ground. This issue becomes more significant over dry, hard ground. An advantage of this technique (Sudduth et al. 2003) is that no calibration or drift control is required.

### 1.2.8 Electrical Resistivity (Capacitively Coupled ER)

Capacitively Coupled ER uses the same principle as described in Sub-section 1.2.7 but instead of inserted electrodes it has plates which capacitively couple with the ground. These plates are towed along the surface of the ground for the purpose of injecting current (and detecting the resulting voltage). The ohmMapper (Geometrics Inc, California, USA: www.geomtrics.com) is the best known of these instruments. The primary advantage of this system is its speed. Dragged behind either an operator or a vehicle, it rapidly maps resistivity.

Walker and Houser (2002) evaluated the ohmMapper and concluded that determining moisture variation within the root zone with this instrument was unlikely due to system noise with short electrode spacings. However, with wider electrode spacings (and hence acceptable noise levels) average soil moisture was mappable for the top few metres. Walker and Houser (2002) also point out that ER (including the traditional electrode type) results are not point measurements but represent a volume of earth similar to the current electrode spacing (i.e. 11 m for a 2.5 m dipole spacing, 0.7 m depth for peak response).

### 1.2.9 Electromagnetic Induction (EMI)

In EMI, a transmitting coil induces eddy currents in the ground. A receiving coil then detects the changing magnetic field from those eddy currents induced in nearby conductors. The magnitude of the received signal (relative to the transmitted field) is then proportional to the ground's bulk electrical conductivity (EC). The coils are usually mounted on either end of a rigid horizontal staff. The instruments most commonly used to investigate the hydrology of the root-zone are the EM31 and EM38 (both designed and manufactured by Geonics Limited;

Mississauga, Ontario, Canada, see Appendix A). Other similar EMI instruments for shallow EC mapping include:

1. The EMP-400 (Geophysical Service Systems Inc., Salem, NH, USA);
2. GEM-2 (Geophex Ltd, Raleigh, NC, USA); and
3. DUALEM-2 & -4 (DUALEM.com, Milton, ON, Canada).

The advantages of EMI include that they are:

1. Highly mobile;
2. Give a localised, almost point response;
3. Rapid-sampling (hence are capable of practical, high-resolution mapping); and
4. Non-invasive.

The limitations of EMI include the fact that they:

1. Can be adversely affected by metallic litter or nearby conducting structures (which is pertinent to this study); and
2. Require calibration and drift control.

## *1.3 EM38 Vineyard Application*

Recently, the EM38 has been accepted as a useful component of precision agriculture (Corwin & Lesch 2003; Corwin et al. 2003), assisting in the monitoring of inputs (e.g. nutrients and water).

Recognition of the magnitude and localised nature of soil variability within vineyards (Bramley & Proffitt 1999) has identified scope for their improved management. Appreciation of the importance of this variability has prompted the inclusion of EM38 soil conductivity surveys within the monitoring of the soil conditions (i.e. in addition to direct monitoring). The efficient collection and density of data provided by an EM38 survey, leverages the value of the slower direct measurements. In this way, the EM38 conductivity data can highlight areas of greater variability with a higher spatial resolution than traditional monitoring techniques (e.g., ~10 m cf. 75 m).

The EM38's important role in the precision management of vineyards has been described by Bramley (2000; 2001; 2003), Bramley and Lanyon (2002), Bramley et al (2003) and Proffitt et al. (2006). In addition to its manual operation, the simplicity and versatility of the EM38 is shown in the variety of mechanised field configurations adapted to maximise efficient geophysical mapping, as shown in Figure 1-1.

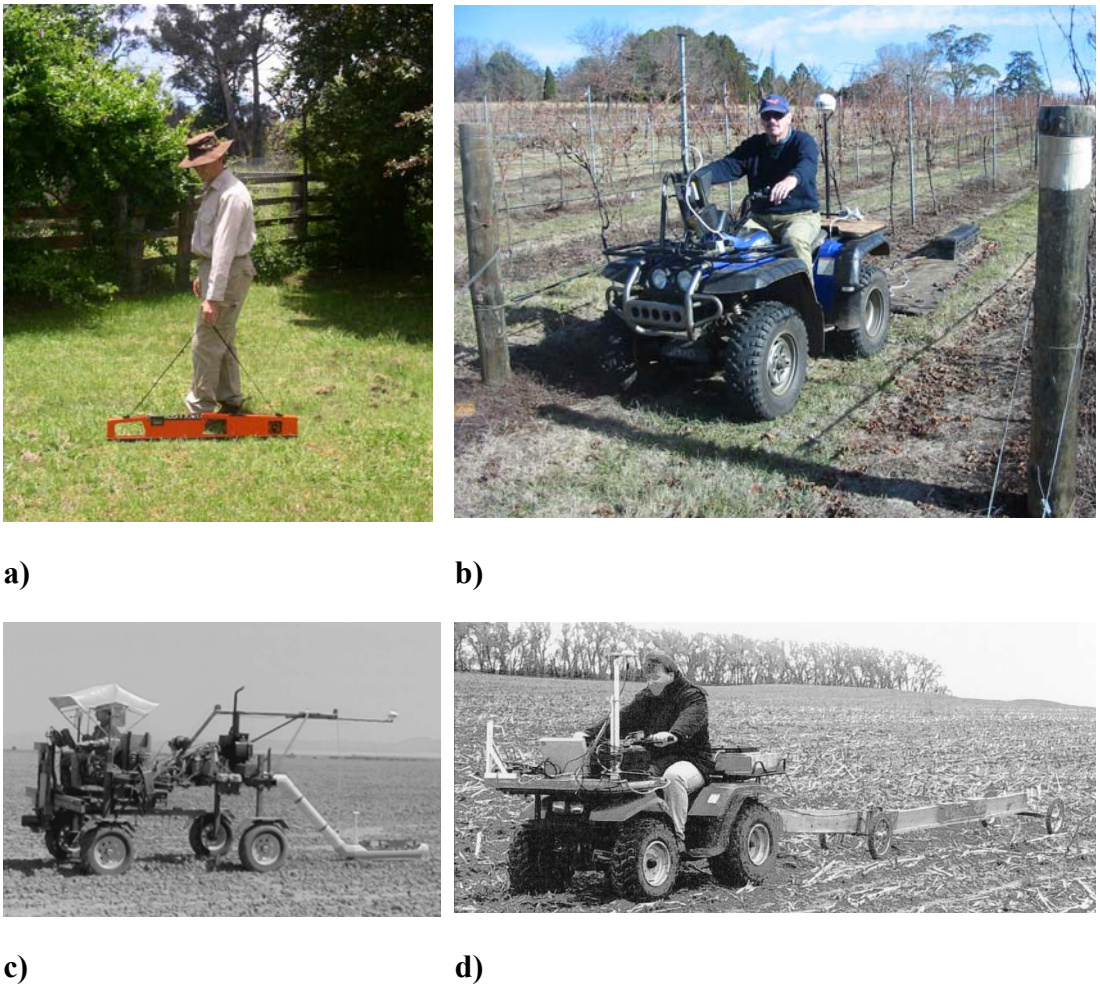

**a)** **b)**

**c)** **d)**

**Figure 1-1. Photographs of the EM38 in operation. a) Manual operation; b) Vehicle-towed sliding mat /GPS operation; c) Vehicle-towed sled operation (Rhoades et. al. 2006); and d) Vehicle-towed wheeled cart (Sudduth, et. al. 2003).**

## *1.4 Vineyard Trellising Distortion of EM38 Measurements*

Wine grape vines are perennial plants, subjected to an annual cycle of pruning, shooting, canopy regrowth, grape growth, harvesting, and leaf fall. Unlike open agricultural fields, wine grape vineyards comprise grape vines trained on to fixed trellis arrangements. Design and management of a vineyard is complicated, intense, and varied, involving many different trellis geometries. A typical trellis

style (and the one used in this investigation) is based on Vertical Shoot Positioning (VSP). As shown in Figure 1-2, this vine style is characterised by the horizontal vine Cordon which is left with buds on the top after pruning. From these buds, the new vine shoots are encouraged to grow vertically and 'grab' onto the wires directly above (the grab wire and then the foliage wires above that). These new shoots will then bear the fruit.

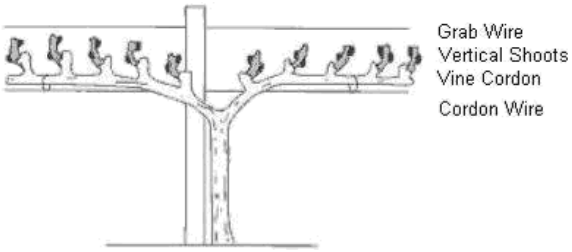


**Figure 1-2. Sketch representation of the Vertical Shoot Positioning (VSP) vine training system commonly used (diagram from Jackson 2008:124). The horizontal vine cordon remains after pruning and in the new season, the shoots grow vertically, 'grabbing' onto the wire(s) directly above.**

Figure 1-3 is a group of photographs showing the steel Gripfast posts and connecting wires providing several vineyard functions. The five steel trellis wires are shown making good contact with the posts. These wires range from the bottom wire (supporting the irrigation pipe at an approximate height of 0.5 m) to the top pair of foliage supporting wires at a height of approximately 2 m.

a) b) c)

**Figure 1-3. Photographs of the galvanised steel Gripfast post. a) The post in a trellis showing the slots in the post for supporting wires; b) With a bottom Dripper wire supporting a plastic irrigation pipe; and c) The higher foliage wire pair for supporting the vines. These are moved up and down depending on the regrowth stage.**

Lamb, Mitchell and Hyde (2005) suspected that during an EM38 inter-trellis survey of a vineyard, the large steel conducting loops of a vineyard trellis could interfere with the integrity of the survey's measurements. These researchers went on to perform a test where they surveyed a grassed field then systematically erected a vineyard-style trellis, while resurveying the same tracks (which became the centreline of the inter-trellis lanes). They repeated the survey with just the steel posts, then with a single bottom (Dripper) wire attached to the posts and then with all (typical trellis) wires emplaced, simulating a full trellis.

Their simulated vineyard trellising had three groups representing different, typical inter-trellis spacings of 2.5 m, 3.0 m, and 3.5 m (Figure 5-1). Lamb, Mitchell and Hyde (2005) reported an elevated response (due to the trellising) of between 10 and 15 mS $m^{-1}$ for the 3 and 3.5 m spaced trellises. These values were mid-lane,

adjacent to the posts. However, the resulting plan images of the entire EM38 data set indicated that the peak trellis interference actually occurred mid-way between the posts (mid-panel, mid-lane) and could be as high as 30 mS $m^{-1}$. In this case, the bare-earth response was approximately 40 mS $m^{-1}$. This means that, due to the steel trellising, there was an overestimation of the soil conductivity by approximately 75 %.

The main geophysical tool used for investigating soil properties in wine grape vineyards is currently the EM38 EMI instrument (Proffit et al. 2006).

Lamb, Mitchell and Hyde (2005) emphasise that the EMI principle of detecting induced eddy currents in the ground is adversely affected by interference from the large conducting loops of the vineyard's steel trellising. Proffit et al. (2006) also warn of the influence of an all-steel trellis on EM38 readings (and that the EM31 should not be used at all because of this). The conductors of concern comprise the steel posts, the contacting wires, and the earth between the posts. The nature of vineyard trellises is that the rows are densely arranged, usually 2.5 to 3.5 m apart, with the EM38 survey conveniently performed down the inter-trellis lanes. This means that the trellis loops are only ~1.5 m either side of the survey track. Lamb (pers. comm. 2005) has also observed distinct increases in EMI response within a vineyard compared to outside the vineyard.

Lamb, Mitchell and Hyde (2005) report on their experiment to measure the effect of the trellising on the EM38 when this instrument is used to map soil conductivity in a vineyard. These researchers mapped the EC of a bare field, remapped it after each stage of a trellis construction (posts; post and bottom wire; and post and all-wires) and then again after removing the trellis. Their conclusion was that the trellising increased the EC readings by up to one-third. The authors identified several aspects of this phenomenon that warranted further investigation:

1. Confirmation of the underlying physics of how the vine trellising influences the mid-lane EC values;
2. A comparison of the influence of wood versus steel trellis posts;
3. The influence (if any) of the water in the irrigation pipe suspended on the trellis;

4. The effect of soil EC beneath the trellis and its interaction with the condition (new or oxidised) of the steel trellis posts; and
5. Determination of whether the trellis influence on measured EC is purely additive.

To date, no investigations of these five aspects have been reported in the scientific literature. They therefore provided the initial direction and impetus for this study.

## 1.5 Scope of the Thesis

The goal of this investigation is to understand the mechanism and degree by which steel vineyard trellising interferes with the response of the widely-used EM38 EMI soil conductivity sensor as deployed following standard industry protocol in vineyards (Lamb, Mitchell & Hyde 2005). From an industry perspective, this work aims to determine whether:

1. Relative conductivity contrasts observed across a vineyard can be relied on to be from the soil rather than a trellis artefact; and/or
2. Data processing or physical trellis intervention strategies may be designed and applied with confidence to accommodate likely trellis effects.

A significant component on this thesis is devoted to understanding (from first principles) the interaction of the EM38 with nearby conducting metallic loops. While simple, single loops can be treated analytically, complicated loop geometries (reflecting an actual multi-wire trellis segment) require numerical techniques. To this end, commercially-available software (FastHenry for circuit inductances) was employed to estimate crucial parameters required for predicting trellis influences.

Thus, the relevant fundamental physics and performance of the EM38 EMI instrument is the starting point for Chapter 2. Analysis of the theory of the instrument's operation and interpretation is in the context of its practical aspects and the soil conductance mechanism. The chapter finishes with a description of the FastHenry software used for numerically estimating inductive coupling between the EM38 instrument and the metallic loops, and the self-inductances (and resistances) of the loops themselves.

Chapter 3 develops, again from first principles, a simple prediction strategy for the EM38 response to basic loops. Testing of this prediction algorithm is by experiment, which led to an evaluation of its limitations.

In Chapter 4, actual trellis geometries are introduced and their interference effect is isolated into key components, each investigated separately. The prediction strategies (developed in Chapter 2) are extended to predict the two significant trellis interference factors: the all-steel loops and the steel-earth loops. Within the context of an EM38 survey, these predictions were then experimentally tested.

Chapter 5 retrospectively evaluates the predicted influences with experimental data, originally described by Lamb, Mitchell and Hyde (2005). This original data set was collected under realistic vineyard surveying conditions (i.e. towed by a quad-cycle and positioned by dGPS). The data set has the advantage of having a trellis-free data subset, collected immediately before and after trellis construction, for comparison with the data subsets collected during various stages of trellis erection.

Chapter 6 brings the underlying physical mechanisms together in a set of robust, practical mitigation strategies which are tested in a local commercial vineyard. The final chapter, Chapter 7, concludes with a summary of key points of understanding and advises on practical processing/mitigation strategies including discussion of further work required.

# Chapter 2 The EM38 Sensor and FastHenry Inductance Modelling Software

## 2.1 Introduction

This chapter begins with a discussion of the fundamental physics relevant to the operation of the EM38 EMI instrument as a soil conductivity meter. An analysis of the theory of the instrument's operation and interpretation (in the context of its practical aspects and the soil conductance mechanism) is then undertaken. The chapter concludes with a description of the FastHenry software used for numerically estimating inductive coupling between the EM38 instrument and the metallic loops, and the self-inductances (and resistances) of the loops themselves.

## 2.2 Definition of Conductivity

The restriction of the conduction of electrical current, electrical resistivity (often shortened to resistivity) is defined in terms of the electrical resistance ($R$) of a cylinder of length, $\ell$, and cross-sectional area, $A$. This can be visualised (in Figure 2-1) as a potential difference (or voltage, $V$) applied to the ends of a cylinder while measuring the resulting current. The resistance ($V/I$, by Ohms Law) is then linearly proportional to $\ell$ and inversely linearly proportional to $A$. The resistivity ($\rho$) is that constant of proportionality, derived from Ohm's Law:

$$R = \frac{V}{I} = \rho \frac{\ell}{A} \Rightarrow \rho = \frac{RA}{\ell}, \qquad \text{Equation 2-1}$$

with units of Ω m. Electrical conductivity, often referred to as conductivity ($\sigma$) is the equivalent of the inverse of resistivity (i.e. $\sigma \equiv 1/\rho$) and has units of $\Omega^{-1}$ $m^{-1}$ or S $m^{-1}$, where S is the abbreviation for Siemens, a unit equivalent to $\Omega^{-1}$.

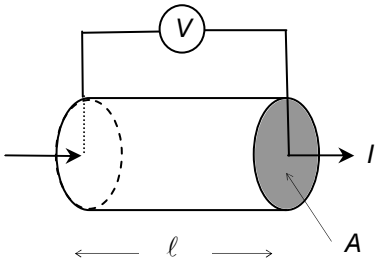


**Figure 2-1. Visualisation for the conceptual definition of resistivity along a homogenous cylinder. The potential difference, *V*, is applied evenly across the entire ends of the cylinder area, *A*.**

In terms of measuring basic soil properties, directly measuring the conductivity of soil involves collecting samples and applying an electrical current to them in a process conceptually similar to that shown in Figure 2-1. However, in practice the process is complex and time-consuming, involving careful collection, preparation of the soil into a paste, extraction of a saline solution and then measurement of its electrical conductivity, $EC_e$, in a laboratory (McNeill, 1986).

## 2.3 Conductivity Surveying

It was Conrad Schlumberger (1912) who provided the first refined conceptualisation for investigating the earth using conductivity:

> to compare the potential distribution resulting from current applied to the real earth to that which would exist if the same current were applied to a homogeneous earth, and to draw from observed differences, conclusions concerning the nature of the real earth (cited in Kunetz, 1966:2).

The first description of electrical conductivity surveying was by Keller and Frischneckt (1926). Their initial investigations were of the galvanic (or direct contact) resistivity types and essentially sought to measure the electrical conductivity of the ground, in situ, thereby bypassing the onerous laboratory measurements of collected samples.

Based on the work of Schlumberger (1912), and in an effort to overcome the problem of electrode contact-resistance, Wenner (1915) developed a four-electrode configuration for measuring electrical conductivity. However, it is the apparent electrical conductivity that is measured ($EC_a$). The apparent term is significant

because $EC_a$ is an abstract quantity based on the geometry of the electrodes and the ratio of the measured voltage to current (which is itself dependent on the complicated current distributions within the earth) and cannot therefore be considered an average of the inhomogeneous, earth conductivities.

The four-electrode configuration is now standard geophysical practice and the equal-spaced, four-electrode operation is the Wenner configuration (Figure 2-2). In this configuration, $EC_a$ is given by:

$$EC_a = \frac{I}{\Delta V 2\pi a}, \qquad \text{Equation 2-2}$$

where $\Delta V$ is the potential voltage difference between electrodes $P_1$ and $P_2$, $a$ is the electrode spacing and $I$ the current injected into the ground through electrodes $C_1$ and $C_2$.

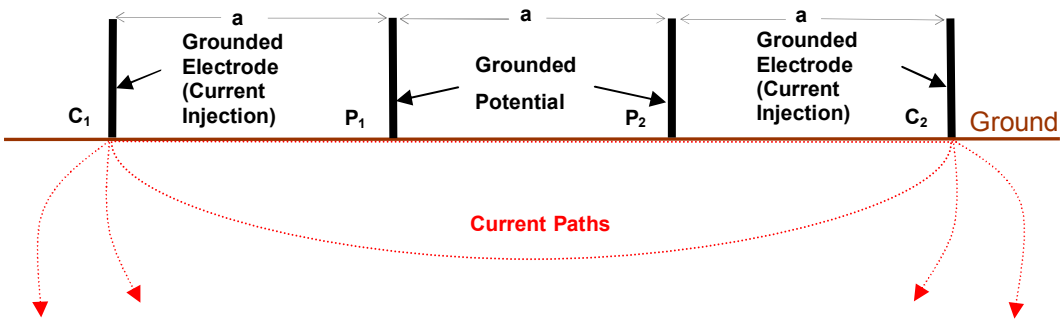


**Figure 2-2. Schematic diagram of the Wenner configuration (equal electrode spacing) for grounded electrode, in situ, electrical conductivity measurements. The red, dotted lines indicate, schematically, some of the injected current paths.**

McCorkle (1931) was the first to use the four-electrode method for field in situ soil moisture and salinity investigations. However, Rhoades and Ingvalson (1971) pioneered the interpretation of in situ apparent conductivity measurements (using grounded electrodes) into $EC_e$ values, as a measure of soil salinity.

However, these galvanic techniques had important limitations. McNeill (1980) points out that resistive variations near the galvanic electrodes lead to significant 'geological noise' which cannot have its source location, depth, or size resolved. The electromagnetic (or inductive) form of measuring the earth's conductivity overcame this disadvantage.

## 2.4 Deducing Soil Properties from Soil Conductivity

The relationship between soil properties and conductivity is complicated and has been the subject of extensive research (see Corwin & Lesch 2003). The mechanism of current flow in the ground is completely electrolytic (McNeill 1986). This process occurs within the soil moisture and its efficiency depends on the availability of suitable ions. Some saline groundwater may have a conductivity as high 20 S $m^{-1}$ compared to normal ground water with conductivity as low as 1 mS $m^{-1}$ (Reynolds 1997). At the other extreme, distilled water, which has few free ions, has a conductivity of just 0.2 mS $m^{-1}$. Normal soil-borne water also contains few free ions which is why the presence of salts, (which provide the free ions) is so readily detectable by conductivity measurements. However, in addition to the presence of salt, the $EC_a$ is also controlled by (at least):

1. Soil saturation (which controls the continuity of moisture paths);
2. Soil porosity (which controls the tortuosity of the moisture paths);
3. Soil temperature (conductivity increases by approximately 2 %/$^{o}$C); and
4. Soil clay content (which, depending on type, provides significant free ions).

Conversely, when $EC_a$ maps soil types, soil water content is an important variable that should be fixed by direct measurement (Brevik, Fenton & Lazari 2006). Even then, it is still a complicated task to normalise the effect of soil moisture in order to produce $EC_a$ based maps of soil-type. Similarly, Sudduth, Drummond and Kitchen (2001) discuss the use of $EC_a$ surveying to map topsoil depth but acknowledge the requirement to monitor soil moisture.

The application of the $EC_a$ to map moisture variations can be achieved, but other factors (as mentioned above) need to be taken into account. Reedy and Scanlon (2003) obtained successful correlations between $EC_a$ measurements and direct soil moisture measurements (via neutron-probe) at a particular site. These authors concluded that once the correlation was established (at that site) EM38 measurements alone were required to monitor the moisture variations.

## 2.5 Electromagnetic Induction (EMI)

Owing to the fact that EMI provides opportunities for non-invasive, non-contact investigation of the sub-surface, EMI-based instruments are likely to have the greatest range of configurations and applications of all the techniques in geophysics. A challenge with EMI is to detect the secondary field in the presence of the much larger primary field. Within the range of instruments, there are two basic approaches to this challenge:

1. Frequency domain (in which the primary field is nulled electronically in the instrument); and
2. Time domain (in which the measurement is made while the primary field is effectively off).

Frequency domain instruments operate at one or more fixed frequencies while time domain measurements occur as a function of time. Time domain measurements involve the transmission of a pulse (or series of pulses) of primary magnetic field and the measurement of the residual, induced secondary magnetic field effects (primarily relaxation effects) after the end of the primary field pulses. Frequency domain instruments (which are relevant to the current research) operate by either nulling the primary magnetic field and detecting the induced secondary magnetic field, or by detecting the combined primary and secondary magnetic fields. In both cases, the strength of the induced secondary magnetic field is related to the primary magnetic field.

The first EMI surveys were for mineral exploration and occurred around 1931 (Reynolds, 1997). Geonics Incorporated have been an EMI instrument developer and producer for over forty years and their instruments are still popular in a broad range of applications around the world. Their instruments are exclusively frequency domain, and operate with a continuous sine wave primary magnetic field output at a single frequency.

## 2.6 Electromagnetic Induction (EMI) Theory

In a technical note published by Geonics, McNeill (1980) explains the basic EMI theory. The principle of the EMI technique starts with a transmit (Tx) coil which is energised at a frequency, *f*. As shown in Figure 2-3, this produces a primary

magnetic field, $H_0$, which is also oscillating at frequency $f$. The equations defining this dipole field, in cylindrical co-ordinates (with the time varying modifier, $\sin \omega t$ assumed) are:

$$H_{0z}(r,z) = \frac{m}{4\pi}\left[\frac{3z^2}{\left(r^2+z^2\right)^{5/2}} - \frac{1}{\left(r^2+z^2\right)^{3/2}}\right], \qquad \text{Equation 2-3}$$

$$H_{0r}(r,z) = \frac{m}{4\pi}\left[\frac{3rz}{\left(r^2+z^2\right)^{5/2}}\right]. \qquad \text{Equation 2-4}$$

In this form, $H_0$ is referred to as a phasor magnetic field equation of angular frequency, $\omega$.

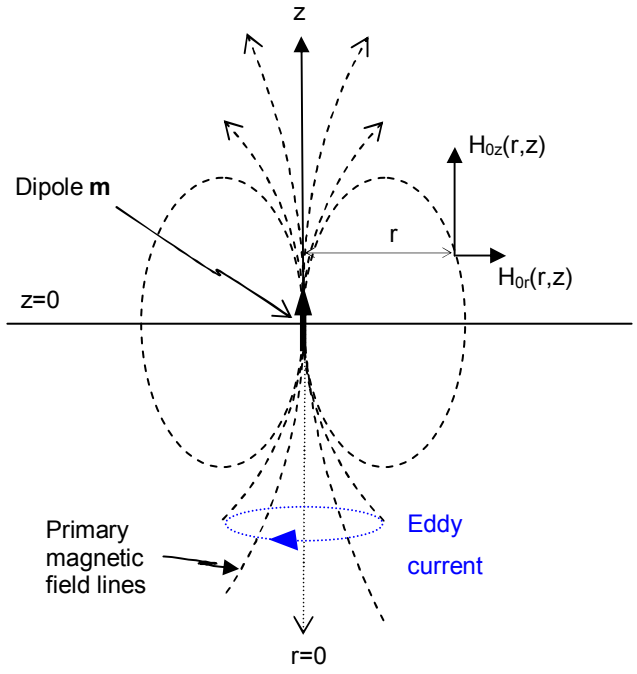


**Figure 2-3. The axial ($H_{0z}$) and radial ($H_{0r}$) components, in cylindrical coordinates, of the primary magnetic field from a point dipole *m*. As currently depicted, the rotational axis of symmetry is the z-axis. An example of an induced eddy current is shown in blue.**

According to Faraday's Law (Kaufman & Eaton 2001:82)

$$\oint_{Loop} E \bullet dl = -\frac{d\Phi}{dt}, \qquad \text{Equation 2-5}$$

the vortex electric field, $E$, around a loop, is defined as the time-rate of change of flux cutting the loop orthogonally (where $dl$ is the incremental length around that

loop; $\Phi$ is the orthogonal flux cutting the loop; and $dt$ the incremental time change). This means that a changing magnetic field produces small circulating currents, referred to as eddy (or sometimes vortex) currents, within nearby conductors. One of many such induced eddy current loops is shown schematically (in blue) directly below the Tx coil in Figure 2-3. These circulating currents are also oscillating at frequency, $f$, and so too produce a changing magnetic field, referred to as the secondary magnetic field, $H_s$. This field (shown in Figure 2-4 in red) is detected when it intercepts the receiving coil. In fact, the receiving coil actually detects the primary field with a distortion due to the secondary field. In summary, the EMI device is sensing the secondary magnetic field effect from eddy currents induced by the primary magnetic field. The detected secondary field is a distortion of the primary field, represented conveniently as a ratio against that primary field (i.e. $H_s/H_0$). Provided the inter-coil (i.e. transmitter to sensor coil) spacing, $s$, and frequency, $f$, meet the condition:

$$\omega \equiv (2\pi f) << \frac{2}{\mu_0 \sigma_a s^2}, \qquad \text{Equation 2-6}$$

then the apparent conductivity ($\sigma_a \equiv EC_a$) can be obtained from the ratio of the secondary to the primary magnetic field according to (McNeill, 1980):

$$\left(\frac{H_s}{H_0}\right) \approx i\frac{\omega \mu_0 s^2}{4}\sigma_a. \qquad \text{Equation 2-7}$$

The symbol $i$ ($i^2 \equiv -1$) denotes the fact that the secondary magnetic field is $\pi/2$ phase-shifted (i.e. leading the primary magnetic field by $\pi/2$). This results from the direct application of Faraday's Law of Induction (Equation 2-5) whereby the induced eddy currents are proportional to the derivative (with respect to time) of the sinusoidal primary magnetic field. Dividing the normalized response, $H_s/H_0$, by the constant of proportionality, $\omega\mu_0 s^2/4$, gives $EC_a$ (in S m$^{-1}$). The requirement to sense a secondary magnetic field that is $\pi/2$ out of phase with the primary magnetic field gives rise to the notion of quadrature detection. In comparison, in-phase detection, as applied to magnetic susceptibility measurements, involves the detection of a secondary magnetic field that is in phase with the primary magnetic field.

Equation 2-6 is the condition for the assumption of a valid quasi-static approximation (where consideration of the wave nature of the signal propagating

out from the EM-38 is ignored). The linearity approximation relates to the fact that the degree of coupling is low and that coupling from one eddy current loop to another is neglected, where the assumption (Equation 2-6) holds.

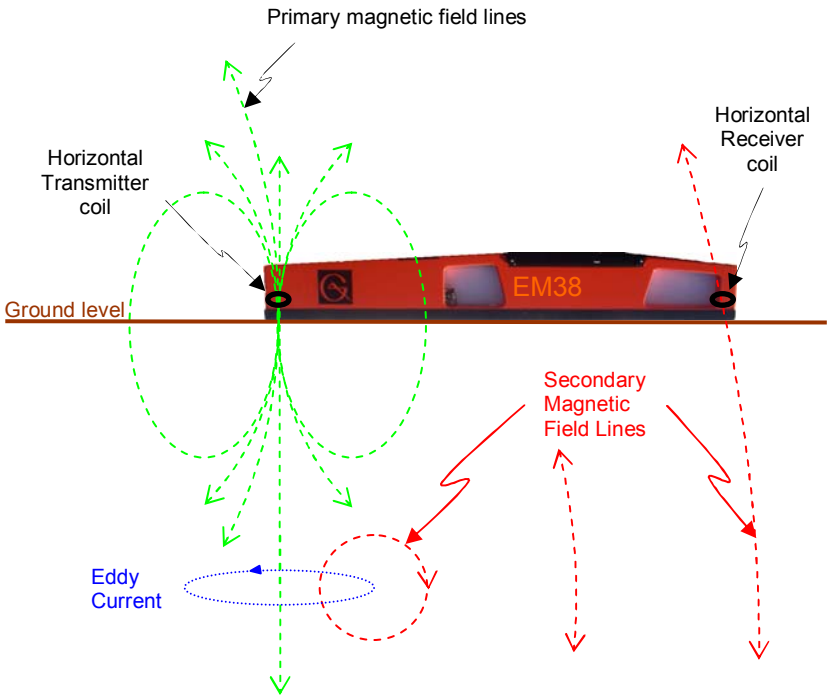


**Figure 2-4. Schematic visualization of the EM38 energising eddy currents in the ground which then produce secondary magnetic fields that can be detected at the receiving coil.**

## 2.7 EMI Depth Function

In Section 2.6 the assumptions were given for the linearity approximation (Equation 2-7). These assumptions were used by Geonics to find the upper limit of frequency for the EM38 (McNeill 1996) where the eddy currents do not significantly couple with one another (McNeill 1980). This constraint, and the fact that within a homogeneous or horizontally layered, half-space, the eddy currents are (due to symmetry) horizontal (Kaufman & Eaton 2001:93), facilitates the derivation of the depth functions. According to Equation 2-3, Equation 2-4 and Figure 2-3, the primary magnetic field interacts differently with underlying soil depending on the orientation of the dipole. That is, the rotational axis of symmetry is usually oriented either vertically (as depicted in Figure 2-3) or horizontally. In both cases, the eddy currents are horizontal (McNeill 1980). These constraints allow the derivation from Equation 2-3 and Equation 2-4, of the normalised, depth response

functions for the vertical and horizontal dipole configurations, given in Equation 2-8 and Equation 2-9, respectively (McNeill 1980). These functions are the contribution from a horizontal slice at depth $z$ of the primary magnetic field and are obtained by integration over that slice from r=0 to infinity. Figure 2-5 shows the depth response functions graphically (for vertical and horizontal orientations).

$$\phi_V(z) = \frac{4z}{\left(4z^2+1\right)^{3/2}}, \qquad \text{Equation 2-8}$$

$$\phi_H(z) = 2 - \frac{4z}{\left(4z^2+1\right)^{1/2}}. \qquad \text{Equation 2-9}$$

The ability to quantify the depth function for both the vertical and horizontal configurations is an advantage of EMI-based conductivity methods over galvanic methods as it allows for the development of the multi-layered response functions (Section 2.8). In addition, it quantifies the different depths of interaction of the primary magnetic field with the underlying soil between the vertical and horizontal dipole configurations. Furthermore, it shows that for the vertical dipole mode there is no response from the surface of the half-space, with the bulk of the response (in a homogenous half-space) coming from between ~0.2 to 1.5 m below the surface. In comparison, the horizontal dipole response has its strongest response from the very near surface (top few decimetres) but tapers off more quickly, with the bulk of the response coming from above a depth of 0.75 m.

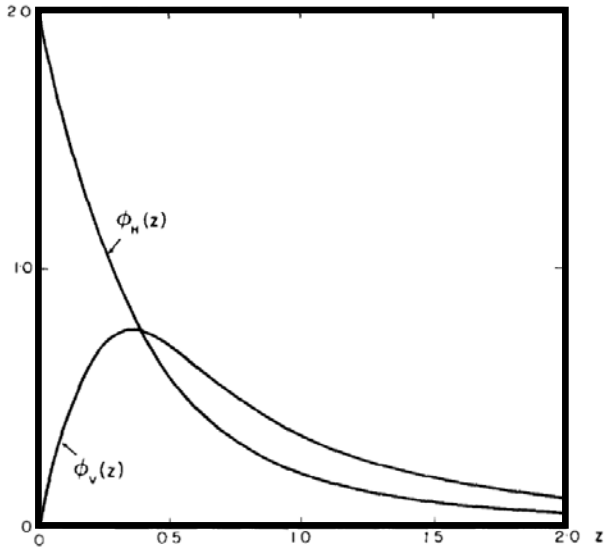


**Figure 2-5. Relative response of EM38 as function of (normalized) depth (McNeill 1992). The horizontal axis is in multiples of the inter-electrode spacing (which is the equivalent of metres for the EM38 because *s*=1).**

Another invaluable aspect of this well-defined depth response function is that the vertical dipole instrument response is approximately twice that of the horizontal dipole deeper than 1.5 m below the surface (see Figure 2-6). This fact is the basis for zeroing the instrument (as will be described in Section 2.10).

## 2.8 EMI Theory for a Horizontally Layered Earth

Figure 2-5 shows the relative responses from horizontal slices at various depths in a homogeneous half-space. Mathematical integration of Equation 2-8 and Equation 2-9 gives the cumulative responses (Equation 2-10 and Equation 2-11) shown graphically in Figure 2-6. These are useful equations for the analysis of multilayer cases.

$$R_V(z) = \frac{1}{\left(4z^2+1\right)^{1/2}} \qquad \text{Equation 2-10}$$

$$R_H(z) = \left(4z^2+1\right)^{1/2} - 2z \qquad \text{Equation 2-11}$$

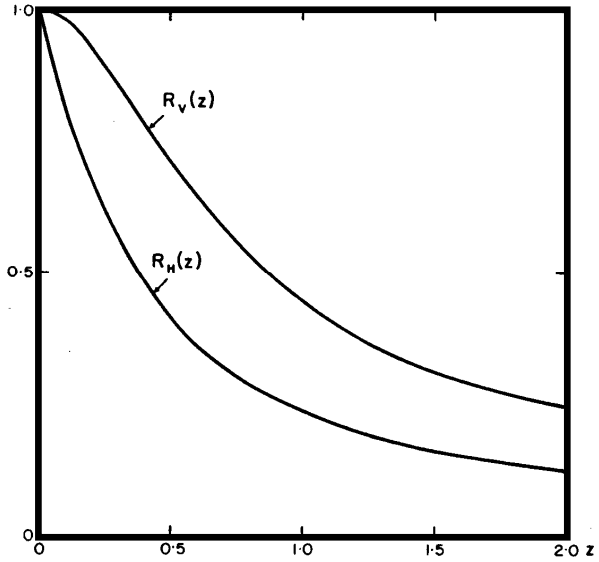


**Figure 2-6. Cumulative response from $z$ to ∞ of EM38 as a function of (normalized) depth (McNeill 1980). $R_V(z)$ and $R_H(z)$ are the cumulative responses for the vertical and horizontal dipole modes, respectively. The horizontal depth axis is in multiples of the inter-electrode spacing (which is the equivalent of metres for the EM38).**

Knowing the relationship for the cumulative $EC_a$ means that the total response value can be calculated if the layer thicknesses and conductivities are known. For example, for the two-layer case, the total $EC_a$ is given by:

$$\sigma_a = \sigma_1\left[1 - R_V(z_1)\right] + \sigma_2 R_V(z_1), \qquad \text{Equation 2-12}$$

where $\sigma_1$ and $\sigma_2$ are the conductivities of the top and lower layer, respectively, while $z_1$ is the depth of the interface between the top and lower layer. This additive relationship can easily be extended to included additional layers. For example, the 3-layer case is given by:

$$\sigma_a = \sigma_1\left[1 - R_V(z_1)\right] + \sigma_2\left[R_V(z_1) - R_V(z_2)\right] + \sigma_3 R_V(z_2). \qquad \text{Equation 2-13}$$

In addition to this forward modelling, the responses shown in Figure 2-5 can be used to analyse the layering in the earth by taking EMI measurements at two separate heights (McNeill 1980).

## 2.9 The EM38 Soil Conductivity Meter

The EMI instrument used in this study is the EM38 DLM (Geonics Inc., Mississauga, Ontario Canada) as depicted in Figure 2-7.

Geonics chose a coil spacing of $s$=1 m for their EM38 instrument to sense the conductivity within the first couple of metres of the earth's surface. Given that constraint, the EM38 frequency of operation ($f$ = 14.6 kHz) was then chosen so that the linear relationship between $H_s/H_0$ and $EC_a$ (Equation 2-7) is valid for a realistic range of $EC_a$ expected for typical soils ($\sigma$<70 mS m$^{-1}$) (McNeill 1980). The reduction of the frequency (to maintain the linearity approximation) was balanced against using frequencies so low that instrument-zeroing issues became impractical (McNeill 1996).

There is no practical advantage in using different EMI frequencies, only technical difficulties (McNeill 1996). That is, to gain any practical benefit, a 1 MHz instrument would be required and at these frequencies electronic equipment manufacture is problematic, while at frequencies lower than that selected for the EM38, drift becomes unmanageable.

The principle motivation for the EM38 development was salinity investigations and that application has been a principle focus of applied research (Rhoades, et. al. 1989a; Rhoades, et. al. 1989b).

However, within this study, only the EM38 quadrature response (which gives conductivity) is relevant. The physical orientation of the primary magnetic field lines from the EM38 and the location of the transmitter and receiver coils are shown in Figure 2-4. Given the physical orientation of the EM38's primary magnetic field lines, operation in vertical and horizontal dipole configurations is as simple as changing the instrument's orientation as depicted in Figure 2-7.


**a)** **b)**

**Figure 2-7. Photographs of the EM38DLM model used in this study oriented for: a) Vertical dipole mode; and b) Horizontal dipole mode.**

The instrument is readily operated in both quadrature and in-phase modes by changing the position of the toggle switch on the console. However, within this study only the relevant EM38 quadrature response (which gives conductivity) is used, and will be referred to simply as $V_Q$ for quadrature readings in the vertical dipole mode, and $H_Q$ when the instrument is in the quadrature, horizontal dipole mode.

## 2.10 EM38 Accuracy, Calibration, Zeroing and Drift

Table 2-1 lists the specifications of the EM38. The accuracy stated in this table is approximately ± 1.5 mS $m^{-1}$ at 30 mS $m^{-1}$ with a noise level of 0.5 mS $m^{-1}$, while the resolution (based on the LCD digital display) is 0.1 mS $m^{-1}$ (for the zero to 100 mS $m^{-1}$ range). These accuracies do not take into account instrument drift and zeroing factors.

Robinson et al (2004) have observed EM38 drift of 20 % and caution against ignoring this factor. A potential cause of the instrument drift is differential heating between the coils and the control panel, where the temperature compensation sensor is located. While the instrument is rated for operation between -30°C to 50°C (Table 2-1) Robinson et al (2004) state that it is only temperature-compensated up to 40°C, which is readily achieved in direct sunlight. The stability of distance between the coils is critical to the instrument's measurement stability (particularly for in-phase measurements) hence the choice of material for construction of the EM38, Canadian cherry wood, which has an exceptionally low coefficient of expansion with temperature (Catalano 2008, pers. comm. 11 September 2008). To minimize this significant temperature factor, the instrument should be shaded from direct sun light and allowed one hour for thermal stabilisation when taken to a new location (or for example, removed from a vehicle into an open field situation).

Sudduth, Drummond and Kitchen (2001) also reported significant EM38 drift (up to 3 mS $m^{-1}$ /hour) which could not be simply compensated for by measuring air-temperature and deducing a correction. Their recommendation is to re-zero the instrument every hour (or ideally every half-hour).

**Table 2-1. EM38 Specifications. (Adapted from Geonics 1992; Geonics 2008).**

| Feature | Specification |
|---|---|
| **MEASURED QUANTITIES** | 1: Apparent conductivity in milliSiemens per metre (mS $m^{-1}$)<br>2: In-phase ratio of secondary to primary magnetic field (ppt) |
| **PRIMARY FIELD SOURCE** | Self-contained dipole transmitter |
| **SENSOR** | Self-contained dipole receiver |
| **INTERCOIL SPACING** | 1 metre |
| **OPERATING FREQUENCY** | 14.6 kHz |
| **POWER SUPPLY** | 9 V battery |
| **MEASURING RANGE** | Conductivity: Autoranging 0- 1000 mS $m^{-1}$. Manual: 100, 1000 mS $m^{-1}$<br>In-phase: ± 29 ppt |
| **MEASUREMENT RESOLUTION** | ± 0.1 % of full scale (4 digit digital meter) |
| **MEASUREMENT ACCURACY** | ± 5 % at 30 mS/m |
| **NOISE LEVELS** | Conductivity: 0.5 mS/m<br>In-phase: 0.02 ppt |
| **BATTERY LIFE** | 30 hours continuous |
| **DIMENSIONS** | Instrument: 106 x 15 x 3.6 cm |
| **TEMPERATURE** | -30°C to 50°C<br>Shipping Case: 117 x 19 x 13 cm |
| **WEIGHTS** | Instrument: 3 kg<br>Shipping: 10 kg |
| **DATA OUTPUT RATE** | 10 Hz |
| **COMMUNICATION PORT** | 10 pin round RS-232 port (up to 115 Kbaud) |
| **DISPLAY** | Large LCD (4 digit digital) |

The procedure for zeroing the EM38 relies on the depth responses given in Figure 2-6 where below a depth of 1.5 m the vertical dipole response is approximately twice the horizontal dipole response (Section 2.7). This forms the basis of the zeroing procedure: Firstly, the instrument is nulled (whilst in-phase mode is selected). The instrument is then switched to quadrature mode and lifted to a height of 1.5 m above the ground (the highest convenient height for frequent field zeroing). The quadrature phase control knob is adjusted so that the instrument reads a value in vertical mode (*V*) that is twice that in horizontal mode (*H*).

Ideally, zeroing would be performed at a great height or in extremely resistive soil (McNeill, 1980). Dabbas and Tabbagh (2003) analyse the error from the assumption, $R_V = 2R_H$ at the nominated 1.5 m elevation and at other heights. Using Equation 2-10 and Equation 2-11 to determine $R_V$ and $R_H$ at various heights allows the calculation of the relative error in zeroing to be tabulated (Table 2-2). Given that the convenient height of 1.5m is used for field zeroing, this table shows that that would give a zeroing error of -2.6 %.

**Table 2-2. EM38 Calculated zeroing error for different heights.**

| Height (m) | $(R_V-2R_H)/R_V$ |
|---|---|
| 0.5 | -17.2 % |
| 1.0 | -5.6 % |
| 1.5 | -2.6 % |
| 2.0 | -1.5 % |
| 2.5 | -1.0 % |
| 10 | -0.1 % |

Dabbas and Tabbagh (2003) also claim, contrary to McNeill 1980, that certain layering in the near surface can introduce a greater error in zeroing the EM38. Dabbas and Tabbagh (2003) point out that the approximation in Equation 2-7 can also introduce errors for higher conductivity soils, for example, 13 % at 100 mS $m^{-1}$ compared to the true values calculated from Maxwell's equations. However, it would be a simple matter to calculate a correction for this effect.

In this study the significant drift and zeroing errors have been acknowledged and side-stepped by measuring (and then subtracting) a background reading immediately after the main reading. This background reading was a repeat reading

but with the target removed and the EM38 left in the same location. This procedure also had the advantage of removing background soil readings when the target being investigated was other than the soil (e.g. a trellis structure) because the EM38 remained at the same location, measuring the same soil.

Where this background removal procedure was not possible, a nearby calibration site was marked and a calibration reading taken after each measurement. In some cases this calibration measurement was performed for a group of measurements, provided they could be taken relatively quickly (e.g. in less than 10 minutes). A linear interpolated value between the calibration readings was then subtracted from the main readings.

## 2.11 Inductance Estimations with FastHenry

The interference to an EM-38 from a large conducting trellis can be analyzed as a circuit network. A simplified schematic of the interaction between two circuit elements (i.e. the EM-38 transmitter coil and the large vertical rectangular loop of the trellis) is shown in Figure 2-8. In this circuit (ignoring the return influence to the receiver) it can be seen that while trellis resistance and self-inductance will be factors, it is the mutual inductance between the two main elements that is the mechanism of interference.

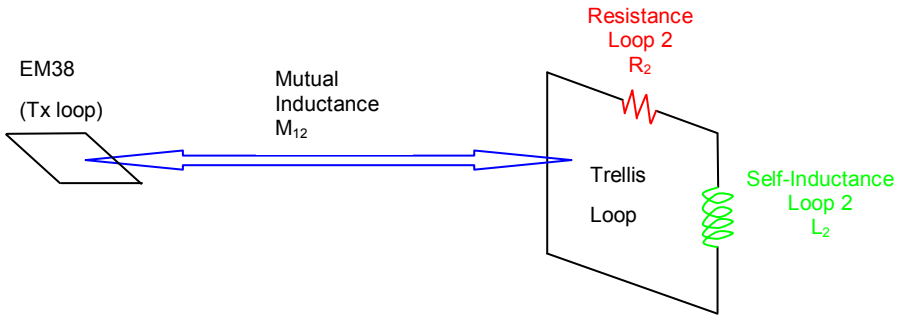


**Figure 2-8. Schematic representation of the mutual inductance between the EM38 Tx coil and a large vertical loop (simulating a trellis). Also of importance is the resistance and self-inductance of the large trellis loop.**

For simple loop shapes, the self-inductance, $L$, is calculated exactly from an analytical formulae derived from first principles. For example, the self-inductance of a thin, circular loop of thin cylindrical wire (Kaufmann & Eaton 2001:99) is:

$$L = r\mu_0\left(\log_e \frac{8r}{r_x} - 1.75\right), \qquad \text{Equation 2-14}$$

where $r_x$ is the wire's cross-sectional radius and $r$ is the loop radius. However, as the shapes become more complicated, the formulas for self-inductance rapidly become unmanageable. This is even more so for mutual inductance where the interaction of (at least) two shapes has to be determined in three-dimensions. There are a number of numerical computer software packages available to solve for the inductances from complicated geometries, and the software used in this research is FastHenry (Kamon, Tsuk & White 1994), developed by the Department of Electrical Engineering and Computer Science, MIT, MA, USA. The FastHenry software calculates frequency dependent inductances and resistances of complicated arrays of linear, conducting filaments. Complicated 3-D structures are constructed by first defining the vertices in 3-D Cartesian coordinates and then defining the straight filaments that connect particular pairs of vertices (Kamon, Smithhisler, & White, 1996). The filaments' cross-sectional area and resistivity are also specified. A circular loop is approximated by a polygon of the same area due to the straight filament requirement (e.g. a hexagon is a convenient and adequate representation of a circular loop for most applications). For each frequency defined, the software reformulates the defined configuration into a system of equations. These are then solved to produce a complex, impedance matrix, *[Z]*, the elements of which provide the basic parameters of the circuit network representing the EM38 interference.

The two terminals where a voltage is applied, and through which the current flows in and out, are referred to as a 'port'. The size of the resultant output matrix depends on the number of ports defined. If only a one-port circuit is defined, then the output will be a 1×1 matrix containing just a single impedance (the resistance and self-inductance) of that constructed circuit as would be 'seen' at that port (Figure 2-9a). That is, if a sinusoidal voltage, $V_1(t)$, is applied to a circuit network, then a certain current, $I_1(t)$, will result. Figure 2-9a shows a one-port system, where the circuit inside the dashed box is unknown (i.e. it is a 'black box') but can be

represented as a simple series circuit of a resistance $R_1$ and self-inductance $L_1$ (ignoring capacitance for this case). The complex impedance of this one-port black box network is:

$$Z_1 = R_1 + i\omega L_1, \qquad \text{Equation 2-15}$$

and the voltage is determined by:

$$V_1(t) = Z_1 I_1(t). \qquad \text{Equation 2-16}$$

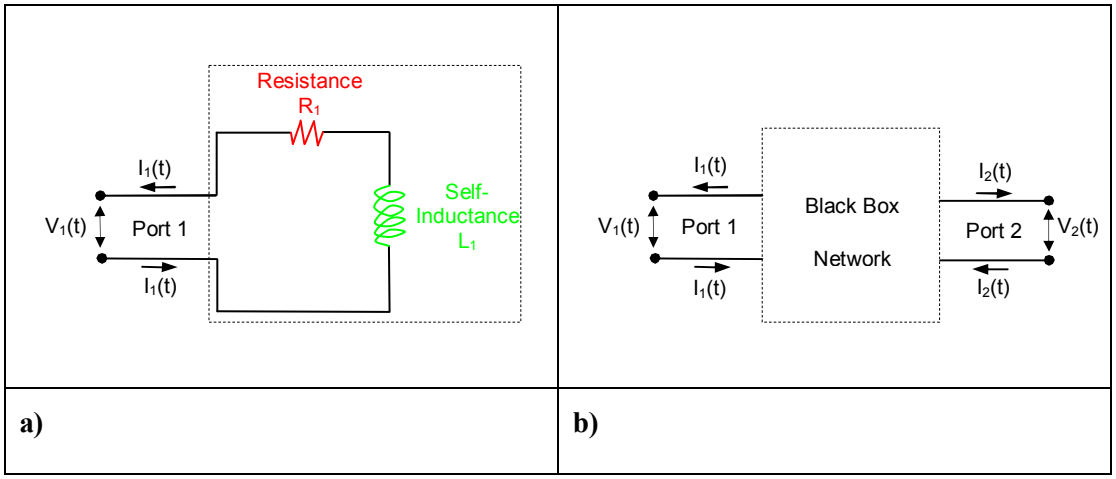


**Figure 2-9. a) a one-port network; and b) a two-port network. The dashed box is a 'black box'.**

If two ports (Figure 2-9b) are defined then the output will be a 2×2 matrix:

$$[Z] = \begin{bmatrix} Z_{11} & Z_{12} \\ Z_{21} & Z_{22} \end{bmatrix} = \begin{bmatrix} R_{11} + i\omega L_{11} & R_{12} + i\omega M_{12} \\ R_{21} + i\omega M_{21} & R_{22} + i\omega L_{22} \end{bmatrix}, \qquad \text{Equation 2-17}$$

with the diagonal elements giving the internal resistance and self-inductance of each circuit element as 'seen' by the relevant port (e.g. the diagonal element on Row 1 refers to Port 1). The off-diagonal elements give the effect at one port if a voltage is applied to another port. However, because these factors have reciprocity, the matrix is symmetric (i.e. $Z_{12}$=$Z_{21}$), For example, in a 2×2 matrix, matrix element, Row 1, Column 2 ($Z_{12}$) is the effect at Port 1 due to voltage applied at Port 2. However, this is reported in the software's output matrix as the impedance encountered between Port 1 and Port 2 and the partial inductance (which in this case is the mutual inductance, $M$, between the two). Partial inductance is defined as the inductance contribution from an element to the total inductance (Grover 2004:2). The total inductance is then the algebraic sum of the partial inductances (i.e. they are additive) (Grover 2004:3). Figure 2-10 shows these representative

matrix elements inside the 'black box' connected to their respective ports and the mutual inductance linking Port 1 and Port 2. In this two-port system, Equation 2-16 is extended to a matrix equation (Chirlian 1969:470):

$$[V]=[Z]\cdot[I], \qquad \text{Equation 2-18}$$

where $[V]=\begin{bmatrix} V_1 \\ V_2 \end{bmatrix}$, $[I]=\begin{bmatrix} I_1 \\ I_2 \end{bmatrix}$ and the function of time *(t)* designation is assumed.

This matrix equation is then the basis for the system of equations that FastHenry solves internally.

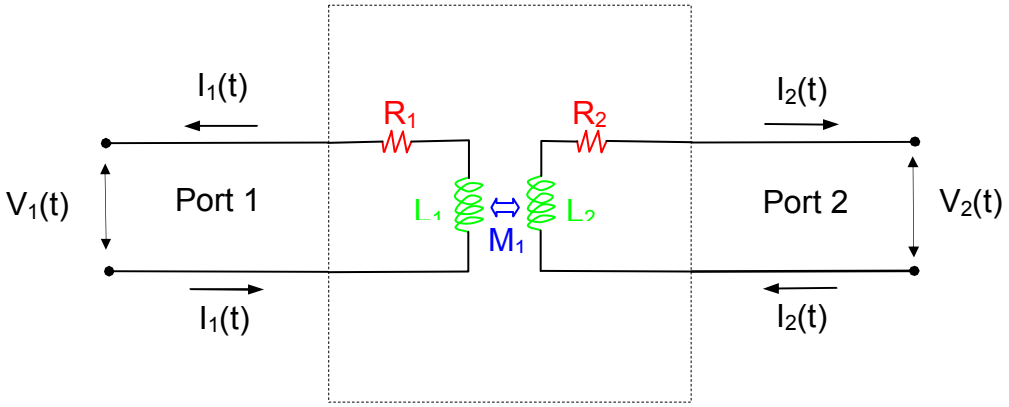


**Figure 2-10. Two-port network with mutual inductance.**

The interaction between an EM38 coil and a vine trellis can be constructed using a two-port system as shown schematically in Figure 2-11. Here one circuit is the Tx coil of the EM38 and the second circuit is the Target Loop (i.e. the steel trellis segment). In this case, the relevant information is $M_{12}$ (= $M_{21}$), $L_2$ and $R_2$. As can be seen from Equation 2-14, the cross-sectional area of the filament is significant, so it is important to build up the loops with filaments with accurate cross-sectional areas (even though only rectangular cross-sections are permitted in FastHenry). Finally, the coupling of the trellis loop back to the Rx coil of the EM38 is modelled (unless symmetry makes it unnecessary). This is achieved by setting up a second 2-port simulation or by using a 3-port set-up (i.e. EM38-Tx to trellis loop and then back to the EM38-Rx).

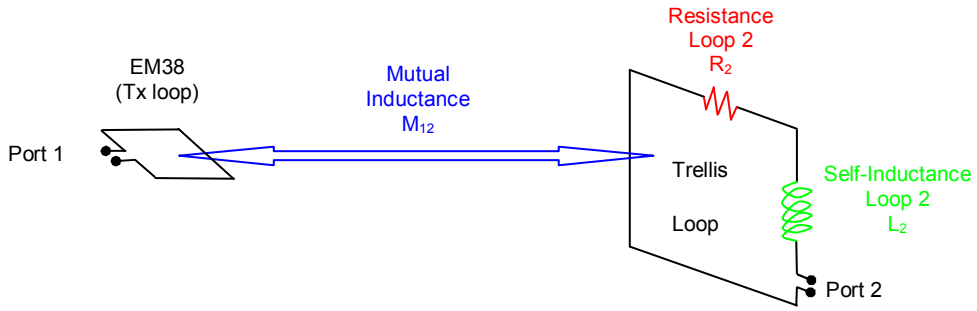


**Figure 2-11. Schematic representation of the straight segment modelling within the FastHenry software to estimate resistance, self-inductance of a large vertical loop (simulating a trellis) and the mutual inductance to the EM38 Tx coil.**

In reality, a trellis will be made up of multiple loops. Hence, the partial mutual inductance from each elementary loop will need to be considered in any analysis. Fortunately, the inductive coupling between the loop elements of a trellis can be ignored (at the quasi-static frequencies used by the EM38). However, because the loops are interconnected, the circuit interactions between each element will be significant and require consideration in an overall circuit network analysis.

## 2.12 Conclusion

In this chapter, the fundamental physics relevant to the operation of the EM38 EMI instrument as a soil conductivity meter have been developed together with an analysis of the theory of the instrument's operation and interpretation. The practical aspects of the EM38's operation, pertinent to the experiments described in subsequent chapters, have also been presented. Finally, a description of the FastHenry software, which was used in this research, has been provided in preparation for its use in predicting trellis interference in EM38 soil surveys. The following chapter (Chapter 3) focuses upon the EM38's response to simple conducting loops. Starting from the fundamental physics, the discussion then develops the concept of mutual induction from the EM38 to simple conducting loops. This leads to a relative prediction of the EM38 response to a loop from its size and orientation.

# Chapter 3 EM38 Response to Simple Conducting Loops

## 3.1 Introduction

The focus of this chapter is upon the EM38's response to simple conducting loops. Starting from the fundamental physics, the concept of mutual induction from the EM38 to simple conducting loops is developed. This concept leads firstly to a relative prediction and then to an absolute prediction which is supported by a series of experiments. The chapter concludes with a derived predictive formula including previously unidentified constants.

To predict the EM38's response to a simple conducting loop, the following four physical effects must be determined for the loop:

1. The mutual inductance from the transmitter loop to the Target Loop;
2. The complex impedance of the Target Loop;
3. The resulting eddy current and its phase in the Target Loop; and
4. The mutual inductance from the Target Loop back to the receiver loop.

In order to reduce the complexity of the interaction between the EM38 transmitter and a nearby conducting loop, the geometry has initially been restricted to circular loops aligned coplanar with the transmitter and receiver coils of the EM38.

## 3.2 Magnetic Field of the EM38 Transmitter

The actual magnetic field strength of the EM38 transmitter does not need to be known by the conventional user as the instrument's response value is normalised against transmitter strength (Equation 2-7). Moreover, the value of the field strength is the manufacturer's proprietary information and is not made available to users.

The small transmitter loop is, for all practical purposes, treated as a point dipole source. The amplitude and direction of a magnetic dipole is the vector moment, $\boldsymbol{m}$, and its amplitude is defined by a plane loop of current, such that:

$$| m |= IA \quad , \qquad \text{Equation 3-1}$$

where $I$ is the current, $A$ the area of that loop of current, and the vector direction is orthogonal to the plane of the current loop (see Figure 3-1).

The EM38 transmitter dipole generates an energizing magnetic field as shown in Figure 3-1. The magnetic field from the vertical magnetic dipole can be represented (in spherical coordinates) by a radial and a transverse magnetic field component. The energising magnetic field lines from the EM38 transmitter dipole in Figure 3-2 are shown coupling with a simple circular, coplanar conducting loop.

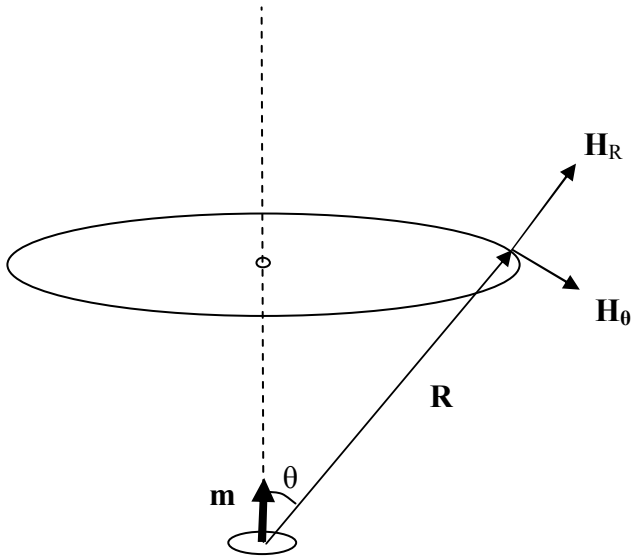


**Figure 3-1. A magnetic dipole whose moment, m, is directed along the z-axis at the origin of a spherical coordinate system. $H_R$ and $H_\theta$ are the radial and transverse magnetic field components due to $m$. Note the schematic has a cylindrical axis of symmetry around the vertical dotted line.**

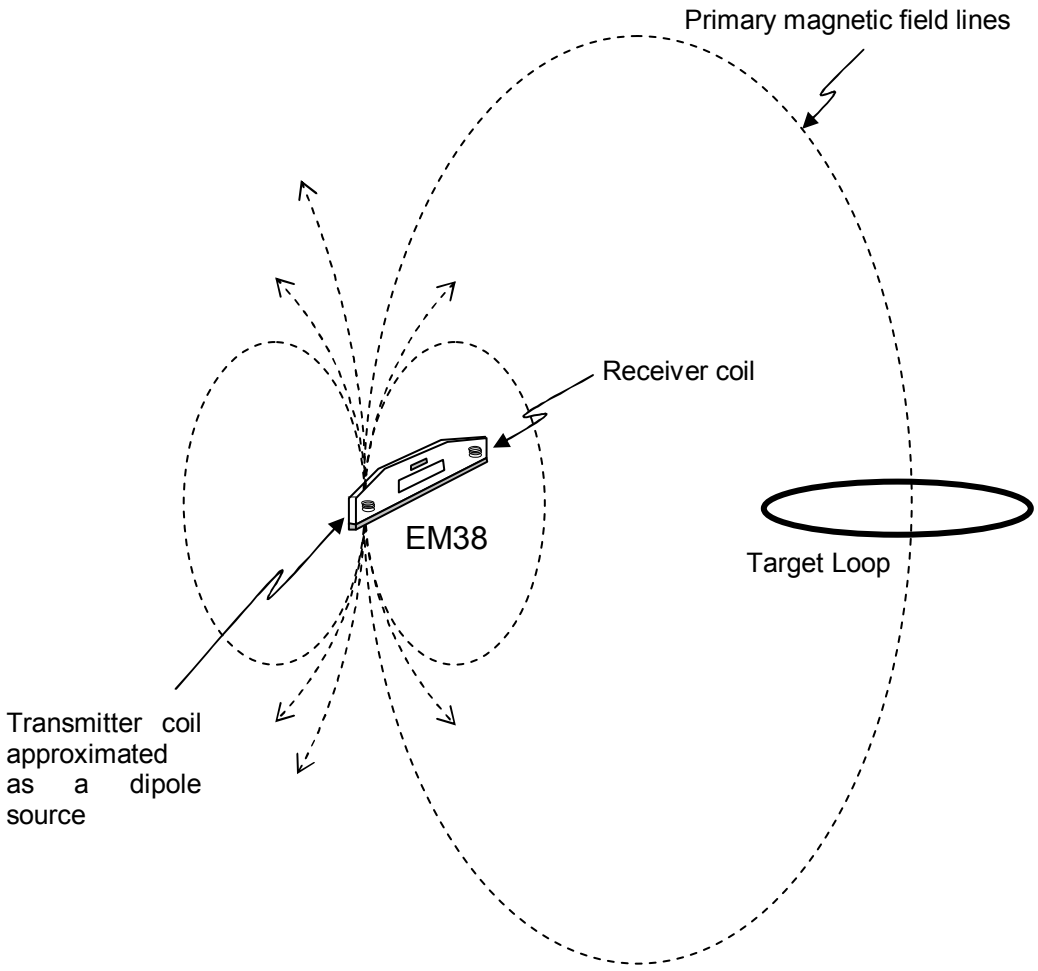


**Figure 3-2. The magnetic dipole representation of the EM38 transmitter, with an example of magnetic field lines (dotted curving lines) coupling with a coplanar Target Loop.**

## *3.3 Mutual Inductance between Two Distant Coplanar Loops*

The vortex electric field in the Target Loop is proportional to the purely geometrical effect of mutual inductance, $M$, and the primary current, $I_0$, in the transmitter. The mutual inductance between coplanar distant loops can be simplified by approximating the magnetic flux over the horizontal Target Loop as a constant. The mutual inductance is then calculated by mathematically integrating this constant magnetic flux over the area of the Target Loop. This is represented diagrammatically in Figure 3-3.

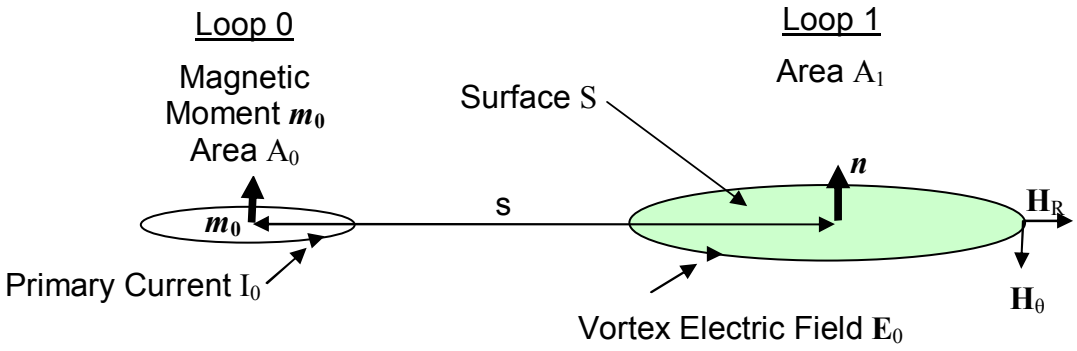


**Figure 3-3. Coplanar loops showing the vortex electric field at the Target Loop (Loop 1) due to the primary magnetic dipole field (induced by the primary magnetic current, $I_0$, in the EM38 transmitter loop, of area $A_0$). $n$ is the normal unit vector, orthogonal to target surface, $S$.**

The vortex electric field, $E_0$, around Loop 1, due to a time varying primary magnetic moment, $\boldsymbol{m}_0(t)$, drives the eddy current around Loop 1. In fact, it is only the time-rate of change of the magnetic flux cutting the surface of Loop 1 (orthogonally) that drives the eddy current. This driver is the electro-motive force, $\xi$, or vortex electric field. Substituting the definition of flux, $\Phi$, (Kaufman & Eaton 2001:81):

$$\Phi = \int_S B \bullet dS \,, \qquad \text{Equation 3-2}$$

into Faraday's Law (Equation 2-5) gives the flux rule:

$$\xi = \oint_{Loop} E \bullet dl = -\frac{\partial}{\partial t}\int_S B \bullet dS \,, \qquad \text{Equation 3-3}$$

where $\boldsymbol{B}$ is the magnetic flux density or magnetic induction and relates to $\boldsymbol{H}$ by $\boldsymbol{B}=\mu\boldsymbol{H}$, where $\mu$ is the magnetic permeability.

In general, it is the relative magnetic effect of the magnitude, phase and geometry of eddy currents (with respect to the EM38 orientation) that is ultimately measured with the EM38.

### *3.3.1 The Magnetic Field of a Dipole*

The first step in calculating the mutual inductance is to calculate the magnetic field at the Target Loop from the primary source. The magnetic field from a magnetic

dipole, ***m,*** is shown in Figure 3-1, where the radial and transverse magnetic field vectors are given by (Kaufman & Eaton 2001: 87):

$$\mathrm{H_R}(t) = \frac{2m}{4\pi s^3}\cos\theta\,, \mathrm{H}_\theta(t) = \frac{m}{4\pi s^3}\sin\theta\,, \qquad \text{Equation 3-4}$$

where $s$ is used here for the length of the radial vector, $R$, (i.e. $s$ denotes loop separation in this study). However, for coplanar loops (as shown in Figure 3-3) the angle $\theta$ is $\pi/2$ and $\boldsymbol{H}$ simplifies to:

$$\mathrm{H_R}(t) = 0, \mathrm{H}_{\theta=0}(t) = \frac{m}{4\pi s^3}. \qquad \text{Equation 3-5}$$

### 3.3.2 Mutual Induction Definition

Mutual inductance is a purely geometrical factor (Kip 1962:299) between two conductors. Mutual inductance is defined as the total magnetic flux cutting the surface at one conductor, per unit-current flowing in the other conductor (Lorrain & Corson 1962:345):

$$M_{01} = \frac{\Phi_{01}}{I_0} \qquad \text{Equation 3-6}$$

where $M_{01}$ is the mutual inductance in Loop 1 due to the current $I_0$ flowing in Loop 0 and $\Phi_{01}$ is the total magnetic flux orthogonally cutting the surface $S$, at Loop 1, due to the primary source. Figure 3-3 shows this for the coplanar loop case. By definition, $\Phi_{01}$ is the integration of the primary magnetic induction vector $\boldsymbol{B_0}$ over $S$:

$$\Phi_{01} = \int_S B_0 \bullet dA_1, \qquad \text{Equation 3-7}$$

where the dot product takes account of the orthogonality requirement.

### 3.3.3 Mutual Induction Approximation for Initial Testing

For well-separated loops ($A_0 << s^2$ and $A_1 << s^2$) the primary magnetic field will be approximately constant over the surface $S$, defined by Loop 1. In addition, $B$ is defined as:

$$B = \mu(H + \text{Magnetisation}), \qquad \text{Equation 3-8}$$

where ***Magnetisation*** is the vector quantity dipole moment per unit-volume contributed by the medium (Lorrain & Corson 1962:384). However, magnetisation can be eliminated by removing all magnetic material from the vicinity of the transmitter (i.e. using copper wire rather that steel wire) and, because the loops are in air, the magnetic permeability, $\mu$, is practically the same as the magnetic permeability of free space, $\mu_0$ (i.e. $\mu \approx \mu_0$) giving:

$$B_0 \approx \mu_0(H_0)\,. \qquad \text{Equation 3-9}$$

Using the approximation for distant loops that $\boldsymbol{B_0}$ is constant over the surface, $S$ (of Loop 1) Equation 3-7 becomes:

$$\Phi_{01} = B_0 A_1\,, \qquad \text{Equation 3-10}$$

and, combining this with Equation 3-9 and Equation 3-5 gives (for distant loops):

$$\Phi_{01} = \mu_0 m(t)\frac{A_1}{4\pi s^3}, s^2 >> A\,. \qquad \text{Equation 3-11}$$

Combining the definition for mutual inductance (Equation 3-6) with the approximation for flux at a distant coplanar loop (Equation 3-11) and the magnetic dipole definition (Equation 3-1) gives:

$$M_{01} = \frac{\Phi_{01}}{I_0} = \mu_0 m_0(t)\frac{A_1}{I_0 4\pi s^3} = \mu_0 A_0 I_0 \frac{A_1}{I_0 4\pi s^3}, s^2 >> A_1\,,$$

which condenses (because $\mu_0 = 4\pi\times10^{-7}$) to:

$$M_{01} = 10^{-7}\frac{A_0 A_1}{s^3}, s^2 >> A_1\,. \qquad \text{Equation 3-12}$$

## 3.4 Relative EM38 Response to a Distant Horizontal, Coplanar Loop

The EM38's predicted response to a distant loop (held coplanar and horizontal with the transmit and receive loops, as illustrated in Figure 3-4) should be proportional to the product of the mutual inductance from the transmit loop to the Target Loop and the mutual inductance from the Target Loop back to the receive loop:

$$[\text{EM38 Response}] \propto M_{01} M_{12}\,. \qquad \text{Equation 3-13}$$

For the assembly shown in Figure 3-4, the loop separations are equal ($s_1=s_2=s$) and using Equation 3-12 for the mutual induction estimation gives a predicted EM38 proportional response:

$$M_{01}M_{12} = \mu_0^2 \frac{A_0 A_1^2 A_2}{(4\pi)^2 s^6} = 10^{-14} \frac{A_0 A_1^2 A_2}{s^6}, s^2 >> A_1, \qquad \text{Equation 3-14}$$

where $A_0$ and $A_2$ are the unknown (but constant) areas of the EM38's transmit and receive loops.

If just the separation to the Target Loop, *s,* is varied, then the complex impedance (self-inductance and real resistance) of the Target Loop is constant. In addition, because the EM38 operates at a fixed frequency (Section 2.6) and the Target Loop area is constant then, according to Equation 3-14, its response should be proportional to the inverse sixth power of the distance from the EM38 transmit loop to the Target Loop centre, *s*. That is,

$$[\text{EM38 Response}] \propto \frac{1}{s^6}, s^2 >> A. \qquad \text{Equation 3-15}$$

Equation 3-15 predicts an inverse-sixth-power relationship between the EM38 response and its separation distance from a conducting loop of fixed size, shape, orientation and conductivity that is not close to the EM38. To test this prediction, an experiment was devised to confirm that the EM38's response could be accurately predicted using this fundamental physical relationship.

The quadrature response of the EM38 ($V_Q$) should be proportional to the simple product of the mutual inductance from the EM38 Tx with the loop vortex current, $I_Q(t)$, and the product of mutual inductance of the Target Loop back to EM38 Rx. Applying the constraint, $M_{01}=M_{12}$ (Figure 3-4), the predicted proportionality relationship is therefore:

$$V_Q \propto M_{01} \times I_Q(t) \times M_{12} = M_{01}^2 \times I_Q(t). \qquad \text{Equation 3-16}$$

### 3.4.1 Materials and Methods: Relative EM38 Response to Distant Coplanar Loops with Distance

The schematic arrangement for this preliminarily test is shown in Figure 3-4 and a photograph of the apparatus used given in Figure 3-5. The measurements were

conducted on a wooden bench approximately 1 metre above the ground. This was to minimise the interference from ground conductivity (i.e. maintaining the free space approximation used in Equation 3-9). However, to ensure that any residual ground effect was kept constant, the Target Loop, not the EM38 was moved. In addition, raising the instrument to a height of 1 m reduced the instrument's sensitivity to changes in the relative ground effects (or sub-surface metal) due to instrument orientation changes (e.g. due to wind, vibration or minor movement in the supporting bench). The EM38 was nulled and calibrated according to the procedure described in Section 2.10. The instrument was then lowered to the bench so that the transmit and receive loops, which are 58 mm above the base of the instrument (M. Bosnar 2005, pers. comm., 19 October) were level with the Target Loop, in order to maintain the coplanar condition required.

Following the protocol from Section 2.10, the instrument was switched on one hour prior to the experiment to allow the EM38 to electronically and thermally stabilize. Subtraction of the background ($V_B$) from each measurement corrected both instrument drift and residual $EC_a$ from the soil below the bench. The background value was the EM38 measurement taken immediately after removal of the Target Loop from the influence of the EM38. Hence, the value of $EC_a$ reported is $V$-$V_B$.

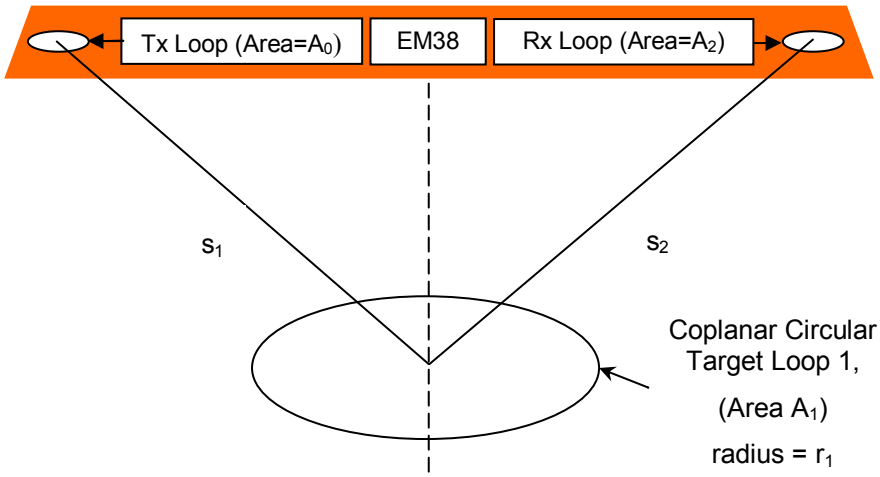


**Figure 3-4. Schematic of the EM38 coplanar loops experimental configuration. Shown are the circular Target Loop of wire, the transmitter (Tx) loop and the receiver (Rx) loop. All three loops were coplanar and horizontal. The Target Loop (of area $A_1$) was moved along the centre-dashed line, maintaining the equality of the distances $s_1$ and $s_2$.**

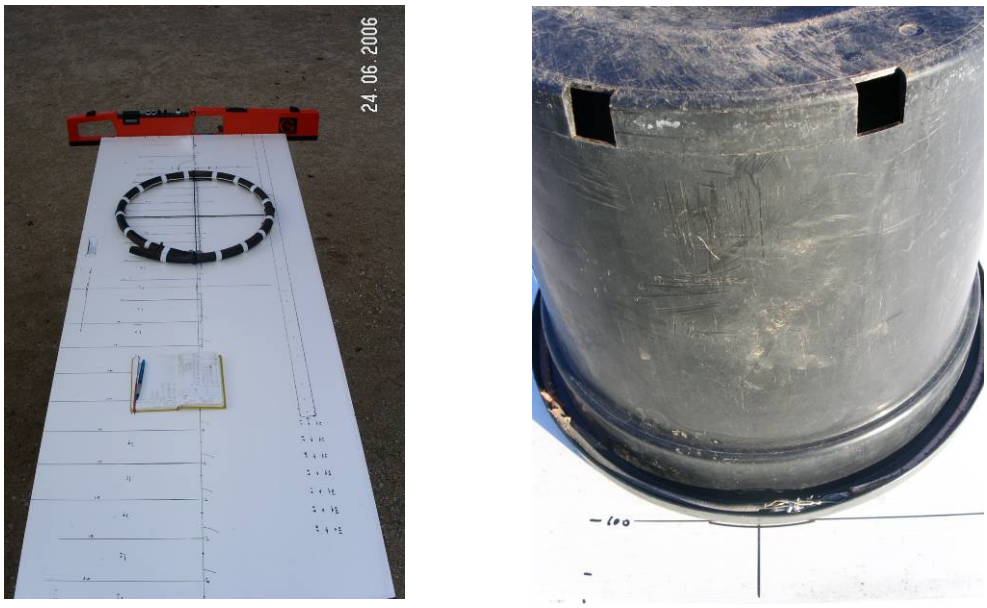


**a)** **b)**

**Figure 3-5. Photographs of the coplanar loops experiment showing: a) The EM38 on the wooden test bench, the top of which was marked with graticules for accurate positioning of the horizontal Target Loops; and b) Plastic form for the 310mm diameter circular Target Loop (single turn copper wire with ends connected (soldered) together).**

Circular Target Loops were formed by wrapping lengths of 1.07 mm diameter copper wire around the circumference of plastic cylinders (e.g. Figure 3-5b). Six loop diameters were fabricated: 0.115 m; 0.134 m; 0.167 m; 0.228 m; 0.310 m; and 0.489 m. The position of the wire loops relative to the EM38 unit were accurately determined using a pre-marked graticule on the wooden bench top. The distance of the loop along the perpendicular bisector between the transmit and receive coils of the EM38 was varied in 50 mm increments from as close as possible to the EM38, up to 1 m, and thereafter in 100 mm increments up to where the signal was negligible (a maximum of 1.8 m for the largest loop). The EM38 output was read directly from the digital display, and as the display was readable from some distance, a minimum observer distance of 1 m was maintained during readings to minimize introduction of distortions to the EM38 response.

Finally, numerically calculated mutual inductances (using the software program FastHenry described earlier in Section 2.11) were compared with the distant loop measurements. (The circular Target Loops were represented 'piecewise' in FastHenry by hexagons of the same area, such that near and far 'pieces' were

modelled.) Whilst the Tx loop dimensions for the EM38 are proprietary (and hence unavailable)(Bosnar, 2005, pers. comm. 15 October), a nominal diameter of 25.4 mm (i.e. 1 inch) was chosen. This was considered the maximum loop size to fit within the wooden case of the EM38 and meet the condition that it be small compared to the separations and Target Loop dimensions.

### 3.4.2 Results and Discussion: Relative EM38 Response to Distant Coplanar Loops with Distance

A graph of EM38 vertical dipole responses ($V_Q$-$V_B$) for each of the six loop sizes, as a function of loop distance, is given in Figure 3-6, along with calculated values for a single size ($M_{12}^2$.amplitude for distant loops normalised to the response for a coil diameter of 0.115 m) for slope comparison. On that graph, both axes (i.e. the EM38 responses to the loops against their separation distances) are plotted on logarithmic scales, and so the inverse power relationship (predicted earlier in Equation 3-15) is confirmed by the linearity of the datasets. A power regression line has been fitted to each group of results and the calculated power is shown, along with the Coefficient of Determination (CD) which is an indicator of the variation of each data set from the regression line. That is, CD is a measure of the fit to a straight line, with one being an exact fit. For example, the predicted response was calculated using the sixth power (Equation 3-15) and its regression result gave a CD of one, to four decimal places (graphed as the black line of dots).

Figure 3-6 illustrates that the response for all loop sizes is close to the predicted inverse-sixth power law, except for the largest loop. Calculated power relationships varied between 5.8 and 6.6 (except for the largest loop, which had a calculated power of 7.0). The amplitude offset (in actual EM38 values) between each loop size is a result of increased magnetic field coupling as the loop size increases. A discussion of the theoretical value of this offset effect is given later in Section 3.5.

A divergence of the EM38 response from the inverse-sixth power law occurs at small separations, and is more evident for larger loop diameters. This is primarily due to a breakdown of the distant-loop approximation. At the other, low amplitude, end of the responses, the variations in ($V_Q$-$V_B$) from linearity in the log-log plots is due to reduced signal-to-noise ratios as the values fall below the instrument's

accuracy (of approximately ±1.5 mS $m^{-1}$); and the limit of the instrument's resolution (0.1 mS $m^{-1}$) is approached (Section 2.10).

The steps in the data sets for loops of diameter 0.489 m, 0.310 m and 0.228 m occur where the EM38's sensitivity range was manually changed from 1000 mS $m^{-1}$ to 100 mS $m^{-1}$. (The smaller loops did not produce a strong enough response to justify a range change.)

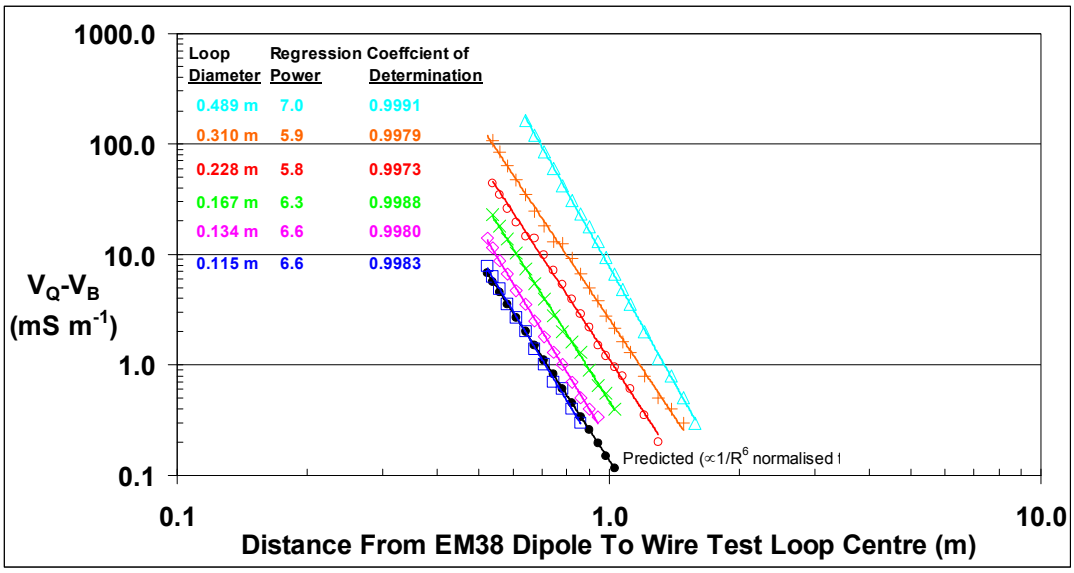


**Figure 3-6. Graph (log-log scale) of the response of the EM38 to coplanar Target Loops versus distance from the EM38's transmit loop (as configured in Figure 3-4). For comparison, the predicted response ($\propto 1/R^6$) is shown in black (normalised to the response from the 0.115 m diameter coil). CD is the coefficient of determination and is a measure of the data fit to the regression line.**

As the separation between the large loops and the EM38 reduces, the distant loop approximation for mutual inductance grows less valid. This can be seen in Figure 3-6 where the largest Target Loop has a power fall-off rate of seven compared to the assumed sixth power. With increasing loop diameter, the sections of the loop closer to the EM38 contribute an appreciably greater amount to the mutual inductance than the distant sections. Thus, the implicit assumption that all regions of the loop contribute equally to the EM38 response, as used in the derivation of Equations 3-13 and 3-14, becomes less valid.

Figure 3-7 is a comparison of the mutual inductance, $M_{01}$, (as estimated using FastHenry) and that using the distant loop approximation (Equation 3-12) against separation for the largest loop (0.489 m diameter). Whereas the distant loop approximation of Equation 3-13 predicts linearity at all separations, the FastHenry

model predictions show a pronounced deviation at both the small and large separation ends of the graph. The deviation at small separation is in keeping with the deviation observed in Figure 3-6 (for comparison to this figure recall from Equation 3-14 that the EM38 response is proportional to $M_{01}^2$). This is because the FastHenry model works on combining the effects of discrete segments of conductors, effectively accommodating the local distance effects described earlier.

However, for separations greater than 1.3 m, the FastHenry calculation overestimates the mutual inductance compared to the distant loop approximation, illustrating a limitation in the software configuration used in the numerical analysis. In fact, using hexagons to estimate the effect of the circular loops was required as the original attempts using 36-sided regular polygons gave only reasonable results for some separations and was numerically unstable for larger distances. Presumably, this was due to the large matrices and small values involved in complicated structures at larger separations (again due to inverse sixth power). This is understandable, considering that FastHenry is a general-purpose inductance and resistance utility, but the main application seem to be at the scale of integrated circuit structures. This example calculation indicates that numerical methods such as FastHenry for complicated and/or distant loop estimations (as required for trellis investigations in 3) have limitations.

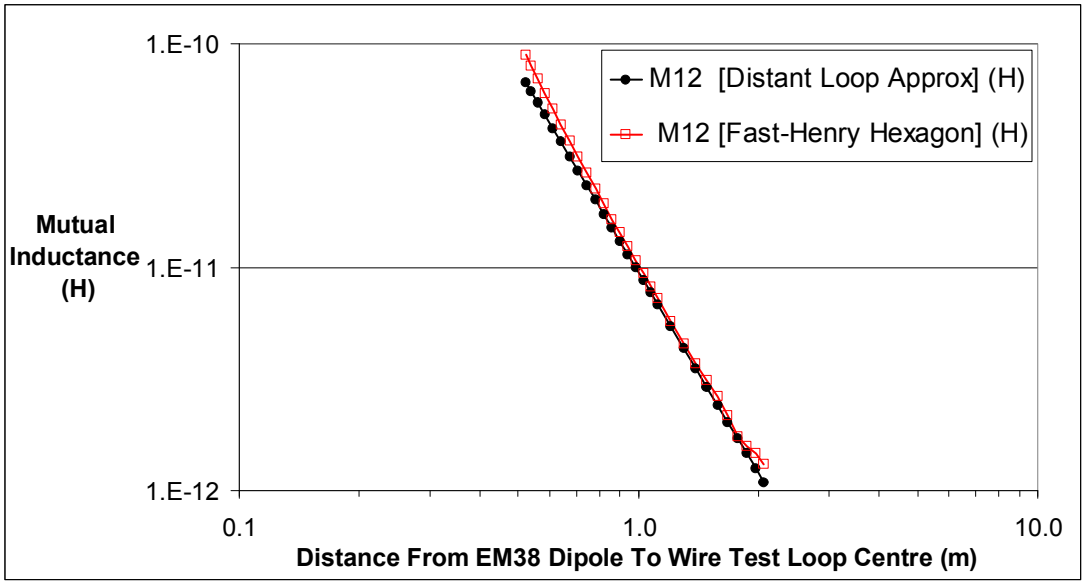


**Figure 3-7. Graph (log-log scale) of the calculated mutual inductance between coplanar loops using the distant-loop approximation (Equation 3-14) and FastHenry calculation methods as a function of distance between the EM38 dipole and a coplanar loop. (Loop diameter = 0.489 m.)**

## 3.5 Relative EM38 Response to Distant Coplanar Loops of Different Size

To predict the effect on the EM38 response due to different loop sizes requires the introduction of additional factors. These factors are electrical resistance and self-inductance, both of which are proportional to the loop size. The interaction of these factors with the mutual induction is treated by returning to the concept of eddy currents (Section 2.6). These currents are driven by the vortex electric field (shown in Figure 3-3 for the coplanar EM38 loop and Target Loop schematic).

Kaufmann and Eaton (2001:105) give the steady-state eddy current induced in a conducting loop due to a sinusoidally varying primary magnetic field (such as produced by an EM38 transmitter) as:

$$I(t) = -\frac{\omega\Phi_0}{R^2 + \omega^2 L^2}\left(R\cos\omega t + \omega L \sin\omega t\right), \qquad \text{Equation 3-17}$$

where $L$ is the self-inductance of the Target Loop, $R$ its real resistance, and $\omega$ the angular frequency of the primary inducing field. This equation can be expressed in phasor notation (i.e. with the sine and cosine components implied) as:

$$I(t) = -\frac{\omega\Phi_0}{R^2 + \omega^2 L^2}\left(R + i\omega L\right). \qquad \text{Equation 3-18}$$

As discussed in Section 2.6, for soil surveying, the EM38 is usually operated in quadrature ($Q$) mode because it is the soil's real electrical resistivity that is the variable of interest. The strong dependence of the EM-response on the conductivity of the soil, and its phase relationship, has already been mentioned in Equation 2-7. By definition, $Q$ mode relates directly to the $\pi/2$ phase-shifted part of Equation 3-17. Consequently, the $Q$ part of Equation 3-17 is:

$$I_Q(t) = -\frac{\omega\Phi_0 R}{R^2 + \omega^2 L^2}\cos\omega t\,, \qquad \text{Equation 3-19}$$

where $I_Q(t)$ refers to the quadrature component of the eddy current in the loop. Again, in phasor notation, this equation becomes:

$$I_Q(t) = -\frac{\omega\Phi_0 R}{R^2 + \omega^2 L^2}\,. \qquad \text{Equation 3-20}$$

Fortunately, the phase separation means that the quadrature component relates only to the soil's conductivity, because in soil R>>ωL.

Equation 3-20 can be evaluated for various loop sizes because the angular frequency, $\omega$, is known, while the real resistance, $R$ and the self-inductance, $L$, can be calculated for a simple loop energized by the EM38. The formula for $L$ of a thin circular loop was given in Equation 2-14.

The resistance of the Target Loops used in this work can be estimated using tabulated values of resistivity for copper ($\rho_{Cu}$ = 16.8 x $10^{-9}$ Ω.m; Howatson, Lund & Todd 1972) and the definition for resistivity:

$$\rho = \frac{RA}{l}, \qquad \text{Equation 3-21}$$

which, for a circular loop of copper wire with a circular-cross section, is given by:

$$R_{Cu} = \frac{16.8 \times 10^{-9} 2\pi r}{\pi r_x^2}. \qquad \text{Equation 3-22}$$

As an exercise in relating a material's resistivity to its resistance, Equation 3-22 was validated for a piece of copper wire by measuring the wire's diameter and its length, and then comparing its calculated resistance value to its measured resistance. Table 3-1 shows that the theoretical resistance of a copper wire with a wire length of 3.54 m and radius of 0.535 mm, differs from the actual measured resistance (conducted using a Hewlett Packard HP34401A, made in the U.S.A., multimeter in 4-port mode) by just 5.5 %. This minor difference may be due to variations from the published typical resistivity to that of the actual wire's material, the temperature-dependence of resistivity, the accuracy of the wire's measured radius and/or the accuracy limit of the resistivity instrument itself. The difference between the measured and calculated values and their estimated variability and accuracies are summarized in Table 3-1.

**Table 3-1. Comparison of Measured and Calculated Resistance of 3.54 m of Copper Wire.**

| Wire's Measured Cross-sectional Radius (mm) | Std. Dev. Wire's Cross-sectional Radius$^2$ ($mm^2$) | Measured Resistance ($R_{Meas.}$) (mΩ) | Std. Dev. ($R_{Meas.}$) (mΩ) | HP 4-Port Resistivity Meter Accuracy (mΩ) | Calculated Resistance ($R_{Calc.}$) (mΩ) | Difference ($R_{Calc.} - R_{Meas.}$) (mΩ) |
|---|---|---|---|---|---|---|
| 0.536 | 0.018 (1.5 %) | 63.4 | 1.5 (2.4 %) | 4.0 (6.6 %) | 67.1 | 3.7 (-5.5 %) |

Therefore, the predicted relative EM38 response to changing loop size is obtained by combining the proportional equation relating the product of $M^2$ and the quadrature vortex current (Equation 3-16) with Equation 3-20 for $I_Q$, in terms of the self-induction and resistance of the Target Loop:

$$V_Q \propto M_{01}^2 \times I_Q(t) = M_{01}^2 \times \frac{\omega \Phi_0 R}{R^2 + \omega^2 L^2}. \qquad \text{Equation 3-23}$$

### 3.5.1 Materials and Methods: Relative EM38 Response to Distant Coplanar Loops of Different Size

The data for this comparison between predicted and measured EM38 responses with loop size merely required the extraction of a data subset from the previous experiment (Section 3.4 on relative fall-off rate with distance for various loop sizes). That is, a subset of the response data (for each of the six different sized loops) was extracted for just a single separation distance (0.64 m).

### 3.5.2 Results and Discussion: Relative EM38 Response to Distant Coplanar Loops of Different Size

The EM38 response to varying loop diameters is given in Figure 3-8. For comparison, the predicted response (based on Equation 3-23 using the distant loop approximation) is shown, normalized to the measured response for a loop diameter of 0.228 m. The comparison between the normalized predicted response and the measured response for varying loop size (Figure 3-8) indicates that incorporation of the quadrature eddy current calculation (Equation 3-20) into the overall EM-response (Equation 3-16) provides good predictability of the relative responses. The measured response matches the normalized predicted response, except for the small discrepancies for the largest and smallest loop diameters. The

variation at the smallest diameter is explained by a combination of small amplitude (being comparable to the instrument's accuracy limit) and increasing relative errors in physical positioning and orientation of the EM38 relative to the coils. The variations at the largest diameter are due to the breakdown of the distant loop assumption used to determine the mutual inductance as discussed earlier (Sub-section 3.4.2).

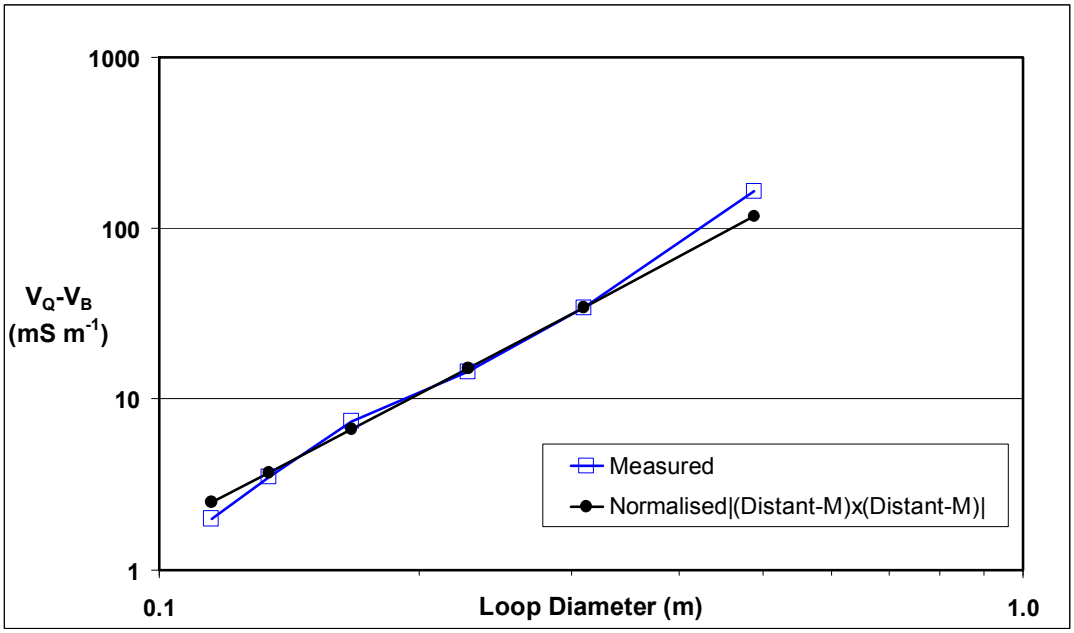


**Figure 3-8. Graph (log-log scale) of the response of the EM38 to different sized Target Loops at a fixed distance of 0.640 m from the EM38's transmit loop (0.4 m from the EM38's midpoint as shown in Figure 3-4). For comparison, the predicted response ($M_{01}^2$) using the distant-loop estimate for mutual inductance, is shown normalized to the amplitude from the measured loop diameter of 0.310 m.**

The FastHenry hexagon estimate for mutual inductance (described earlier in Sub-section 3.4.2) improves the predicted response from that shown in Figure 3-8 to that shown in Figure 3-9. That is, the use of FastHenry to estimate the mutual induction overcomes the shortcomings of the distant-loop estimate method, when the loop is, in fact, not distant.

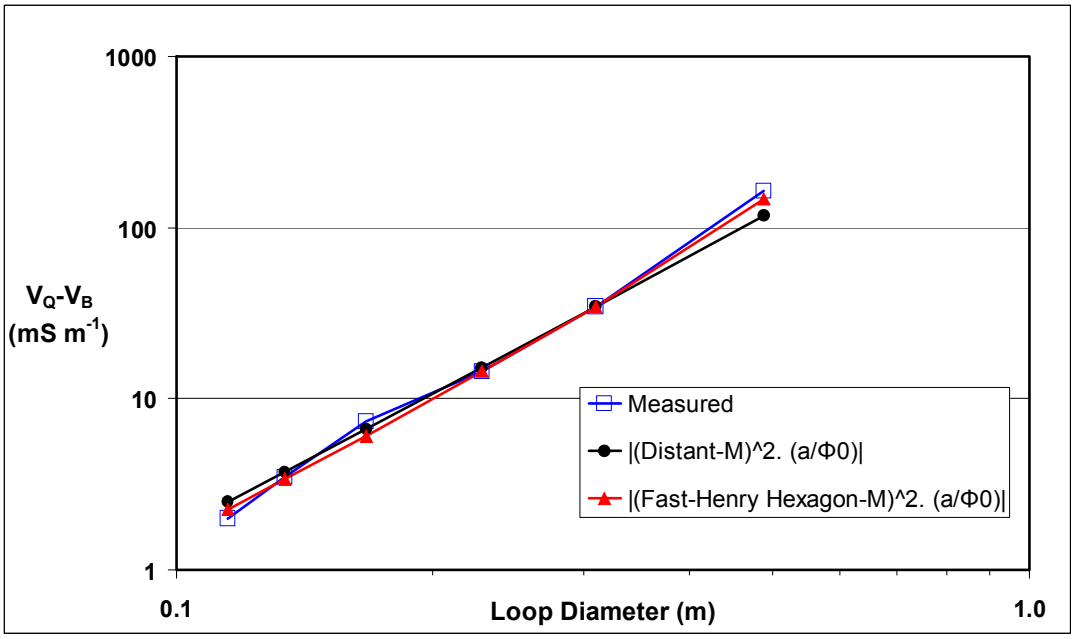


**Figure 3-9. Graph (log-log) showing the improvement in predicted response for the larger loops (compared to the response shown in Figure 3-8) when the more accurate FastHenry estimates of mutual inductance are used.**

## 3.6 Absolute EM38 Response to Distant Horizontal, Coplanar Loops

To predict the actual quadrature amplitude response of the EM38 to conducting loops, rather than just the relative response demonstrated in the previous two experiments (Sections 3.4 and 3.5), requires a formula that predicts $H_s/H_0$, the ratio of the secondary magnetic field at the receiver coil to the primary magnetic field generated by the transmitter coil. Conversion of $H_s/H_0$ to $V_Q$ requires multiplication by the constant of proportionality given earlier in Equation 2-7.

Developing an equation for $H_s/H_0$ requires an expression for the secondary magnetic field, $H_s$, at the receiver coil, which then needs to be expressed as a function of the primary magnetic field, $H_0$, via coupling with the Target Loop.

Starting with the magnetic field at the receiver loop ($H_s$, radius $r_2$), and assuming it is always relatively small, then changing the subscripts to reflect the loop designations and combining Equation 3-9 and Equation 3-10, gives:

$$H_s = \frac{\Phi_{12}}{\mu_0 \pi r_2^2}, \qquad \text{Equation 3-24}$$

where $\Phi_{12}$ is the flux cutting the receiver loop (Loop 2) originating from the Target Loop (Loop 1). This flux is a simple function of both the mutual inductance from, and the current in, Loop 1. So by substituting a simple rearrangement of the definition of mutual inductance (Equation 3-6):

$$\Phi_{12} = M_{12} I_1 , \qquad \text{Equation 3-25}$$

into Equation 3-24 gives:

$$H_s = \frac{M_{12} I_1}{\mu_0 \pi r_2^2} \qquad \text{Equation 3-26}$$

Equation 3-20 then links the quadrature current in the Target Loop, $I_1$, to the flux from the primary source, $\Phi_{01}$, when the resistance and inductance of Loop 1 are known. Again, using the definition of mutual inductance and then substituting Equation 3-20 into Equation 3-26, gives:

$$H_s = \frac{M_{12}}{\mu_0 \pi r_2^2} \frac{\omega R}{(R^2 + \omega^2 L^2)} M_{01} I_0 . \qquad \text{Equation 3-27}$$

Now, dividing Equation 3-27 by the primary magnetic field, $H_0$, at the centre of a circular loop of radius, $r_0$

$$H_0 = \frac{I_0}{2 r_0} , \qquad \text{Equation 3-28}$$

gives the required ratio:

$$\left( \frac{H_s}{H_0} \right) = \frac{M_{12}}{\mu_0 \pi r_2^2} \frac{\omega R}{(R^2 + \omega^2 L^2)} M_{01} 2 r_0 . \qquad \text{Equation 3-29}$$

Equation 3-29 indicates that the EM38 response is a function of the effective transmitter and receiver coil radii. This can, nonetheless, be confirmed as a reasonable outcome because the equation is unit-less, as expected.

Finally, the constant of proportionality (from Equation 2-7, with s=1 m for the EM38) and the $10^3$ factor (because the EM38 output is in milli-Siemens $m^{-1}$) can now be included to predict the quadrature response, $V_Q$:

$$V_Q = \frac{10^3 \times 4}{\omega \mu_0} \left( \frac{H_s}{H_0} \right) = \frac{10^3 4}{\omega \mu_0} \frac{M_{12}}{\mu_0 \pi r_2^2} \frac{\omega R}{(R^2 + \omega^2 L^2)} M_{01} 2 r_0 , \qquad \text{Equation 3-30}$$

which condenses to:

$$V_Q = \frac{8\times10^3}{\mu_0^2}\frac{M_{01}M_{12}r_0}{\pi r_2^2}\frac{R}{(R^2+\omega^2L^2)}$$

Equation 3-31

However, the actual values for $r_0$ and $r_2$ in the EM38 unit are, again, not available as they are considered proprietary information by the manufacturer. Consequently, arbitrary values $r_0=r_2=0.0127\ m$ (based on a 1 inch diameter as described in Sub-section 3.4.1) were used. In addition, the EM38 requires a strong transmit signal, given the typical, relatively weak signals emanating from eddy currents. To achieve adequate signal amplitudes at low power (the EM38 can be operated using a standard 9 V transistor battery for up to 12 hours) it must also be assumed that both the transmit, and receive loops are solenoids. It is generally assumed that the solenoids can be approximated as point dipole sources and geometrical solenoid effects ignored; thus both mutual inductances are simply multiplied by an effective number of turns, *N,* which combines the aforementioned unknown parameters (i.e. Tx and Rx coil size/shape and number of turns) into a single factor, $N^2$. Assuming that the transmitter and receiver coils have the same number of turns, Equation 3-31 becomes:

$$V_Q = \frac{10^3 8}{\pi\mu_0^2 r_0}\frac{R}{(R^2+\omega^2L^2)}N^2M_{12}M_{01}$$

Equation 3-32

Solving for $N$ and then using the measured values of $V_Q$ from the previous experiment (Section 3.4) gives the empirical value for $N$ listed in Table 3-2 for various loop sizes and separations. The average value of 894 was obtained with a standard deviation of 6.4 % using 53 samples (using only $V_Q$ values greater than 1 mS $m^{-1}$). This value for *N,* combined with the associated assumed $r_0$ value and the calculated mutual inductance from the transmit and receive coils to the trellis, should allow the calculation of the absolute EM38 response to the loops that constitute vine trellis structures. This could form the basis for calculating a component of a trellis correction.

**Table 3-2. Empirically determined values for the effective number of turns, *N*, of the EM38 transmit and receive coils. Various measured values of $V_Q$ were combined with Equation 3-32 to calculate the values of *N*. The cells without values had a measured EM38 response value of less than 1 mS $m^{-1}$, considered below the accuracy limit of the instrument, and were therefore not used.**

| Loop Sep. (m) | 0.640 | 0.670 | 0.710 | 0.740 | 0.770 | 0.820 | 0.860 | 0.900 | 0.940 | 0.980 | 1.03 | 1.07 | 1.18 | 1.21 | 1.30 |
|---|---|---|---|---|---|---|---|---|---|---|---|---|---|---|---|
| **Loop Dia. (m)** | | | | | | | | | | | | | | | |
| **0.115** | 805 | 793 | 778 | | | | | | | | | | | | |
| **0.134** | 865 | 867 | 854 | 843 | | | | | | | | | | | |
| **0.167** | 948 | 953 | 941 | 926 | 1075 | 940 | 978 | | | | | | | | |
| **0.228** | 855 | 980 | 958 | 920 | 916 | 901 | 918 | 958 | 905 | 902 | | | | | |
| **0.310** | 853 | 840 | 837 | 833 | 955 | 955 | 938 | 926 | 934 | 881 | 881 | 927 | 944 | | |
| **0.489** | 902 | 912 | 900 | 893 | 883 | 879 | 899 | 908 | 892 | 873 | 842 | 870 | 839 | 801 | 756 |

## 3.7 Conclusion

In light of the above discussion, the key findings of this chapter were:

1. An analytical expression based on the distant loop approximation (i.e. assuming a uniform inducing field and coplanar orientations) for mutual inductance gives reasonable predictions of the EM38 response for both practical EM38-loop distances and loops of varying sizes;
2. FastHenry, accounts for the actual inducing field, individual loop segments, their distances and their geometry from the EM38. Therefore it does a better job of estimating the mutual inductance, critical to predicting the EM38 response, than the distant-loop estimate of mutual inductance, especially involving larger loops at smaller distances. As a result, in this research, FastHenry will be used as the prediction tool in realistic dimensioned vine trellis loops; and
3. Using first-principle understanding of how the EM38 works and interacts with loops, instrument parameters have been inferred (e.g. *N*) which were otherwise unavailable, due to proprietary constraints. These parameters

will be necessary when applying FastHenry to predict absolute interference responses and compare them to observed responses from realistic vine trellis components.

Having now discussed the EM38 response to simple conducting loops and developed a method for the absolute prediction of the interference on the EM38 from said loops, the next chapter expands the absolute prediction method to cover more complex, realistic trellis shaped loops.

# Chapter 4 EM38 Response to Components of an All-Steel Vine Trellis

## 4.1 Introduction

In this chapter, actual trellis geometries are introduced and their interference effect is isolated into key components, and each investigated separately. The prediction strategies (developed in Chapter 2) are extended to predict the two significant trellis interference factors: the all-steel loops and the steel-earth loops. Within the context of an EM38 survey, these predictions are then experimentally tested.

The EM38 response from an all-steel, vine trellis system will be a combination of the following four factors:

1. The steel posts;
2. The steel wire;
3. The various conductive loops created by the wires and the posts; and
4. The loops made from the wires, the posts and the ground paths.

The potential complexity of these numerous, interacting loops is indicated schematically in Figure 4-1. In order to reveal the relative contributions of each of these factors, each will be investigated separately, and then in combination.

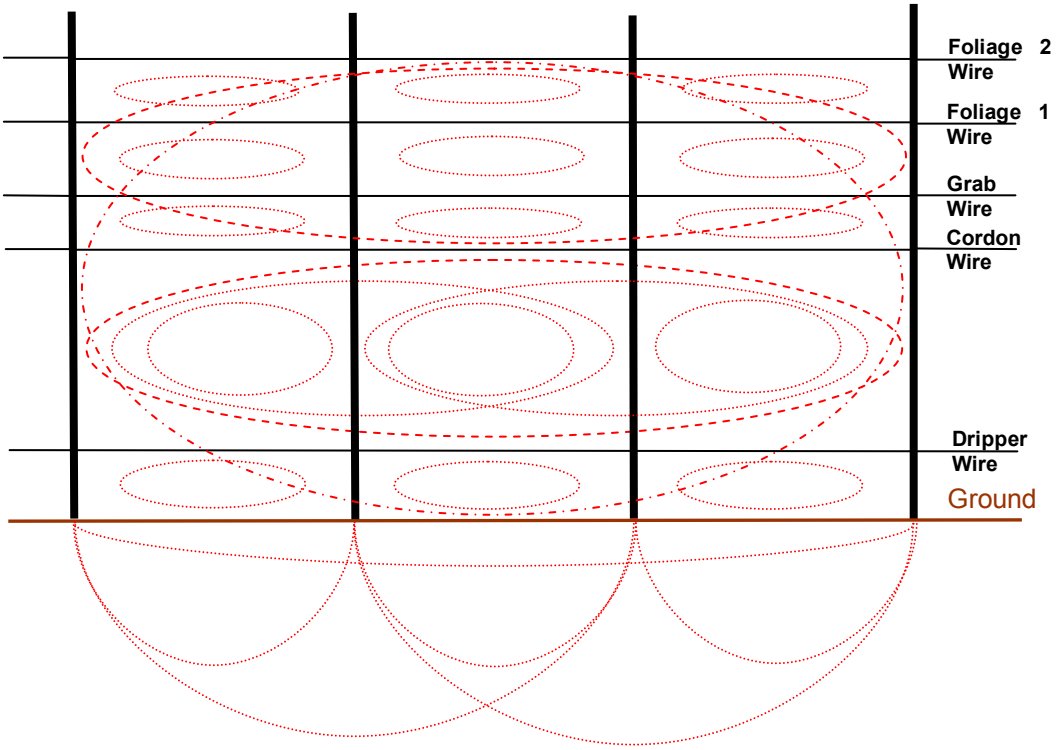


**Figure 4-1. Schematic diagram of a segment of an all-steel trellis illustrating the complexity of the eddy current networks. The dotted and dashed red lines indicate some of the possible eddy current loops.**

Based on the simple flux rule given earlier in Equation 3-3, the first two factors should contribute negligible influence due to their small available coupling area, (i.e. the cross-sectional area of the wire and posts themselves) relative to their separations from the EM38. In contrast, the last two factors (which form substantial conducting loops) should have a significant effect due to their relatively large coupling area.

In relation to factor three, the effect of the numerous, large conducting loops made up from the wires and the posts, the investigations will be restricted to just single trellis panels comprising two posts and associated wires. To restrict the complexity further, single, rectangular loops of just pairs of adjacent horizontal wires and vertical Gripfast post segments will initially be used. The insights from these simple, four-segmented, rectangular loops will then form the basis of further analyses. Extending these analyses to include the addition of more wires and then more panels will lead to a closer representation of a real-world trellis.

The fourth and final factor will likely be the most complicated and difficult to parameterise. To investigate this factor, the ground effect (i.e. including the ground

paths) will first be measured from a simple loop configuration comprising just a single wire, two posts, and the earth. Introducing the earth will significantly increase the complexity of the system, as it is difficult to control and/or measure the specific electrical characteristics of the soil volume interacting with the system as well as the post-earth contact resistance. Finally, the effect of multiple, connected panels will be expected to modify the overall response. This is due to the addition of parallel ground paths, that reduce parts of the network resistance.

## 4.2 EM38 Response from Gripfast Steel Posts

As discussed earlier in Section 1.4, galvanised steel Gripfast trellis posts are commonly used in commercial trellis systems, especially in recently established vineyards. Figure 4-2 contains photographs of the Gripfast post in side-, and end-view, showing the post's six-lobed cross-section.

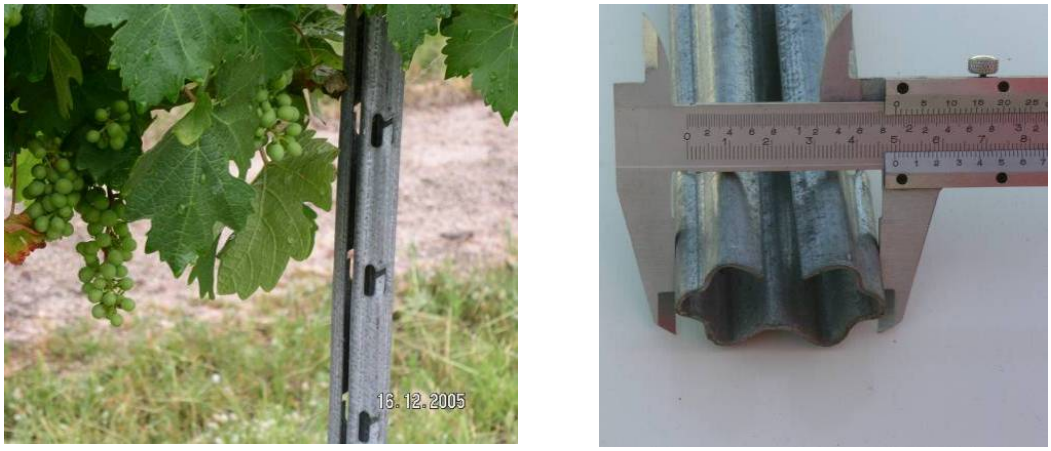


**a)** **b)**

**Figure 4-2. Photograph of the galvanised steel Gripfast post. a) Side view showing the angled slots for supporting the trellis wire; and b) The six-crescented cross-sectional profile and its width dimension of 50 mm (depth is 30 mm and it is made from 1.4 mm thick, galvanised, steel).**

Within the work of Lamb, Mitchell and Hyde (2005), the on-ground, EM38 response as a function of perpendicular distance away from individual Gripfast steel posts was recorded. In these measurements, the EM38 was moved along the ground, and aligned such that the post bisected the EM38 unit. Figure 4-3 is a graph of a subset of the data from the Gripfast post test performed by Lamb, Mitchell and Hyde (2005).

In this particular experiment, there was an array of posts spaced on a 6 m by 3 m grid. The EM38 responses to six of these posts have been replotted here as Figure 4-4. While these results show variable responses within 1 m of those posts (most likely due to variations in the post-earth interaction) it nonetheless confirms that the influence of the post is negligible (i.e. ≤ to the instrument's accuracy of 1.5 mS $m^{-1}$) at separations of greater than 1.25 m.

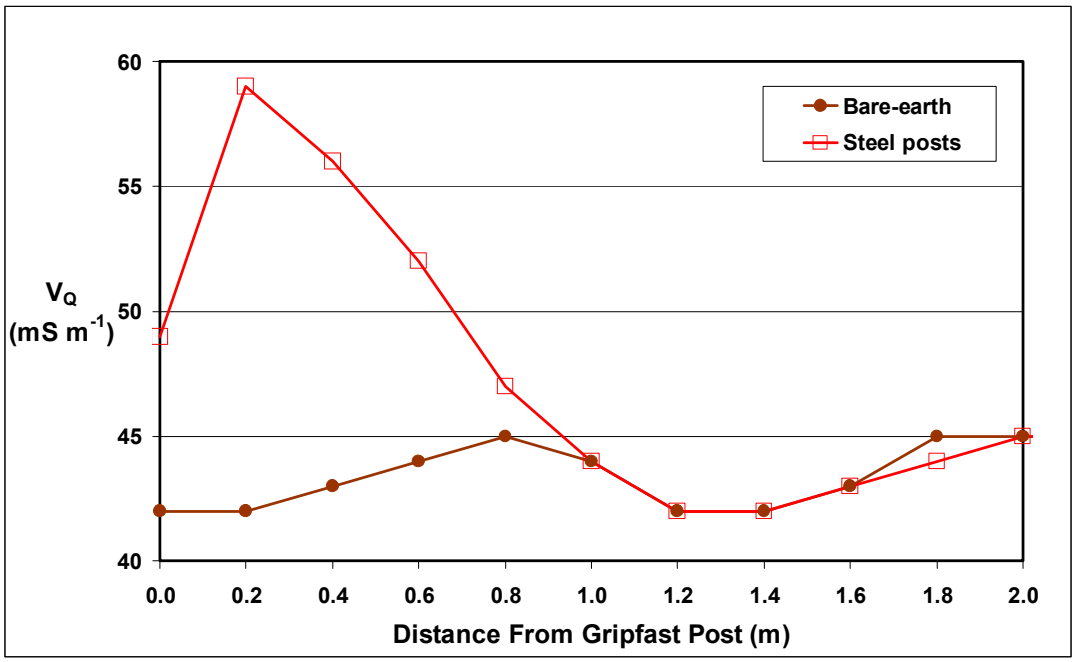


**Figure 4-3. EM38 (vertical dipole) response ($V_Q$) as a function of distance from an isolated, vertical Gripfast steel post (which had just been driven into the ground). The zero distance position occurs when the side of the EM38 is touching the post. The response units are to the nearest integer. The response from the bare-earth (i.e. without the post) is shown for comparison. (Data extracted from Lamb, Mitchell & Hyde 2005: Figure 7).**

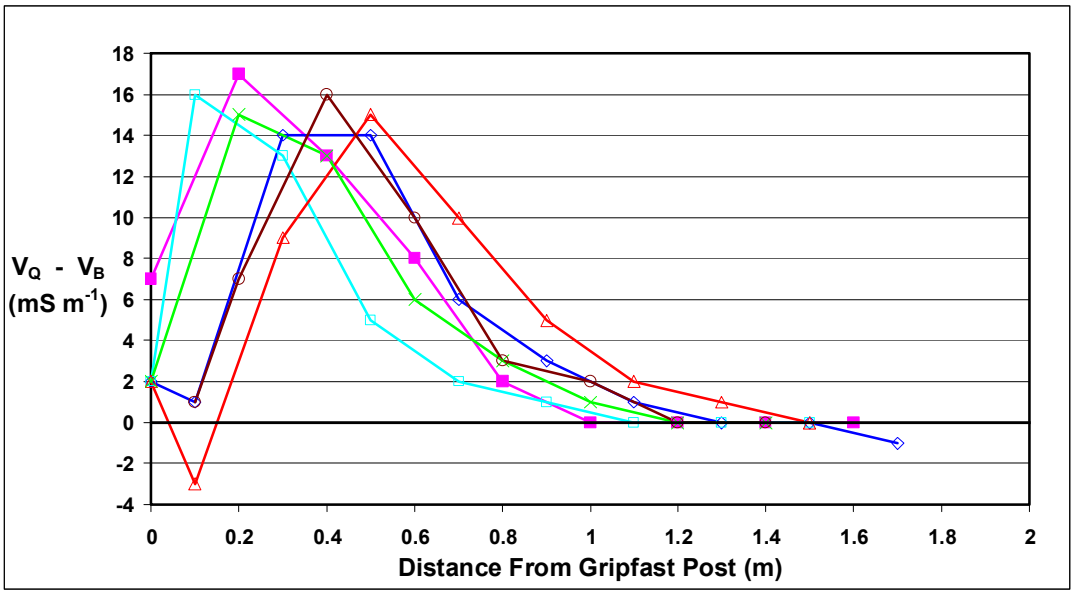


**Figure 4-4. EM38 (vertical dipole) response ($V_Q - V_B$) as a function of distance from six isolated, vertical Gripfast steel posts. The zero distance position occurs when the side of the EM38 instrument is touching the post. The data set of Lamb, Mitchell and Hyde (2005) has been modified by subtracting the bare-earth response ($V_B$). The response units are to the nearest integer.**

### *4.2.1 Materials and Methods: EM38 Response to Gripfast Posts*

To confirm the negligible effect of individual posts on the EM38 response indicated in previous work, Lamb, Mitchell and Hyde's (2005) simple experiment was repeated. The EM38 signal was measured while increasing the separations from the posts out to a distance of 2.0 m. The experiment was extended to include a pair of posts, each 1.5 m offset laterally from the centre of the EM38 (i.e. 3 m apart), as shown schematically in Figure 4-5b. However, unlike the previous work of Lamb, Mitchell and Hyde (2005), the actual posts were moved relative to the EM38, in order to eliminate change from the spatially variable ground-effects beneath the EM38 sensor. To remove the constant bare-earth effect, the EM38 measurements were repeated at the same position on the ground both with and without the post(s) in place. Holes for the posts were prepared by driving a post into the ground at pre-marked locations and then removing it, every 0.25 m along a line away from the EM38 (shown schematically in Figure 4-5).

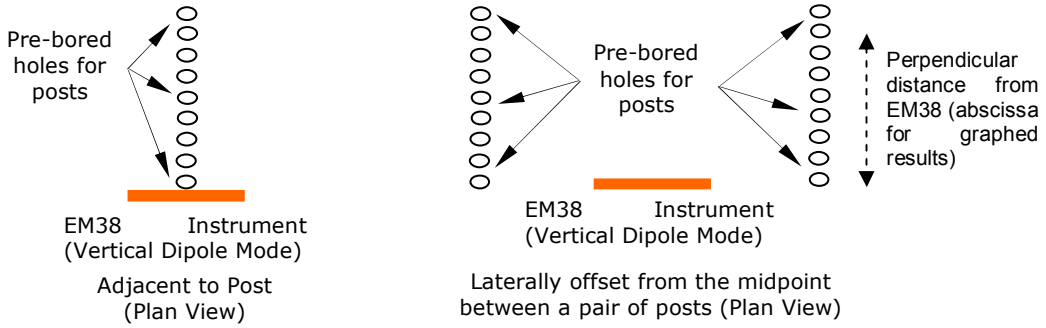


**a)** **b)**

**Figure 4-5. Schematic plan view of the experimental configuration for investigating the effect of the Gripfast posts with the EM38 instrument kept stationary and then the post(s) moved along a straight line (in 0.25 m increments). a) Adjacent to a single post; and b) Laterally offset from the mid-point between a pair of posts (3 m apart).**

### *4.2.2 Results and Discussion: EM38 Response to Gripfast Posts*

The on-ground EM38 response as a function of distance from a single post and a pair of posts (configured as in Figure 4-5) is graphed in Figure 4-6. The only significant EM38 response from a single, isolated post occurs when it is closer than 1.25 m. The EM38 response at just 0.5 m from the post (shown in Figure 4-5 and Figure 4-6) varies between 5 and 15 mS $m^{-1}$. This response is a function of the EM38-to-post mutual inductance, the post's conductivity, and its interaction with the ground. However, the dominant variable of this response is clearly the separation between the post and the EM38.

Irrespective of the absolute differences in EM38 response to both single and paired Gripfast posts, the experimental results confirm that the contribution of the posts to the EM38 response is less than 3.5 mS $m^{-1}$ at distances greater than 1.0 m, consistent with the earlier results of Lamb, Mitchell and Hyde (2005). This distance is less than what would be considered a normal EM38 to trellis distance encountered in commercial surveys. This is because most trellis rows (in Australia) are separated by at least 2.5 m and a typical EM38 survey involves moving the sensor down the centre of the inter-row spacing with only small off-centre deviations (Lamb, Mitchell & Hyde, 2005). Thus, it is unlikely that the EM38

response in a commercial survey would be significantly affected by the interference from the individual posts themselves.

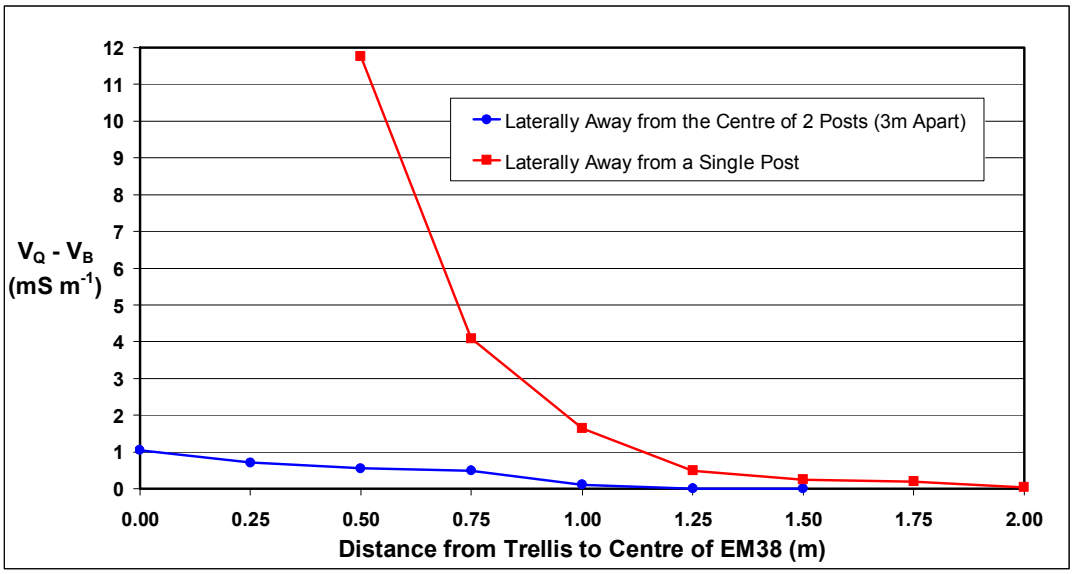


**Figure 4-6. EM38 (vertical dipole) response as a function of distance from vertical Gripfast steel post(s) for single and paired posts. The response from the bare-earth was measured after each post measurement and then subtracted.**

As was the case with Lamb, Mitchell & Hyde (2005), one aspect of the present research that has yet to be clarified is that of the impact of the electrical connection formed between the steel post and soil on the EM38 response to individual posts.

### *4.2.3 Materials and Methods: Impact of Gripfast Post-Earth Interaction on EM38 Response*

To investigate the interaction between individual Gripfast posts and the earth, an experiment was set up on a location of moderately conductive soil ($EC_a \approx 40$ to 46 mS $m^{-1}$). The background EM38 responses versus distance along two separate test lines (start locations were marked for latter post insertions and were nominated as the zero position) were measured to a separation of 1.0 m, at intervals of 0.1 m. The values were corrected for instrument drift by measuring the change in response at a nearby marked reference point before and after each line of measurements. The drift was then interpolated and used to correct the actual measurements by subtraction. Posts 1 and 2 were then inserted into the ground (penetrating to a depth of 0.7 m) at the zero location of each test line and the EM38 line of measurements retaken. This configuration was similar to that shown schematically in Figure 4-7. The posts were then watered-in: Post 1 with 2.5 litres

of fresh water; and Post 2 with 2.5 litres of water containing 0.25 kg of dissolved salt (i.e. a solution of 10 % NaCl), and the EM38 response profiles retaken. These profiles were collected immediately after watering in, minimising the chance that the introduced water would change the bulk soil $EC_a$ characteristics within the sensing volume of the EM38.

Secondly, the EM38 response to the post-in-air was compared to the response when the post was inserted into the ground. The EM38 was placed on the ground adjacent to a Gripfast post (midway between the transmit and receive coils) with the post inserted into the ground at increasing depths (0.0 m to 0.7 m in 0.05 or 0.1 m increments). The measurements were then repeated with the post suspended entirely above the ground (i.e. post galvanicaly disconnected from the ground). For the suspended post measurements, the EM38 was maintained in a fixed position approximately 1 m above the ground and the horizontal post progressively moved axially along the instrument, recreating the same post-EM38 orientation as for the on-ground measurements.

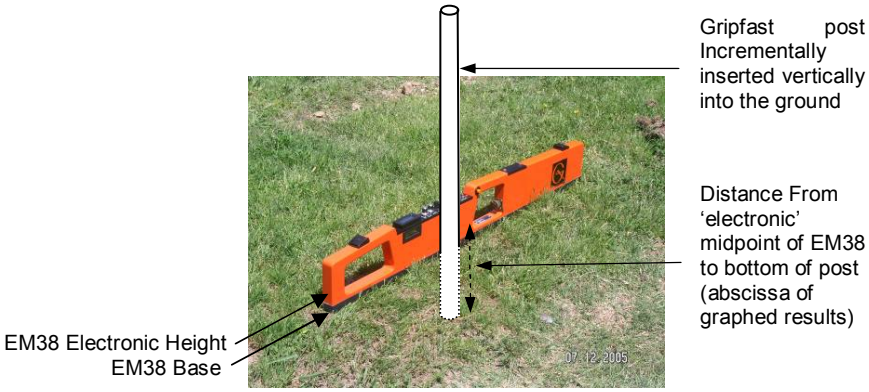


**Figure 4-7. EM38 schematic configuration for measuring the vertical dipole response from a Gripfast post as it was incrementally inserted into the ground.**

### *4.2.4 Results and Discussion: Impact of Gripfast Post-Earth Interaction on EM38 Response*

The EM38 response from the bare-earth as a function of distance from the locations marked for post insertion (i.e. but with the posts not yet in place) is given in Figure 4-8.

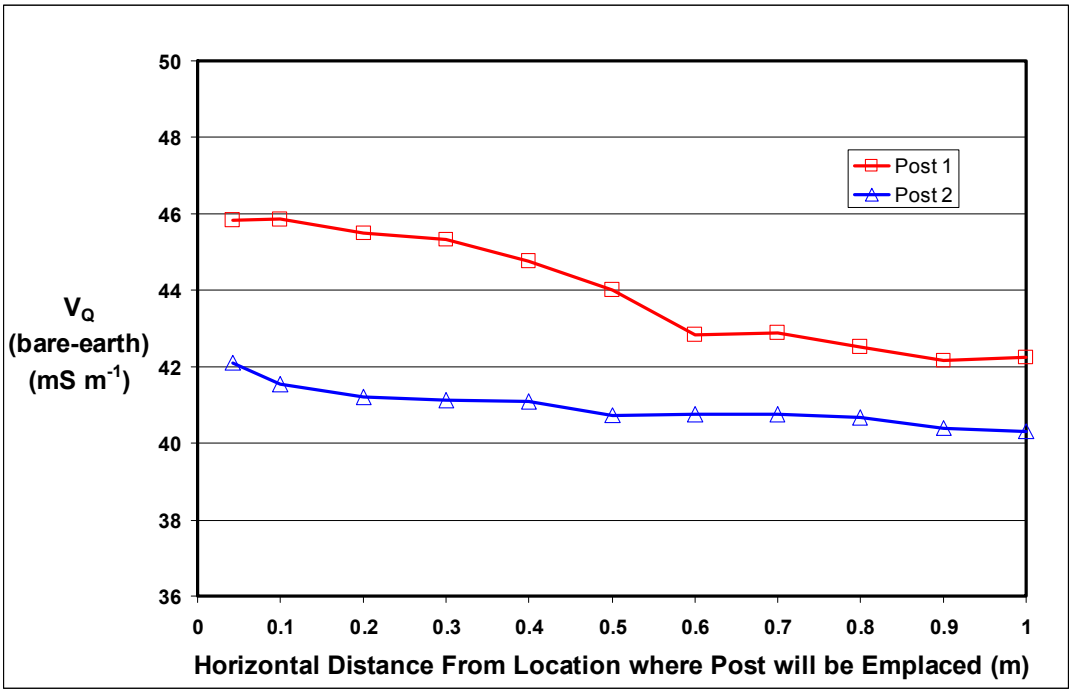


**Figure 4-8. EM38 (vertical dipole) bare-earth responses as a function of distance from post insertion points (i.e. posts not inserted for this background measurement). (Instrument drift corrected using a measured reference values at a nearby test point.)**

Figure 4-9 shows the EM38 response as a function of distance from the post locations with the posts in place. Instrument drift (which was observed to be ≤1 mS $m^{-1}$) was corrected using measurements from a nearby reference point and the bare-earth values were then subtracted. The with and without post responses were indistinguishable when the separations were more than 0.5 m. Nearer the posts, the responses differed by no more than 2 mS $m^{-1}$. Interestingly, closer than 0.2 m to the posts, the responses reduced as the separation decreased.

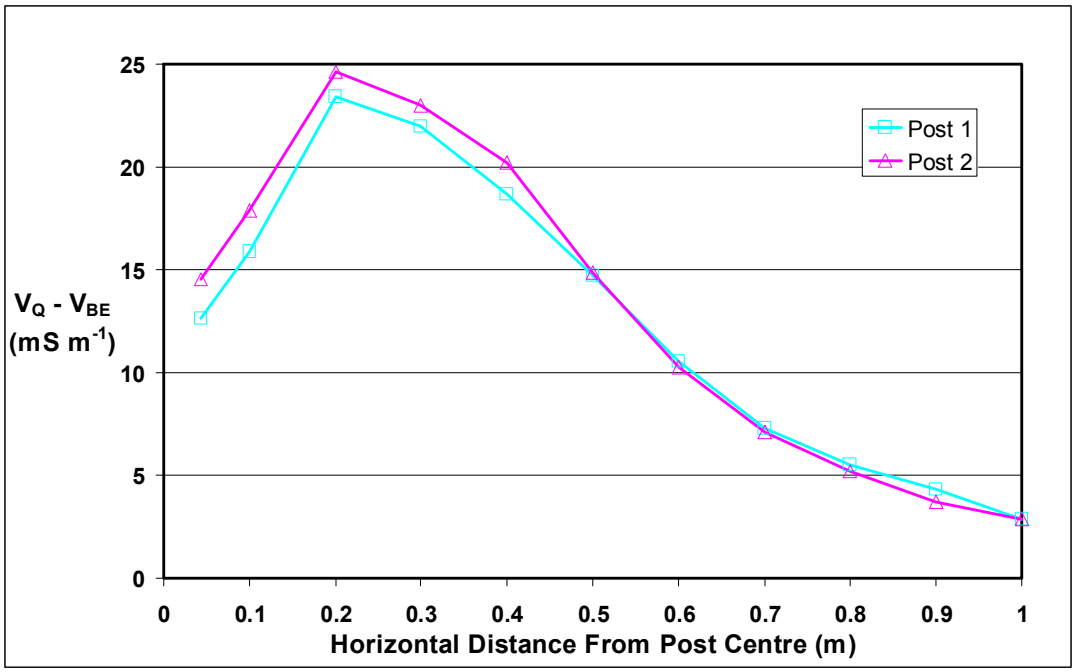


**Figure 4-9. EM38 (vertical dipole) responses as a function of distance from two isolated, vertical Gripfast posts. (Instrument drift was corrected using a measured reference values at a nearby test point and then the bare-earth values, $V_{BE}$, were subtracted.)**

The EM38 response as a function of distance from the post locations (again corrected for instrument drift and bare-earth values) is shown in Figure 4-10, with the before watering-in measurements included for comparison with the after watered-in measurements. Watering-in the posts did not influence the EM38 response beyond 0.6 m away from the posts. Interestingly, this comparison shows that watering-in the posts decreased the EM38 response at distances less than 0.6 m. Furthermore, the introduction of the saline water into post–earth interface further reduced the EM38 response (≈5 mS $m^{-1}$ for salt-water compared to ≈1 mS $m^{-1}$ for fresh-water). The net result of Figure 4-10 is that increasing the post-earth galvanic coupling decreases the EM38 response to the post.

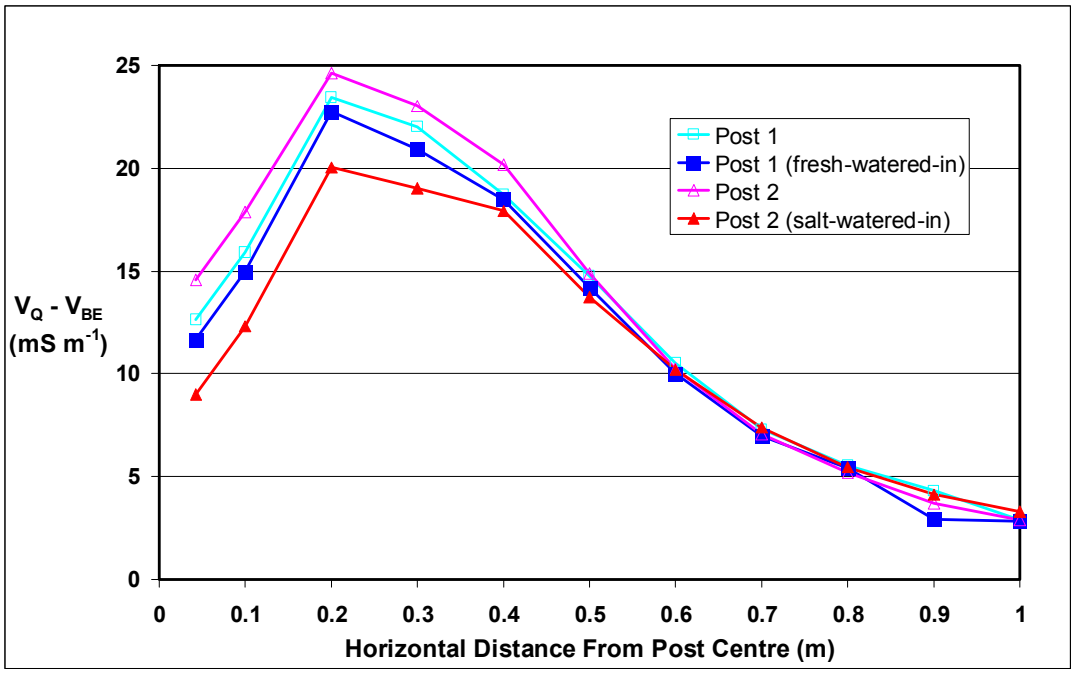


**Figure 4-10. EM38 (vertical dipole) responses whilst moving away from two isolated, grounded, vertical Gripfast posts, before and after watering-in. Post 1 had 2.5 litres of fresh water and Post 2 had 2.5 litres of 10 % NaCl solution poured down the inside of the posts. The after measurements were taken immediately following the watering-in.**

Figure 4-11 depicts the EM38 response when placed adjacent to the post for increasing distance of the EM38's midpoint from the end of the post. (The electronic midpoint of the EM38 is midway between the transmit and receive coils and 58 mm above its base and is referred to here as the EM38's midpoint). The response with the post in air (blue curve) can then be compared with when the EM38 is placed on the ground while incrementally inserting the post into the soil (red curve). The abscissa of Figure 4-11 is the position of the EM38's midpoint along the post, relative to post's bottom end. The EM38 response for the post in air for positions 0 to 0.1 m (blue curve) mimics that when the EM38 is placed on the ground and the post inserted into the soil up to 0.1 m (red curve). This indicates there is little post-ground galvanic coupling (relevant to the EM38's response) up to 0.1 m insertion depth into the soil. However, for progressively larger insertion depths the EM38 response is significantly lower than the equivalent measurements in air. This again demonstrates that increasing the post-ground coupling reduces the EM38 response to the presence of the post.

Both increasing the depth of the post in the soil, or adding water/saline to the post-soil interface, will improve the galvanic coupling between the post and the

soil. Increasing the post depth increases the contact surface area (with the soil) and decreases resistance, while wetting the soil also decreases resistance between the post and the soil (and decreases the resistivity of the soil in the critical few centimetres adjacent to the post). However, it would be expected that simply reducing post-soil contact resistance would increase the current flow between the post and soil, ostensibly increasing the conductivity and hence the EM38 response. However, the opposite was observed. This observation is consistent with the phenomenon (to be discussed in Sub-section 4.5.2) where a very low resistance encountered by the eddy current (i.e. by the dominating presence of a conductor) actually reduces the quadrature response (Equation 4-2).

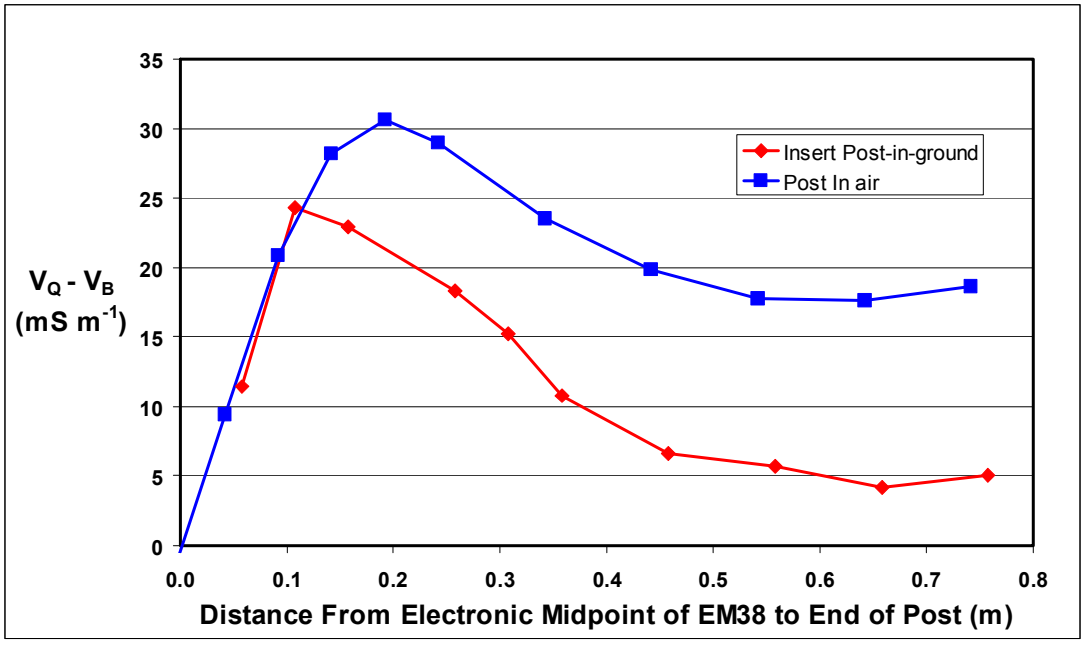


**Figure 4-11. EM38 (vertical dipole) responses when placed adjacent to a post (Figure 4-7) as a function of distance of EM38 midpoint from the end of the post. The curves are for a post progressively inserted into the ground (red) and when the post is suspended entirely in the air (blue).**

## *4.3 EM38 Response to a Single Steel Trellis Wire*

Trellis wire will play a significant role in any EM38 response to vine trellising by potentially forming large, current loops when in electrical contact with vertical steel posts in the trellis assembly. However, it is also necessary to investigate the influence of the wire itself (i.e. independent of forming large conducting loops) on the EM38 response. Commercially available vine trellis wire comes in several diameters. While a 1.5 mm wire is sufficient for the dripper wire to support small

plastic irrigation pipes, a 2.5 mm wire is usually sufficient to support foliage and fruit. Occasionally, for high wind loads or for heavy foliage and fruit, a 3 mm wire is used. For the purposes of this research, however, a representative 2.5 mm diameter wire is used. The resistivity (using Equation 3-21) of 2.5 mm diameter steel wire can be readily made from a measurement of the series resistance of a pair of foliage wires, their total length, and cross-sectional area. Via this method, the resistivity value of $1.54\times10^{-7}$ Ωm found for the wire in this present research is consistent with the quoted value for high carbon AISI 1000 series steel (used for high tensile strength fencing/trellising wire) of $\rho$=$1.42\times10^{-7}$ to $1.80\times10^{-7}$ Ωm (MATWEB 2008). Expressed another way, this wire has a resistance of 34.12 mΩ $m^{-1}$. Interestingly, the temperature coefficient of resistance of steel is $0.003^{o}C^{-1}$ (Kuphaldt, 2007) which means that the resistance will increase by 3 percent for every rise in temperature of $10^{o}$ C.

### 4.3.1 Materials and Methods: EM38 Response to a Single Trellis Wire

An unearthed, straight length of wire was oriented parallel to the long axis of the EM38 and its response recorded as a function of horizontal separation from that instrument. The 3 m long wire was attached to a PVC pipe (with plastic cable ties) to ensure that it was held straight. Figure 4-12 shows this experimental configuration. The experiment was performed with the wire at two heights (relative to the electronic height of the EM38). The first was at the same height as the electronic dipoles of the EM38 (58 mm above the base of the EM38 unit), and the second with the wire at a height of 0.25 m.

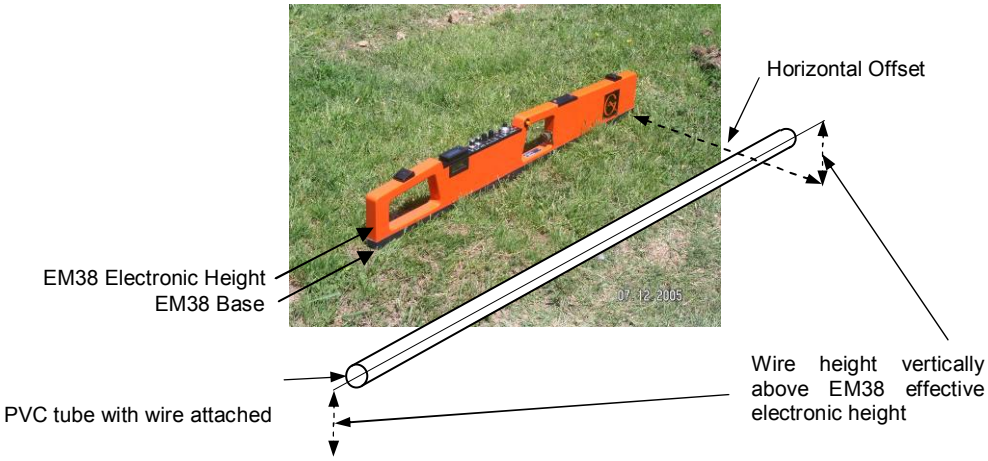


**Figure 4-12. EM38 configuration for measuring the vertical dipole response from an isolated, parallel, horizontal 2.5 mm diameter steel trellis wire.**

### *4.3.2 Results and Discussion: EM38 Response to a Single Trellis Wire*

Figure 4-13 is the resulting EM38 response against increasing horizontal separation from an isolated wire, at the two heights. There is little EM38 response to the nearby wire when it is located in the plane of the dipole (height = 0.0 m) although Figure 4-13 suggests a minor effect may appear when the wire is at a separation of 0.05 m from the EM38. The response is larger, but still relatively small (i.e. ~7 mS $m^{-1}$) for a wire height of 0.25 m above the EM38 dipole level. This small amplitude is understandable given the relatively small area of the wire available for coupling (compared to a large conductive loop). The important result is that, at both wire heights, there is negligible influence (<1 $mS^{-1}m$) on the EM38 response beyond a horizontal EM38-to-wire separation of 0.5 m.

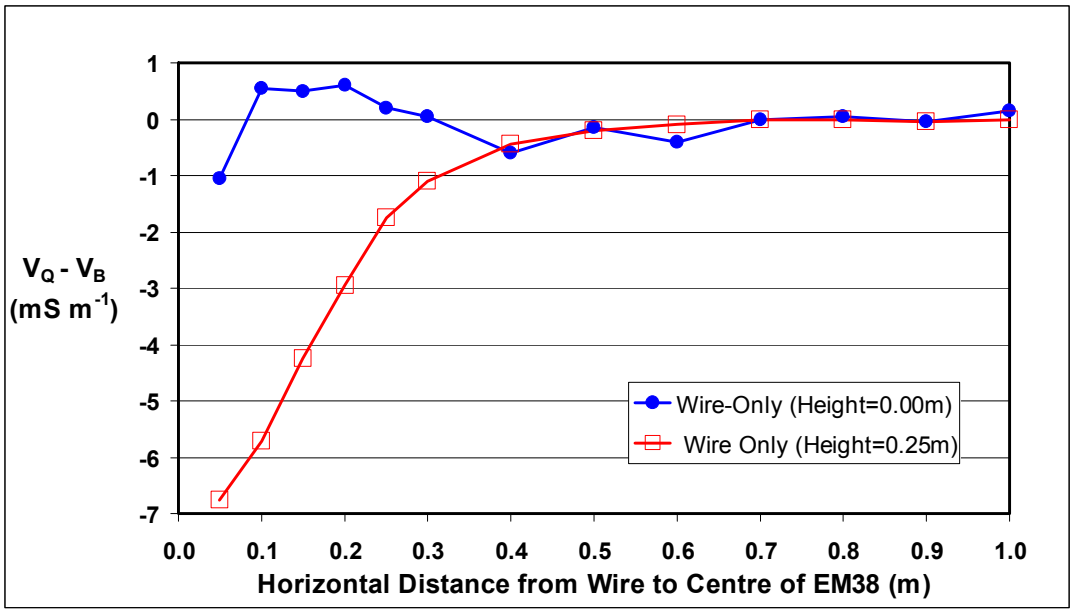


**Figure 4-13. EM38 (vertical dipole) response from a parallel, horizontal, unearthed 2.5 mm steel trellis wire as a function of horizontal separation distance. Wire heights were relative to the vertical position of the EM38's electronic height. The background response (including that from the bare-earth) was subtracted after each measurement.**

## *4.4 EM38 Response to a Vertical Trellis Loop (Unearthed)*

Sections 4.2 and 4.3 indicated that single, isolated trellis posts and wires provide a negligible EM38 response of approximately 2 mS $m^{-1}$ for EM38 distances of only tens of centimetres from the target. Whilst some of the response patterns observed remain unexplained, in all cases the EM38 response decreased to levels comparable to signal-noise limits of the EM38 at separations from the trellis that would occur during a commercial survey. This section now examines the effect on the EM38 response of combining the trellis posts and wires into a large, single conducting loop insulated from the earth.

### *4.4.1 Materials and Methods: EM38 Response to a Vertical Loop of Trellis Wire (Unearthed)*

Figure 4-14 shows the experimental configuration used to measure the EM38 response to a vertical, trellis-sized, closed rectangle of conducting wire. A 3 m (wide) by 2 m (high) rectangular frame, constructed from PVC pipe, supported the wire loop. At a height of 2 m above the ground, the EM38 was suspended, level with the top of the loop. To change the horizontal separation distance of the EM38 to the loop, the loop itself was moved rather than the EM38. This maintained the

background effects from the bare-earth or other nearby conductors at a constant value. Horizontal EM38-to-loop separations started at 0.5 m and were incremented up to a final separation of 5 m.


**a)** **b)**

**Figure 4-14. Photographs of the non-grounded (unearthed) single trellis loop experiment configuration. a) The 3 m by 2 m rectangular PVC pipe frame, with the EM38 supported on a wooden plank, 2 m above the ground, b) close up of the supporting frame showing the conducting wire attached to the PVC frame and the electrical connector used for opening and closing the loop.**

To confirm that the ground had no significant interaction with the loop, the EM38 was lowered to ground level and the experiment repeated.

To examine further the effect on the EM38 of a vertical rectangular loop, another series of measurements were performed with the EM38 raised 1 m off the ground, such that as the loop was moved, the EM38 maintained alignment along a 2-D line of symmetry through the middle of the loop. Along this line of symmetry, the predicted response was expected to be zero because of the zero net flux coupling with the loop. The relative positions of the EM38, the loop and the axes of symmetry for the three EM38 heights, are shown schematically in Figure 4-15.

In all cases, the drift was corrected by disconnecting the loop (Figure 4-14b), immediately retaking a background measurement and then subtracting it from the connected-loop measurement.

To predict the effect of the loop on the EM38 response, the program FastHenry was used to calculate the mutual inductance between the EM38 and the Target Loop, along with the loop's self-inductance and resistance. These electrical parameters

were calculated from the FastHenry software by specifying the vertices of the rectangular loop and the required straight connecting wires (including wire cross-sectional area and resistivity) in an input file. The relative position of the vertices specified can be visualised in the schematic shown in Figure 2-11. From this input file, FastHenry then estimated electrical parameters (at the two ports shown in the schematic of Figure 2-11) for substitution into Equation 3-32, giving the estimated EM38 response to the rectangular wire loop. Since the EM38 was orientated parallel to, and mid-way between the vertical ends of the wire-loop, the EM38's mid-point (between the Tx and Rx dipoles) was moved along a vertical plane of symmetry with respect to the wire loop. Hence, only one mutual inductance estimate from the EM38 dipole to the wire loop was required (i.e. $M_{01}=M_{12}$). The experimental configuration for the three EM38 heights is shown in Figure 4-15.

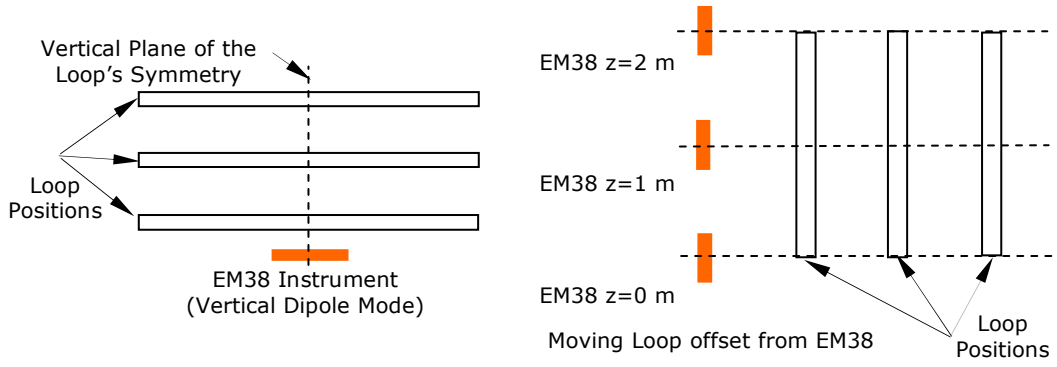


**a) Plan View** **b) Side View**

**Figure 4-15. Schematic views of the experimental configuration for investigating the effect of 3 m wide by 2 m high closed vertical rectangular loop of wire on the EM38 instrument kept stationary (but at three heights: 0, 1, and 2 m). The loop was moved horizontally along a straight line and maintained parallel to the EM38.**

### *4.4.2 Results and Discussion: EM38 Response to a Vertical Loop of Trellis Wire (Unearthed)*

The EM38 response adjacent to the horizontal and vertical centre of the rectangular wire-loop (i.e. With the EM38 suspended 1 m off the ground), was measured and found to be less than 0.3 m $Sm^{-1}$, at loop separations ≥0.5 m. This confirms the expected zero result (within the accuracy of the instrument), due to the

measurements being along the horizontal and vertical axis of symmetry orthogonal to the loop and therefore not coupling with the loop.

The comparison of the measured EM38 response, with the instrument on the ground, and the prediction, calculated from parameters estimated by the FastHenry model, are both shown in Figure 4-16. The graphed prediction shows good agreement with the measured values, both in the fall-off rate and absolute value, across several orders of magnitude. There was no significant difference between the response with the EM38 suspended 2 m in the air, or placed on the ground. This is not surprising as the field from the ground eddy currents would be mostly horizontal, producing an approximately vertical field which would not couple with the vertical wire loop. In addition, it is feasible that the magnitude of any such secondary coupling would be negligible.

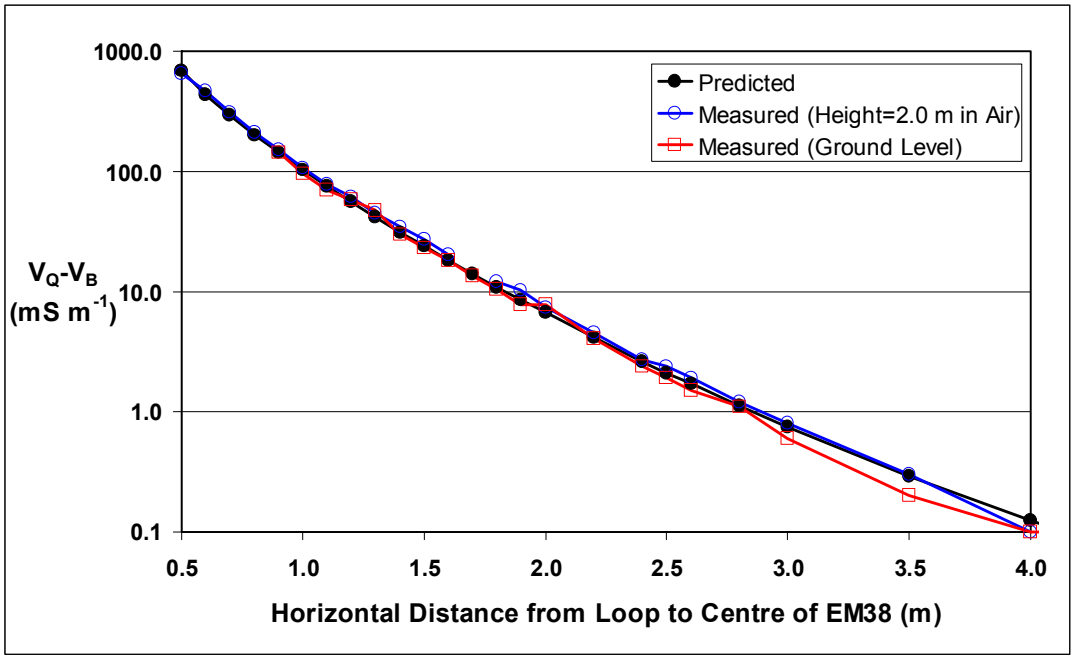


**Figure 4-16. EM38 (vertical dipole) response as a function of horizontal distance from a vertical, unearthed trellis loop. The response from the bare-earth was measured by breaking the loop's electrical continuity after each measurement, and then subtracted. Measurements were conducted with EM38 placed on the ground and then repeated with it suspended 2 m above the ground.**

The consistent slight under-prediction of the calculated values in Figure 4-16 indicates that the effective number-of-turns determined for the EM38 using the small horizontal loops (Sub-section 3.6) was too low. Matching the predicted values with the actual readings in Figure 4-16 requires this parameter be increased from the earlier calculated 894 to a new value of 1035. The need to adjust this

value is attributed to the fact that the EM38 transmitter and receiver (in vertical dipole mode) are behaving differently for vertical loops compared to the horizontal loops. It is also possible that the smaller scale of the earlier measurements exaggerated the uncertainty in positioning or orientation of the EM38 relative to the test coils. Figure 4-17 shows the same data but using the refined value for *N* (with a restricted abscissa range of horizontal separations of the EM38 to the trellis loop of 1.2 to 1.8 m, typical of an EM38 to trellis survey separation). This result shows improved agreement between the measured and predicted values. These response values also indicate that the order of magnitude of EM38 response from a single (unearthed) trellis panel, at these typical separations, will be in the range of 10 to 55 mS $m^{-1}$, a result consistent with the trellis-induced distortions observed by Lamb, Mitchell and Hyde (2005).

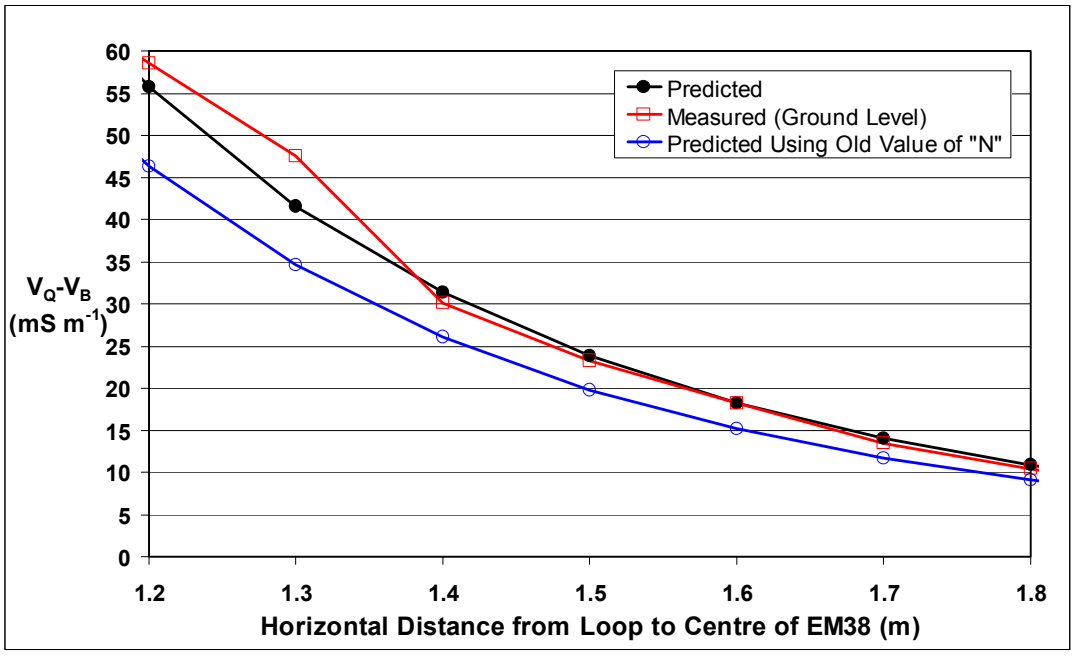


**Figure 4-17. EM38 (vertical dipole) response from a parallel, vertical, non-earthed trellis-sized loop at separations normally encountered during an inter-row EM38 survey. The response from the bare-earth was subtracted from each loop measurement. The predicted responses are shown with the old and the new refined value of *N*.**

## *4.5 EM38 Response to Individual Steel Trellis Panel Loops*

To investigate the response from a real trellis panel, a test trellis was constructed in line with the earlier descriptions of commonly used trellising systems (described in Section 1.4). Figure 4-18 shows the schematic of the trellis configuration used in

this research. The trellis panel shown has ten conducting rectangular loops comprising two vertical Gripfast post segments and two sets of horizontal wires. The Foliage 1 and Foliage 2 horizontal loop segments were considered as single sides of a rectangle even though they are pairs of wires (i.e. one on each side of the post but at the same height). There are ten possible rectangular single loop configurations from these five sets of horizontal wires (listed in Table 4-1).

### 4.5.1 Materials and Methods: EM38 Response to Individual Steel Trellis Panel Loops

A single row of test trellising was constructed with six panels (each 3 m long) as shown in Figure 4-19. This multiple panel trellis was tensioned with electric fence tensioners to give a realistic physical contact from each wire with the slots in the Gripfast posts. The electric fence tensioners also insulated the wires from the steel strainer posts at one end and electric fence type ceramic insulation blocks performed the same function at the opposite end. These two types of ceramic insulators are shown in Figure 4-20 for the ends of the trellis row.

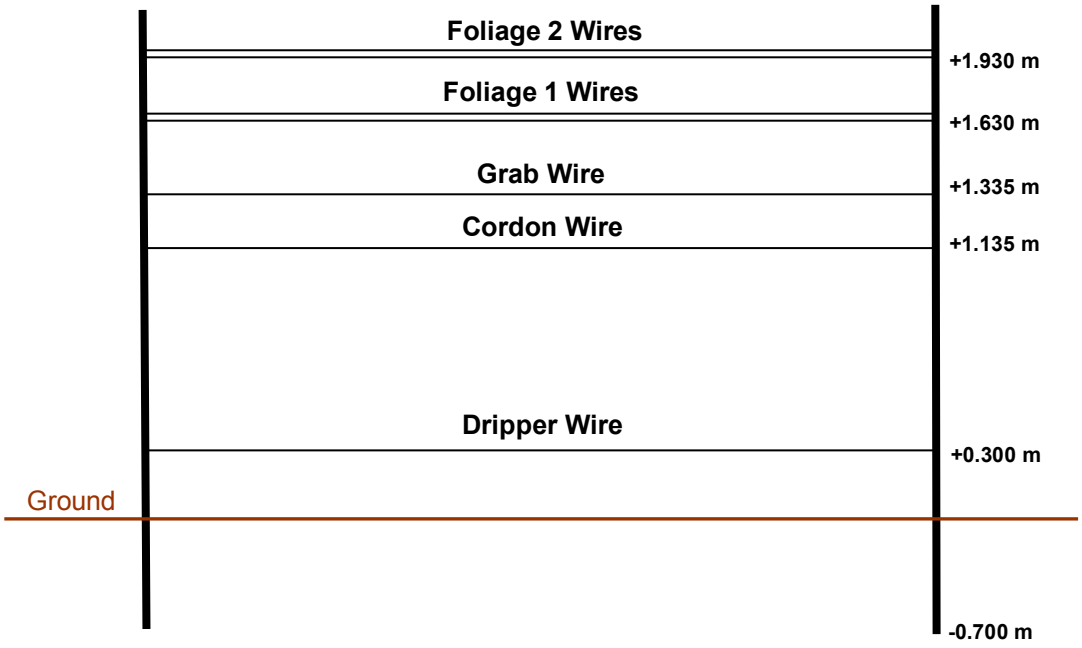


**Figure 4-18. Schematic diagram of a single panel of the constructed test trellis.**


**a)** **b)**

**Figure 4-19. Single trellis row established for controlled testing of its effect on the EM38 responses. a) Steel strainer post and trellis without wires. b) Trellis row with wires and EM38 in position for testing.**

**a)** **b)**

**Figure 4-20. Insulators used to electrically isolate the trellis from the steel strainer posts on each end of the test trellis row. a) Ceramic and steel electric fence strainer. b) Ceramic insulators at the other end of the trellis.**

The activation of individual (or combination of) loops within the trellis configuration was controlled by insulating various wire-post connections. This was achieved by wrapping 30 mm by 30 mm squares of 1.5 mm thick truck tyre inner tube rubber sheet around the specific trellis wire and sliding it along the wire into the post's wire holding slot (Figure 4-21). When in place, the integrity of the wire-post insulation was checked with a digital multimeter (RadioShack Corporation, USA). The EM38 response was measured with the instrument located

at a horizontal distance of 1.5 m away from the trellis. The EM38 was placed on the ground and measurements were completed with the relevant trellis loop(s) activated. The measurements were then repeated with the loop deactivated so that the background bare-earth values could be subtracted.

To predict the EM38 response to each trellis loop configuration, FastHenry estimations of mutual inductance, loop resistance, and loop self-inductance parameters (from the relevant simple rectangles) were substituted into Equation 3-32. It was assumed from the flux–rule (Equation 3-3) that the mutual inductance would be influenced only by the large loop area, rather than the details of the post shape. However, while the Gripfast posts have a complicated cross-sectional pattern, a simple square cross-section of the same area ensured that the anticipated critical resistance was correctly simulated. The effects of the complicated post shape and the magnetic permeability of the steel wire and posts on the self-inductance were ignored.


**a)** **b)**

**Figure 4-21. Photographs showing how the wires are held by the Gripfast post slot and how they were selectively insulated. a) Wire is held in the Gripfast post wire slot. b) Insulating rubber inserted to control which wires are electrically isolated from the posts.**

### *4.5.2 Results and Discussion: EM38 Response to Individual Steel Trellis Panel Loops*

The predicted and measured EM38 response for each of the ten simple loops of a single trellis panel are graphed in Figure 4-22. This comparison graph shows that the measured responses were significantly greater than predicted for the

Dripper-Foliage 1 and Dripper-Foliage 2 configurations, the largest, D-F2 loop providing a 75% increase in response compared to the prediction. In fact, Figure 4-22 indicates the largest loops always measured significantly higher than predicted.

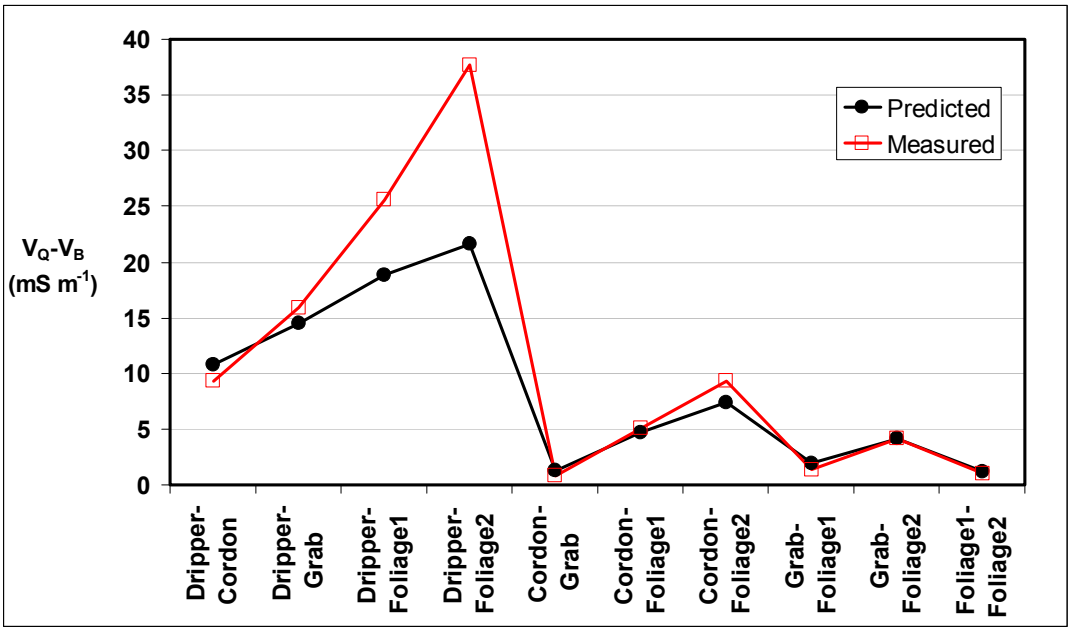


**Figure 4-22. Comparison between predicted and measured EM38 (vertical dipole) response to various single loops in a single trellis panel (3 m trellis segment).**

To understand why the measured response was significantly larger than that predicted requires a review of Equation 3-32. For a fixed loop-to-EM38 configuration (which makes the mutual inductance constant), the EM38 response becomes a function of just loop resistance and its self-inductance. Thus, Equation 3-32 can be re-expressed directly as the proportionality:

$$V_Q \propto \frac{R}{(R^2 + \omega^2 L^2)}$$

Equation 4-1

To evaluate this relationship, actual values for resistance and self-inductance for the ten, rectangular, trellis loops were calculated using FastHenry (listed in Table 4-1). Note that the loops containing the F1 or F2 wire segments have the lowest resistances. This is because those segments consisted of a pair of wires, effectively halving the resistance compared to a single wire segment due to being electrically parallel. Inspection of Table 4-1 shows that $R^2$ is over one order of magnitude smaller than $\omega^2 L^2$.

**Table 4-1. Calculated values of $R^2$, $\omega^2L^2$ and their ratios for the ten individual loops of the experimental configuration (3 m panel) shown in Figure 4-19.**

| Trellis Loop | $R^2$ ($\Omega^2$) | $\omega^2L^2$ ($H^2s^{-2}$) | $\frac{\omega^2L^2}{R^2}$ | $\frac{R^2}{\omega^2L^2}$ |
|---|---|---|---|---|
| Dripper-Cordon (D-C) | 0.023 | 0.717 | 31.23 | 3.20E-02 |
| Dripper-Grab (D-G) | 0.023 | 0.816 | 35.45 | 2.82E-02 |
| Dripper-Foliage1 (D-F1) | 0.013 | 0.766 | 58.41 | 1.71E-02 |
| Dripper-Foliage2 (D-F2) | 0.013 | 0.905 | 68.60 | 1.46E-02 |
| Cordon-Grab (C-G) | 0.023 | 0.358 | 15.75 | 6.35E-02 |
| Cordon-Foliage1 (C-F1) | 0.013 | 0.396 | 30.79 | 3.25E-02 |
| Cordon-Foliage2 (C-F2) | 0.013 | 0.530 | 40.86 | 2.45E-02 |
| Grab-Foliage1 (G-F1) | 0.013 | 0.298 | 23.24 | 4.30E-02 |
| Grab-Foliage2 (G-F2) | 0.013 | 0.442 | 34.23 | 2.92E-02 |
| Foliage1-Foliage2 (F1-F2) | 0.006 | 0.195 | 34.03 | 2.94E-02 |

This means that Equation 4-1 can be approximated as:

$$V_Q \propto \frac{R}{\omega^2 L^2}, R^2 << \omega^2 L^2 \quad \text{Equation 4-2}$$

Now, for a particular loop (of fixed size and shape), the inductance will not vary, in which case Equation 4-2 indicates, counter-intuitively, that the EM38 response is approximately proportional to the resistance. In reality, the total eddy current would decrease with increasing resistance, but in this case, (where the resistance is low due to the conductors being metallic rather than earth) the quadrature phase component actually increases.

It is important to note that, in light of these findings, Equation 2-7 (which relates the EM38 response to the linear proportionality of ground conductivity) will only be valid for the resistances typical for soils. It will not, however, be valid for resistances associated with conductive metals such as steel. This sensitivity to the loop resistance is significant, as both thinner wires and/or increased contact resistances will increase the trellis interference to the EM38 significantly. Therefore, Equation 4-2 indicates that contact resistance between the wires and the posts will increase the EM38 response. The proportions of the contact resistance to

the calculated loop resistance (Table 4-2) indicate that the contact resistance is a significant factor, adding up to 55 % to the loop resistance.

In addition, to make the measurements, one of the four contacts (at a rectangular loop vertex) had to be broken to allow a port for the resistance meter. Hence, the measured contact resistances in Table 4-2 will be approximately three-quarters of the real value. This provides a lower-end estimate of the true contact resistance. The significant magnitude of the measured contact resistance (considered along with proportionality of the EM38 response to loop resistance in Equation 4-2) provides a plausible explanation for the under-prediction of the responses indicated in Figure 4-22.

**Table 4-2. Comparison of measured loop resistance values to calculated values for a 3 m trellis panel.**

| Trellis Loop | Calculated Resistance $R_c$ (mΩ) | Measured Resistance $R_m$ (mΩ) | Difference Resistance $R_m$-$R_c$ (mΩ) | $\frac{R_m-R_c}{R_c}$ (%) |
|---|---|---|---|---|
| **Dripper-Cordon** | 151.5 | 205 | 53.5 | 35 % |
| **Dripper-Grab** | 151.8 | 210 | 58.2 | 38 % |
| **Dripper-Foliage1** | 114.5 | 163 | 48.5 | 42 % |
| **Dripper-Foliage2** | 114.9 | 178 | 63.1 | 55 % |
| **Cordon-Grab** | 150.7 | | | |
| **Cordon-Foliage1** | 113.5 | 174 | 60.5 | 53 % |
| **Cordon-Foliage2** | 113.8 | | | |
| **Grab-Foliage1** | 113.2 | | | |
| **Grab-Foliage2** | 113.6 | | | |
| **Foliage1-Foliage2** | 75.6 | | | |

The role of contact resistance in the under-prediction of the measured loop resistances was confirmed by retaking the EM38 response measurements with the wire-post connections electrically shorted using brass screw-type electrical joiners (effectively making the contact resistance negligible). A plot of the predicted and the retaken EM38 measured responses is given in Figure 4-23, with good agreement between the predicted and re-measured EM38 response.

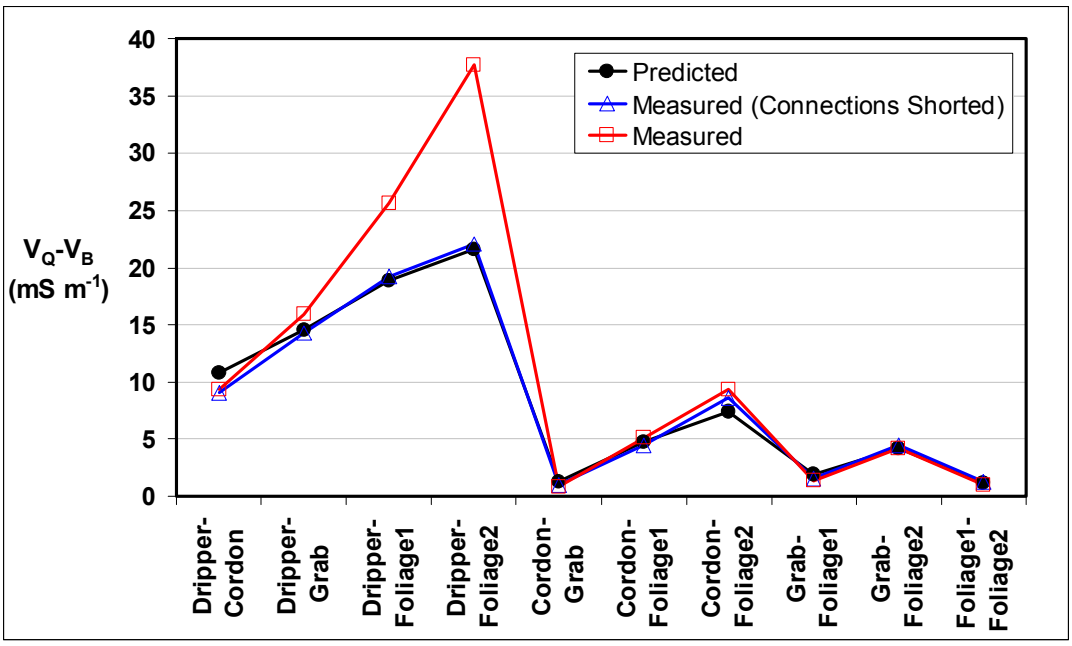


**Figure 4-23. Comparison between the predicted and measured EM38 (vertical dipole) responses to single trellis loops (3 m trellis panel) after improving the wire-post connections (blue curve). The previous EM38 response with significant contact resistance (red curve) has been retained to highlight the improved match.**

Similarly, predicted and measured EM38 responses, for a 6 m long trellis panel (i.e. two consecutive 3 m panels on the test trellis, with the centre post isolated from the wires) are given in Figure 4-24. Again, practically eliminating the wire-post contact resistance by shorting the wire-post connections yields good agreement between the predicted and measured responses for simple loops within a 6 m long trellis panel.

These results clearly indicate the role of appreciable wire-post contact resistance in the EM38 response to these loops. The three most probable causes for the significant contact resistance between the wire and the Gripfast post are: the formation of an electrical insulating layer, either from oxides formed by corrosion on the steel wires and/or galvanizing material on the posts; a small contact area; and/or a lack of contact force between the post and the wire.

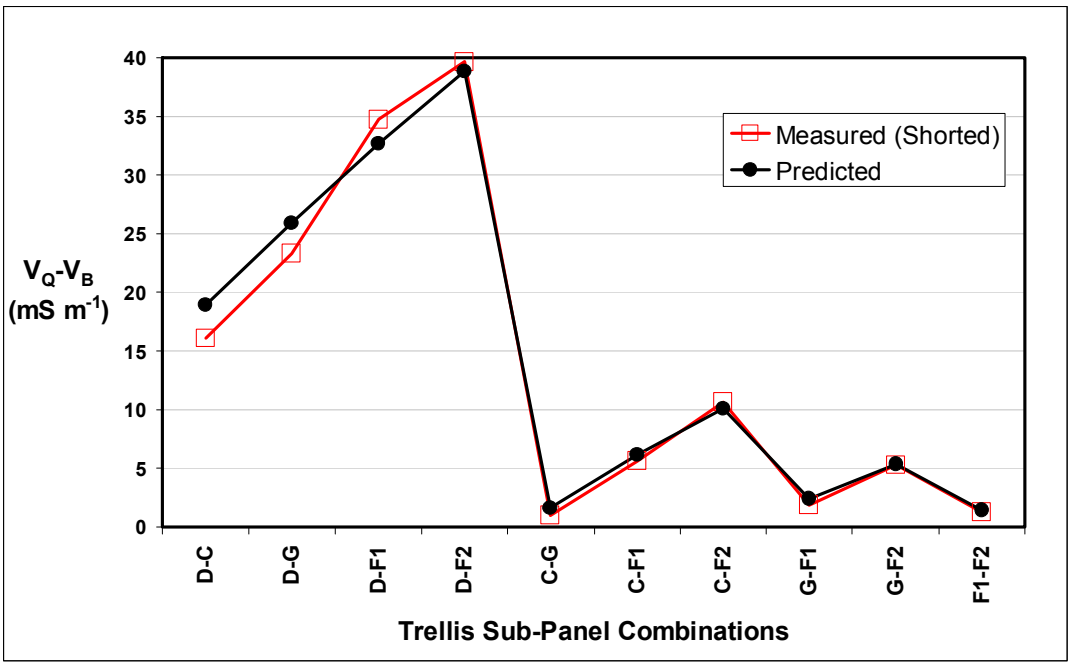


**Figure 4-24. Comparison between the predicted and measured EM38 (vertical dipole) responses to single trellis loops (6 m trellis panel) with electrically shorted post-wire contacts. (EM38 horizontal distance from the trellis was 1.25 m.)**

## *4.6 Mid-Panel EM38 Response to Multiple Loops in a Single Trellis Panel*

The previous Section 4.5 obtained good agreement between predicted responses and measured responses for single rectangular components of a trellis panel. In reality, these component rectangles form a network of rectangular elements that interacts with the EM38. The schematics showing some of the possible network elements (Figure 4-1 and Figure 4-18) indicate the rapid escalation of the complexity of this circuit network when attempting to predict the EM38 response to an actual trellis panel.

### *4.6.1 Using FastHenry to Predict EM38 Response to Multiple Loops in a Single Trellis Panel*

A steel trellis is a complicated combination of loops. Within the one trellis panel (as shown schematically in Figure 4-18), and excluding the ground path, there are twenty-three loop combinations (Table 4-3). Including the ground path as a loop segment doubles the number of combinations. Furthermore, when the ground path and each individual wire loop are included, this brings the total number of trellis loops to fifty-one. Theoretically, all these loops will inductively couple with each

other. In addition, each loop interacts with every other panel in the row and other rows. This illustrates the theoretical complexity of the system. Fortunately, these inductive couplings will be negligible, due to the low operating frequency of the EM38 (see Section 2.6).

**Table 4-3. Loop combinations within a typical trellis panel (as shown schematically in Figure 4-18**).

| Loop Combination Number | Trellis Loop | Abbreviation |
|---|---|---|
| 1 | Dripper-Cordon | D-C |
| 2 | Dripper-Cordon-Grab | D-C-G |
| 3 | Dripper-Cordon-Grab-Foliage 1 | D-C-G-F1 |
| 4 | Dripper-Cordon-Grab-Foliage 1-Foliage 2 | D-C-G-F1-F2 |
| 5 | Dripper-Cordon-Grab-Foliage 2 | D-C-G-F2 |
| 6 | Dripper-Grab | D-G |
| 7 | Dripper-Grab-Foliage 1 | D-G-F1 |
| 8 | Dripper-Grab-Foliage 1-Foliage 2 | D-G-F1-F2 |
| 9 | Dripper-Grab-Foliage 2 | D-G-F2 |
| 10 | Dripper-Foliage 1 | D-F1 |
| 11 | Dripper-Foliage1-Foliage 2 | D-F1-F2 |
| 12 | Dripper-Foliage 2 | D-F2 |
| 13 | Cordon-Grab | C-G |
| 14 | Cordon-Grab-Foliage 1 | C-G-F1 |
| 15 | Cordon-Grab-Foliage 1-Foliage 2 | C-G-F1-F2 |
| 16 | Cordon-Grab-Foliage 2 | C-G-F2 |
| 17 | Cordon-Foliage 1 | C-F1 |
| 18 | Cordon-Foliage 1-Foliage 2 | C-F1-F2 |
| 19 | Cordon-Foliage 2 | C-F2 |
| 20 | Grab-Foliage 1 | G-F1 |
| 21 | Grab-Foliage 1-Foliage 2 | G-F1-F2 |
| 22 | Grab-Foliage 2 | G-F2 |
| 23 | Foliage 1-Foliage 2 | F1-F2 |

Equation 3-32 shows that the response factors (within a trellis panel) will be the effective resistance around the loops, their self-inductance, the mutual inductance from the EM38 to the combined conductive loops and back again, and the circuit network interactions. To estimate these parameters for substitution into Equation 3-32 (in order to calculate a predicted response), requires a choice of where to place the FastHenry measurement port (Section 2.11) within the

multi-loop, trellis panel. Figure 4-25 shows two different trellis port location options; one in the side of the D-C loop and one in the side of C-G loop. While both options do not give significantly different total loop resistances, the mutual inductance estimate with the port in the D-C loop is 24 % higher than having the port in the C-G loop. Self-inductance values differed by only 6 %. While this demonstrates the complexity of the system, it also highlights the difficulty in applying FastHenry to predicting an EM38 response from a multi-loop system.

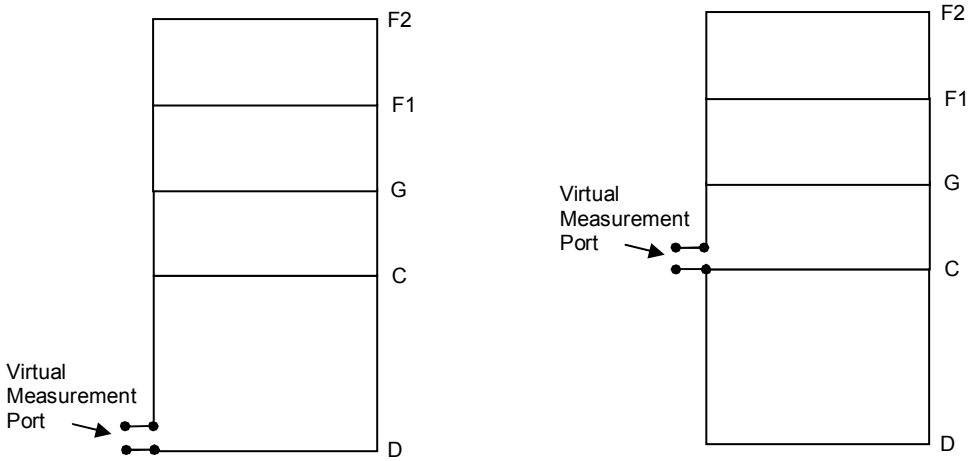


**Fast Henry Estimated Parameters: M=2.26x10-11 H R=0.1267 Ω**

**a)**

**Fast Henry Estimated Parameters: M=1.71x10-11 H R=0.1253 Ω**

**b)**

**Figure 4-25. Schematic drawing of a multi-loop trellis panel with different measurement ports as used by the FastHenry software to estimate the mutual inductance, self-inductance, and resistance; a) Measurement port in the D-C loop. b) Measurement port in the C-G loop. Loop reference conventions follows Table 4-3.**

To predict the EM38 response, requires the choice of a measurement port location. However, as the predicted loop resistance does not vary significantly with the choice of measurement port location, this factor does not impinge upon the decision. Consideration must be given, however, to the fact that the mutual inductance from the EM38 to the D-C loop dominates the contribution from the other loops. This can be justified by reviewing Equation 3-32 and then extending Equation 4-2 to include the critical $M^2$ factor so the EM38 response can be seen as proportional to the two factors, $M^2$ and $R/\omega^2L^2$:

$$V_Q \propto M^2 \frac{R}{\omega^2 L^2}, R^2 << \omega^2 L^2 . \qquad \text{Equation 4-3}$$

These two factors, therefore, are the only factors of any real significance when considerations regarding port choices are made. Figure 4-26 is a graph of these two factors for the four rectangular loops comprising adjacent trellis wires. This graph shows that the amplitude of the $R/\omega^2L^2$ factor for the three higher trellis loops (C-G, G-F1, F1-F2) is almost double that of the lowest loop (D-C). However, it is the $M^2$ factor of the bottom D-C loop that is over one order of magnitude greater than the other three loops. Both these factors combine (as shown in Equation 4-3) to reinforce the fact that the D-C loop is not only the dominant component of the trellis-induced response signal, but also that the higher loops are negligible, if treated in isolation.

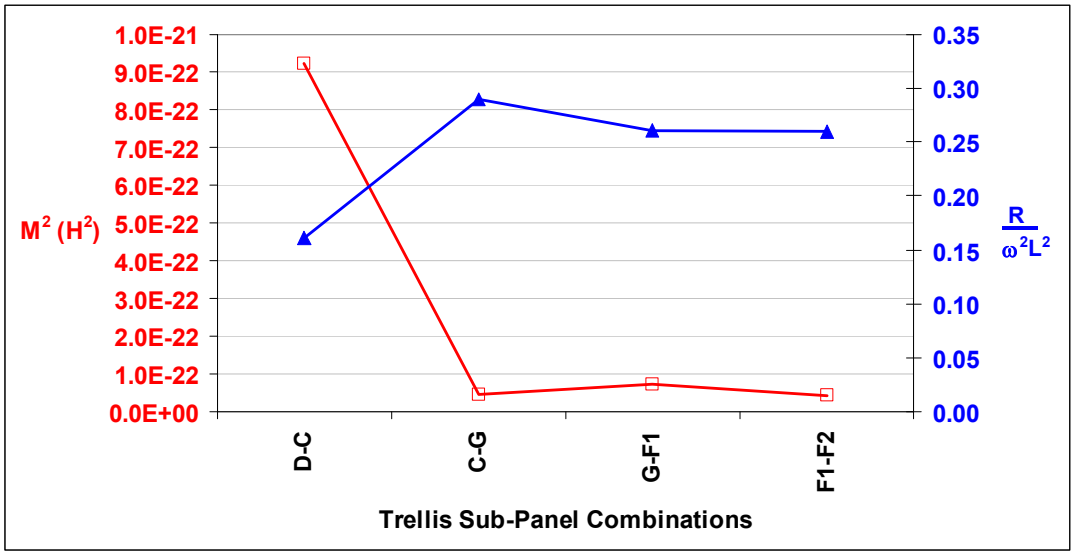


**Figure 4-26. Graph of the mutual inductance-squared for the four basic rectangular loops comprising adjacent trellis wires. The other contributing factor of Equation 4-3, $R/\omega^2L^2$, is also shown.**

However, the contribution of the loops including wire segments above D-C loop, are not, in fact, negligible. Figure 4-27 shows the effect on $M^2$ for the largest loop (D-F2) as progressively more intermediate trellis wires (creating more sub-loops) are added into the FastHenry model. The overall $M^2$ factor reduces significantly as more wires (sub-loops) are introduced. That is, the $M^2$ of the D-F2 loop is reduced by 42 % with the introduction of the four intermediate wires. However, Figure 4-27 indicates the $R/\omega^2L^2$ factor is reduced by 43 % as those same intermediate wires are removed. Therefore, the two factors controlling the trellis interference on the EM38 effectively cancel each other out.

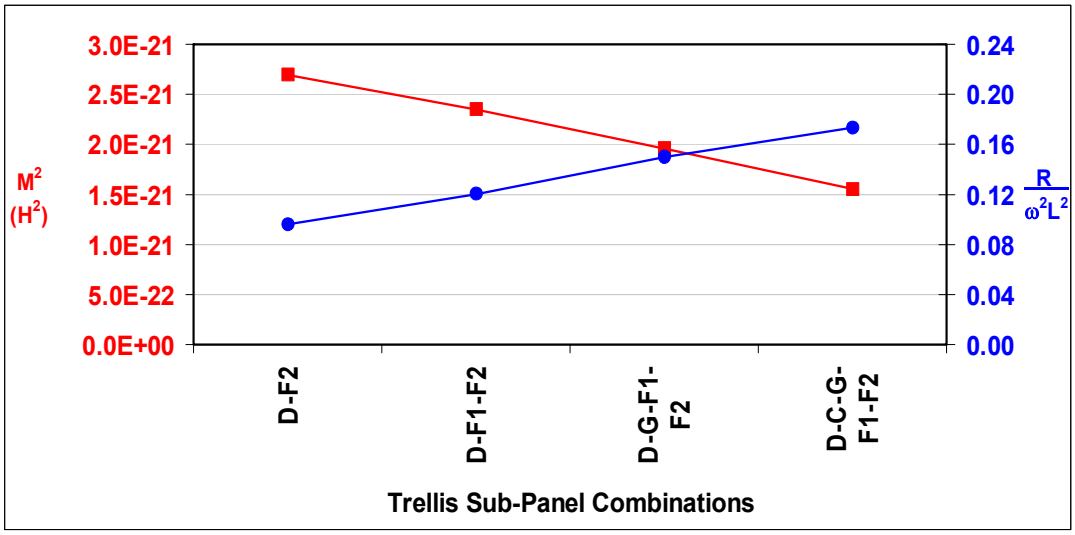


**Figure 4-27. Graph of the mutual inductance-squared for the large rectangular loop (D-F2) with progressively more intermediate wires added. The other contributing factor, $R/\omega^2L^2$, is also shown.**

Therefore, a choice of a FastHenry measurement port in the D-C loop allows a mutual inductance and electrical resistance to be estimated for various loop combinations and hence the calculation of the predicted trellis interference on the EM38.

### *4.6.2 Materials and Methods: Mid-Panel EM38 Response to Multiple Steel Trellis Panel Loops*

Using the same test trellis, the EM38 was positioned on the pre-marked wooden graticule board (shown in Figure 4-19) with the EM38's midpoint co-aligned with the centre of the panel (and parallel to it). The readings were corrected for drift and background by immediately repeating each measurement, but with all the wires insulated from the post. This is the ideal method of correction as it precludes significant time elapsing between the wires-connected measurement and the wires-insulated measurement.

The values for this test were predicted using Equation 3-32 and parameters estimated with FastHenry (with the selected port position in the side of the D-C loop of the multi-wire trellis panel, as shown in Figure 4-25a).

### 4.6.3 Results and Discussion: Mid-Panel EM38 Response to Multiple Steel Trellis Panel Loops

The predicted and measured EM38 response for the large D-F2 loop, as intermediate wires are progressively added, is shown in Figure 4-28. This figure shows only small variations in the predicted response with introduction of sub-loops, confirming the earlier observation (Sub-section 4.6.1) that the consequent reduction of $M^2$, with the addition of intermediate wires, was compensated for by the increase in $R/\omega^2 L^2$.

The measured EM38 response is still approximately 10 % higher than predicted and this could be due to the earth path between the two Gripfast posts forming additional loop structures, even though the soil was relativley resitive. The impact of earth loops will be investigated in detail in Section 4.9.

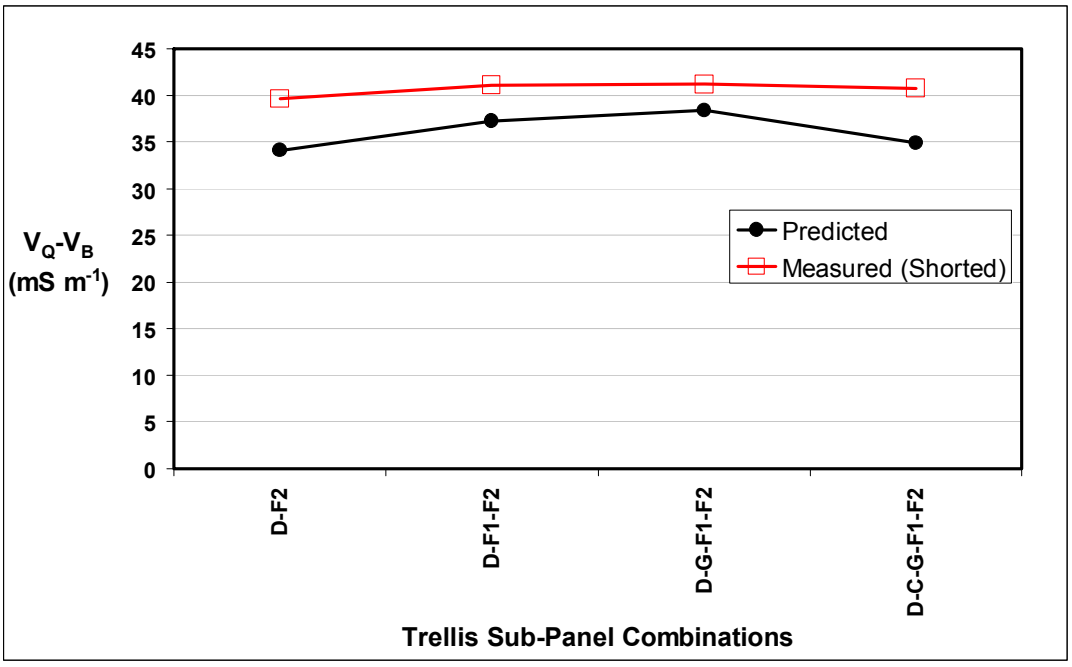


**Figure 4-28. Comparison of the predicted and measured EM38 (vertical dipole) response for an EM38 located 1.25 m horizontally from various multiple loop combinations in a single (6 m long) trellis panel, commencing with the largest D-F2 loop, and then progressively connecting intermediate wires to create sub-loops. Wire-post connections were electrically shorted.**

An alternate explanation for the discrepancy may lie in the fact that the predicted response is inversely proportional to the square of the loop's self-inductance, $L$ (Equation 4-2). Hence, the details of the calculation of $L$ (which have been

ignored) may be relevant. The self-inductance of a rectangular loop of round wire is given by Grover (2004:60):

$$L \approx 0.2l\left[\log_e \frac{2l}{r_x} - \alpha + \frac{\mu}{4}\right]. \qquad \text{Equation 4-4}$$

where $l$ is the perimeter of the rectangle, $r_x$ the radius of the wire, $\mu$ the relative magnetic permeability of the wire (which has a value of one for non-magnetic materials), and $\alpha$ is a shape parameter (aspect ratio for rectangles) determined from a 'look-up' table. For the aspect ratio of the D-F2 loop (of ~0.25), $\alpha$ has a value of ~3.27 (using the 'lookup' table in Grover 2004:61). Clearly, the size (perimeter) of the loop is the overriding factor. The first term of this equation (inside the brackets) for the 6 m D-F2 loop is the dominant term over the second term by a factor of approximately three. Inspection of this dominant first term shows it has a strong dependence on the radius of the round wire. This, perhaps, is where the approximations to the trellis loop are not ideal, due to the relatively large radius and complicated shape of the vertical Gripfast posts. However, this effect may be minimised by the fact that the post only makes up 27 % of the loop. In addition, the final term includes $\mu$, which, for non-magnetic materials, has a value of practically unity. Of course, that is not the case for high-tensile steel trellis wires and mild-steel posts, which are made of ferromagnetic materials. This type of highly magnetic material has a significant and variable (by orders of magnitude) magnetic permeability which is dependant on the strength of the magnetic field, material composition, production processes, heat-treatment, and stress, and would usually have magnitudes (at the weak field values induced by the EM38 and the earth) of approximately 30 to 300. This means that this third term could be larger than the second (or even the first) term in magnitude and is, therefore, not negligible. Hence, this highlights that a simple estimation of self-inductance has limitations.

Figure 4-29 is a graph of the predicted and measured EM38 responses to various 3-, 4- and 5-loop configurations. This graph, again, shows that the model, based on FastHenry, slightly under predicts the measured result. Notably, Figure 4-30 shows that loop configurations that include the bottom (Dripper) wire, give the strongest responses. In addition, this figure shows that the stronger responses include both

the bottom (DW) and top wires (F1 and/or F2). This indicates that both the largest and closest loops (to the EM38) dominate the EM38 response, and confirms the importance of coupling area and loop proximity expressed in Equation 3-14 and Equation 3-32.

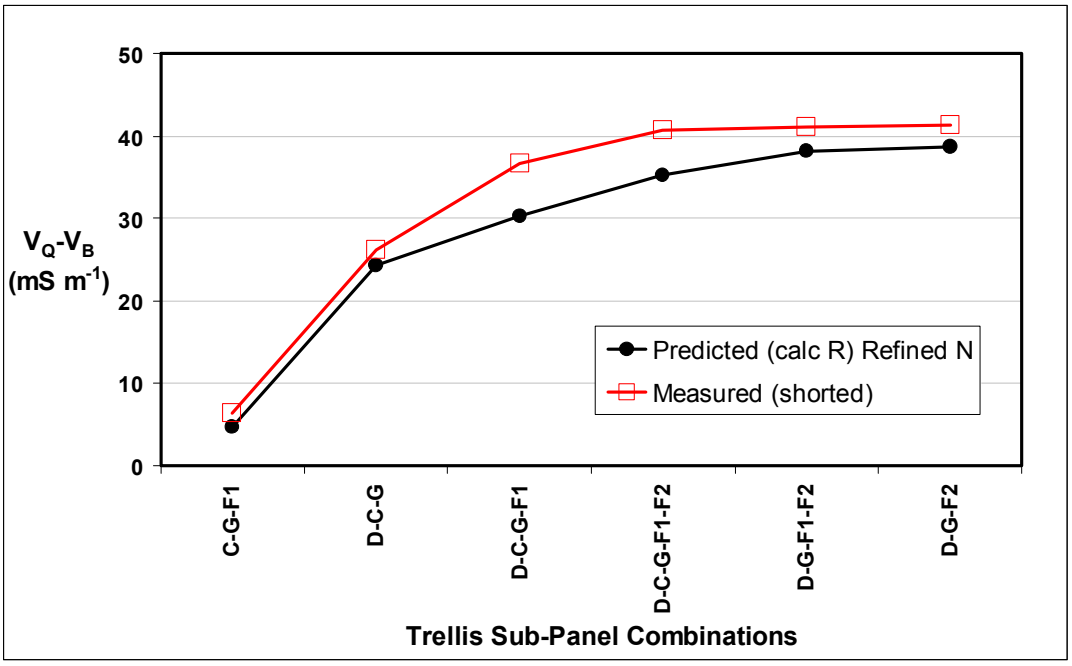


**Figure 4-29. Comparison between the predicted and measured EM38 (vertical dipole) responses for various multi-loop configurations. The responses are 1.25 m horizontally from various multiple loop combinations in an actual single (6 m long) trellis panel. (Wire-post connections were electrically shorted.)**

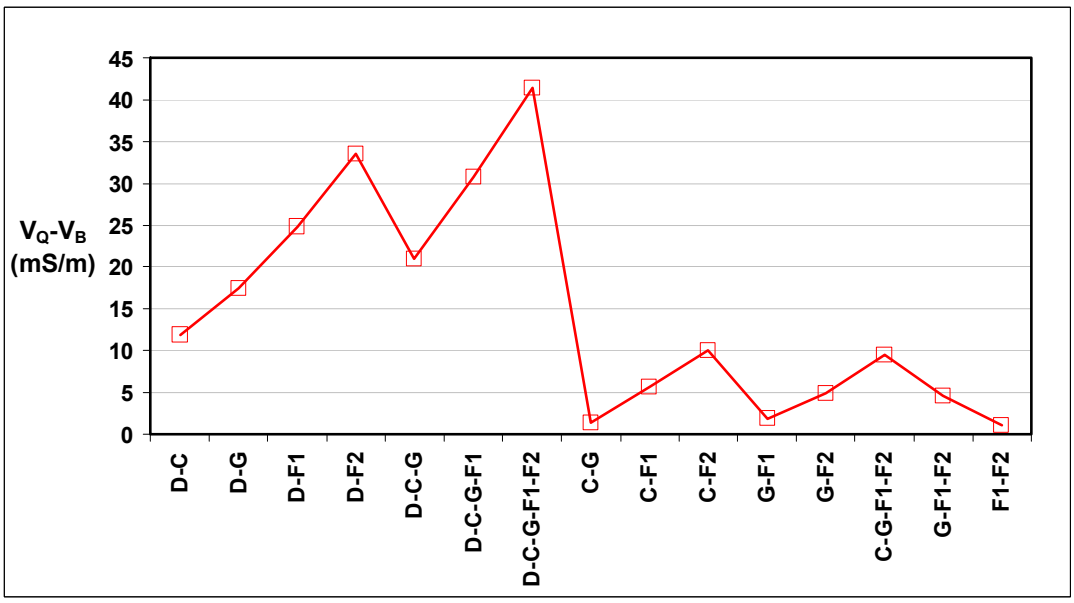


**Figure 4-30. Comparison between the measured EM38 (vertical dipole) responses to single trellis loops for loop configurations containing the bottom Dripper wire and those that do not (3 m trellis panel with un-shorted post-wire connections). (EM38 horizontal distance from the test trellis was 1.5 m.)**

## 4.7 EM38 Response with Distance from a Multiple Wire Trellis Panel

One assumption during a standard inter-trellis EM38 survey is that the instrument travels down the centre of the lane. However, in practice, this assumption may not hold consistently. Variations due to driver attention, terrain, and speed (for vehicle-towed operation) may cause the instrument to move away from the centre-line towards the trellis structure on either side. This may be as much as 30 % of the inter-row spacing, (i.e. ~1 m as estimated by D. Schneider 2008, UNE Precision Agriculture Research Group, Pers. Comm., 3 November). The results of Lamb, Mitchell and Hyde (2005) illustrated the trellis-induced distortion of the EM38 signal to be sensitive to EM38-to-trellis distance. From these data, Lamb, Mitchell and Hyde (2005) recommended that surveys be conducted with no more than 0.4 m lateral drift of the EM38 from the centre of the lane in order to keep trellis-induced distortions to less than 27 %. However, the data of Lamb, Mitchell and Hyde (2005) was limited in that the EM38 responses were only recorded with distance from opposite the steel trellis post, which, when the trellis wires were assembled, meant that the results were those for the EM38 located at the edges of trellis loops rather than adjacent to the centre of the trellis panel (mid-loop). The subsequent (2-D) survey data of Lamb, Mitchell and Hyde (2005) for the established trellis segments showed the EM38 response to be modulated with the instruments relative position along the trellis panels. That is, a maximum response occurred at the mid-loop position. Thus, whilst the change in the trellis effect with horizontal separation from the trellis is relevant because it is a measure of how across-track error in a real EM38 survey will influence the result, the work of Lamb, Mitchell and Hyde (2005) must be extended to include positions along the panels other than just adjacent to the posts.

### 4.7.1 Materials and Methods: Mid-Loop EM38 Response with Sensor-Loop Distance from a Multiple Wire Trellis

Using the test trellis (as described in previous tests, Sub-section 4.5.1) the EM38 was positioned on the pre-marked wooden graticule board (shown in Figure 4-19b).

The readings were corrected for drift and background effects by repeating the measurements with all the wires insulated from the post.

To show the effect of a trellis either side of the lane (as would normally be the case) a computer-simulated test was performed. The values for this test were predicted using Equation 3-32, with parameters estimated with FastHenry for a 3 m panel. This simulated fall-off profile was then mirrored, as if the same trellis configuration occurred on the other edge of the lane, and the coincident values added together.

### *4.7.2 Results and Discussion: Mid-Loop EM38 Response with Sensor-Loop Distance from a Multiple Wire Trellis*

Figure 4-31 shows the variation in the EM38 response as a function of the horizontal distance between the EM38 and the trellis as well as the rate-of-change of EM38 response with decreasing horizontal separation. This graph shows that the peak rate-of-change (of over 10 mS $m^{-1}$ per decimetre) occurs at a horizontal separation of approximately 1.4 m from the panel's midpoint.

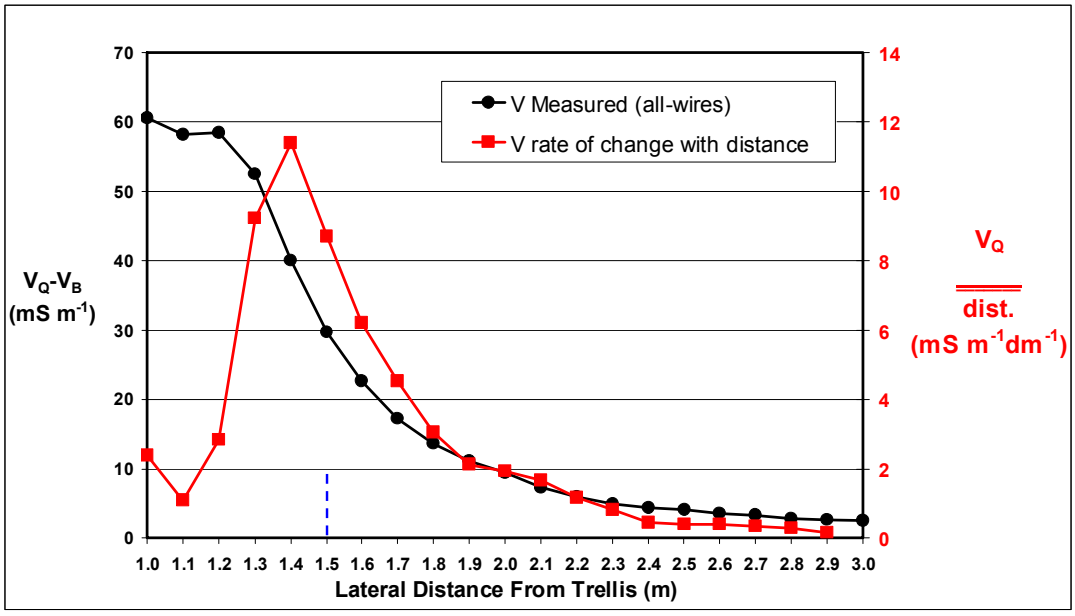


**Figure 4-31. Measured EM38 (vertical dipole) response from a single 3 m trellis panel (all-wires connected) and gradient (or fall-off rate in units of mS $m^{-1}$ / decimetre) as a function of horizontal distance away from the trellis mid-panel. The trellis panel is located at x = 0.0 m (The dashed blue line indicates the location of the mid-lane for a 3 m spaced trellis rows.)**

However, this rapid fall-off is mitigated when there is a trellis either side of the measurement point. Figure 4-32 shows the calculated response between a pair of trellis panels separated by an inter-row spacing of 3.0 m. That is, the second

simulated panel would be at the position 3.0 m along the abscissa of the graph. This graph shows that midway between the panels, the rate of change with EM38-to-trellis distance would be 0 mS $m^{-1}$ / decimetre. However, in practice it unlikely to be exactly zero due to individual trellis variations.

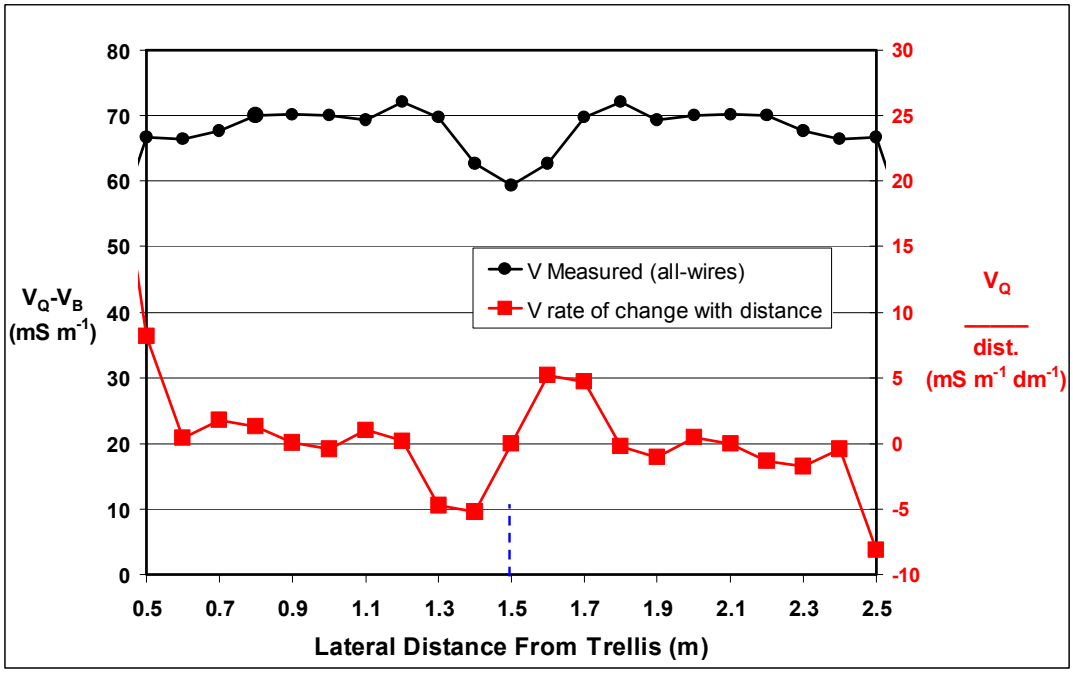


**Figure 4-32. Calculated EM38 (vertical dipole) response with horizontal position between a pair of trellis panels separated by an inter-row spacing of 3.0 m (all-wires connected) and gradient (or fall-off rate in units of mS $m^{-1}$ / decimetre). One trellis panel is located at x = 0.0 m and the second trellis panel at x= 3.0 m. The dashed blue line marks the mid-row location between the two panels.**

## *4.8 EM38 Response to a Trellis Panel Edge*

The predicted and measured EM38 responses from various conductive loops covered in previous sections have been restricted to a point adjacent to the centre of the trellis panel (mid-loop) with the exception of a brief mention of the adjacent-to-the-post response in the previous Section 4.7. Generally, the measurement points have all been at an elevation representing a configuration simulating a practical EM38 survey with the instrument on the ground and the vertical trellis above it, as shown in Figure 4-19b. This measurement location is along a vertical plane of symmetry where the mutual inductance from the Tx and Rx coils to the loops are identical. However, as the measurement location moves along parallel to the trellis loop, and horizontally away from the mid-loop position, and towards the panel edge (as it would during a real survey), each coil of the

EM38 couples with different proportions of the loops. That is, the mutual inductance values vary with different positions, relative to the mid-loop.

### 4.8.1 Materials and Methods: EM38 Response to a Trellis Panel Edge

For measurements adjacent to the edge of the panel, no modifications to the experiment setup were required from that described in the previous Section 4.7, except to slide the EM38 parallel to the trellis from the mid-loop position until it was adjacent to the post. Just the Dripper and Grab wires were connected (D-G) in a 3 m panel configuration. Background and drift measurements were performed in the standard method by insulating all wires from the posts and taking a background reading ($V_B$) immediately after each primary measurement. The combined background/drift correction was then made by subtraction from the primary measurement. However, in order to extend the experiment to investigate the effect adjacent to a post with a panel connected either side (similar to what would occur in a real trellis), a second 3 m panel was connected to the target post.

The predicted response, when two adjacent panels are connected was estimated by doubling the predicted response off the edge of a single panel. This was justified by using symmetry and assuming that the vertical post acts as an electrical short-circuit (relative to the resistance of the wires), effectively allowing the eddy current in the two panels to be treated independently. To investigate the variation in mutual inductance between a single panel and the EM38 as it slides parallel to it, the FastHenry parameters were estimated from the geometry of the configuration.

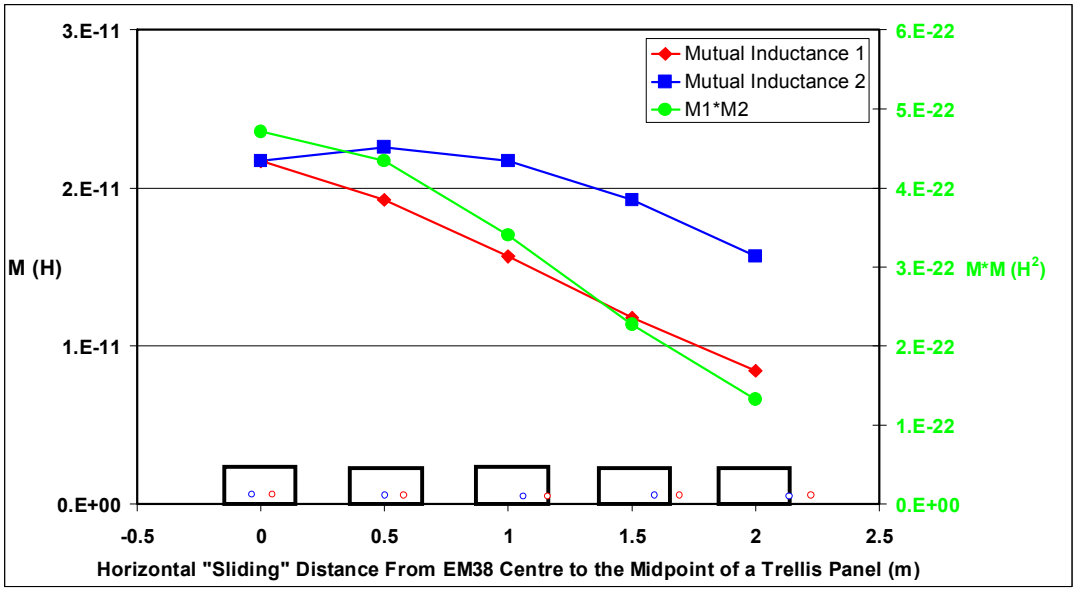


**Figure 4-33. Modelled EM38 mutual inductances to a trellis panel, where the distance axis is horizontal distance of the EM38 relative to the centre of the trellis panel, but parallel to both the trellis and the EM38. The responses are along a line parallel to, but 1.5 m horizontally away from, a single 3 m long D-G trellis panel. Mutual Inductance 1 is to the end of the EM38 that is still overlapping the main panel (blue circle) when the centre of the EM38 is opposite the edge of the panel. Mutual Inductance 2 is to the end of the EM38 that is outside the main panel (red circle) when the centre of the EM38 is opposite the edge of the panel.**

### *4.8.2 Results and Discussion: EM38 Response to a Trellis Panel Edge*

The calculated mutual inductances are shown in Figure 4-33. This graph shows the significant changes in mutual inductance at various positions along the panel. That is, when the EM38's midpoint is adjacent to the edge of the panel, one coil-end (blue symbol) of the EM38 has mutual inductance coupling with the panel loop of approximately two-thirds of the value when it is opposite the centre of the panel. However, for the other coil-end (red symbol, which has passed outside the edge of the panel), the value has dropped to approximately one-third. The total EM38 response is linearly proportional to the product of the two mutual inductances, one from each end of the coil (Equation 4-3). The value of this product ($M_1 \times M_2$, as shown in Figure 4-33) adjacent to the edge of the panel is approximately half that at the centre of the panel.

Figure 4-34 is a comparison graph between EM38 measurements adjacent to the centre of a panel compared to its edge. This graph shows that the response from the middle of the panel is significantly stronger than from its edge. In addition, the

response opposite the edge is still less than from the panel's mid-loop position, even when a second panel was connected to this edge. That is, the response from the middle of a single trellis panel is stronger than adjacent to a post in the middle of the two panels.

Figure 4-34 also shows the predicted responses from a panel's centre, its edge and from the middle of a double panel. The predicted response matches the measured response reasonably well.

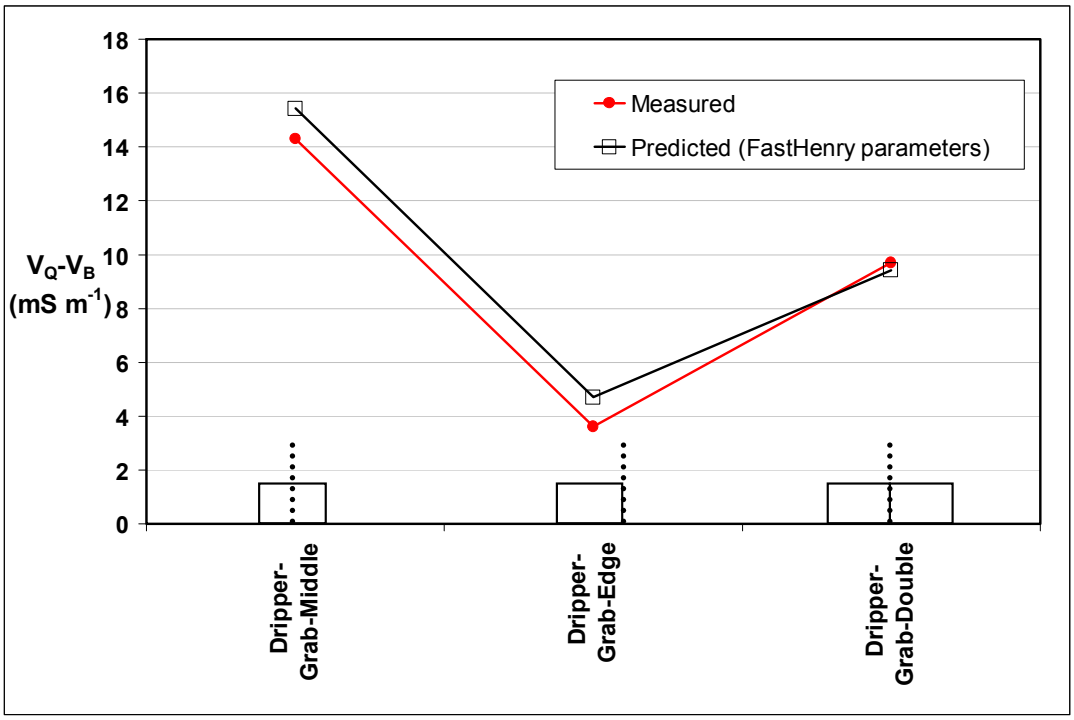


**Figure 4-34. Measured EM38 (vertical dipole) responses from the middle of a panel, from the edge of the panel and finally from the edge of a panel but with an additional adjacent panel connected. The dotted line in the schematic along the abscissa shows the measurement point relative to the panel(s). The responses are 1.5 m horizontally from 3 m long trellis panel(s).**

The addition of extra trellis panels will not significantly affect the EM38 response at the centre of a panel. This is because the addition of any extra panels will not significantly affect the mutual inductance, since the distances will be too great to the adjacent panel(s). In addition to the lack of contribution from increased coupling, the addition of extra panels will not significantly reduce the resistance of the system by allowing additional parallel current paths. This is because the vertical posts provide a relative electrical short compared to the resistance of the wires in the additional panels.

## 4.9 EM38 Response from a Single, Grounded Wire Loop

The experiments and modelling thus far have ignored the effects of the ground loop formed between the trellis loops and the earth via the posts. An experiment was devised involving a single wire ground loop configuration to investigate this. This grounding effect is expected to be comprised of the post-earth resistance interface, the earth resistivity within a few centimetres of the post, and the bulk earth resistivity.

### 4.9.1 Materials and Methods: EM38 Response from a Single Grounded Wire

The experimental configuration is shown in Figure 4-35. To investigate the significance of the post-earth interface, measurements were made both before and after water was poured into the hollow of the posts. This watering in was expected to affect the post-earth interface and the resistance in the first few centrimetres out from the post but not the bulk earth resistivity.

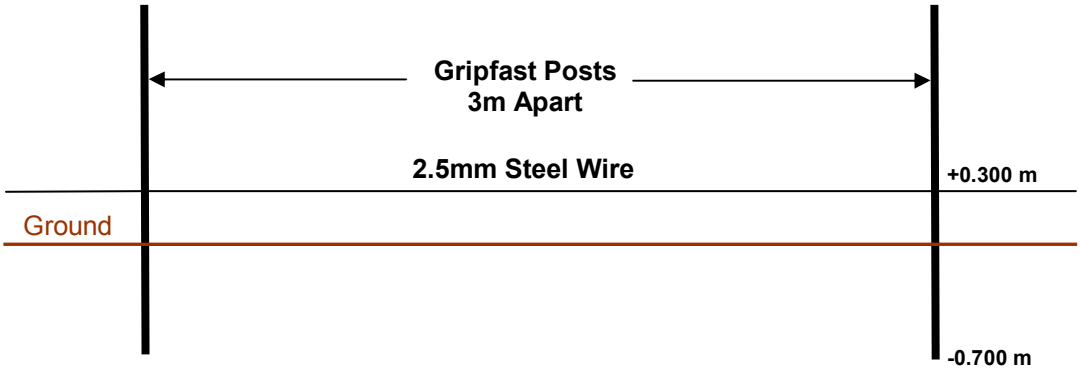


**Figure 4-35. Schematic of the earthed, single trellis wire experimental loop configuration.**

Figure 4-36 shows a photograph of the earthed single wire trellis loop experimental configuration. The wires were attached to the strainer posts with insulated tensioners (and insulated from other Gripfast posts in the test trellis) so that earthing only occurred through the intended pair of Gripfast posts (similar to the setup shown in Figure 4-20). With the wire in this configuration, EM38 measurements were taken on the ground, at increasing separations from, and parallel to, the wire (as shown in Figure 4-36). To investigate the significance of the post-earth conductance, these measurements were taken before the posts were

watered, after watering (20 L water), and again after being heavily watered (40 L water).

**Figure 4-36. Photograph of the single trellis wire, earthed via a pair of Gripfast posts. The EM38 is shown on a wooden graticule board to ensure that the EM38 was vertical and parallel to the wire. The instrument could then be precisely positioned at various horizontal separations from the wire.**

The predicted response was calculated using Equation 3-32 and the program FastHenry to calculate the mutual-inductance between the EM38 and the wire-earth loop, its self-inductance and the loop resistance. Initially, the earth segment of the loop was simulated in FastHenry by using its ground plane facility. Using this feature, a plane was defined horizontally by three points and assigned a conductivity value and a thickness. Internal to FastHenry, the ground-plane was represented numerically by a single layer of rectangular sub-blocks, each electrically connected to the adjacent sub-block. Both horizontal dimensions of the ground plane were arbitrarily chosen and were defined to be larger than the trellis panel. The conductivity of the ground plane was then chosen so that the amplitude of the predicted response matched the measured amplitude. This allowed the shape of the predicted and measured response (against distance) to be compared graphically.

### 4.9.2 Results and Discussion: EM38 Response from a Single Grounded Wire

Figure 4-37 shows the EM38 measured response from an earthed wire compared to the predicted response. The conductivity of the ground plane chosen (10 mS $m^{-1}$) to give a match between the predicted amplitude and the measured response was different to the actual EM38 bulk conductivity measured (in the absence of the grounding wire) of approximately 0 $\pm$2 mS $m^{-1}$. This is understandable due to complexities of the ground current distribution; the dominance of the post-earth contact; the earth within a few centimetres of the post; and the depth response of the instrument (shown in Figure 2-5). This concept (that the earth very close to the post dominates the current density distribution) is supported by the rapid rate of change of the EM38 response after watering the posts. That is, by pouring a small amount of water down the posts, a significant effect was detectable within minutes. The water would only have had time to affect the post-earth interface and to have soaked into the ground a small distance compared to the bulk of earth sampled by the EM38.

However, replacing the ground-plane with a simple resistor at an arbitrary depth of 9 m within the FastHenry circuit model gave the same predicted EM38 response shape as shown in Figure 4-37. To match the amplitude of the response, a resistor value of 705 ohms was required. This indicates that the combined effect of the post-wire resistance, the first few centrimetres of the soil adjacent to the post, and the earth's bulk resistance affects the impedance of the wire-earth system and, therefore, the amount of eddy current flowing in the wire.

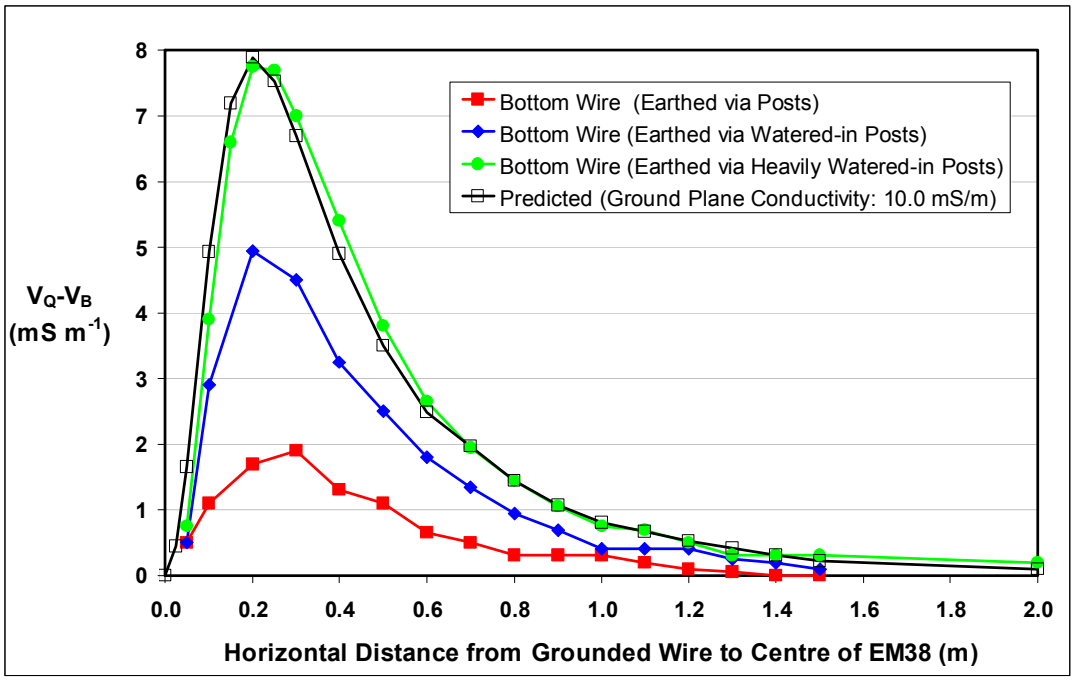


**Figure 4-37. EM38 vertical dipole responses from an earthed single-wire showing the increased response as the posts were progressively watered. The response from the bare-earth (with the wire insulated from the posts) was measured after each measurement and then subtracted.**

When this experiment was repeated with a single wire at a height of 1.93 m, there were no detectable responses at any horizontal separation. Assuming that the resistance provided by the extra post-length involved in this bigger circuit is negligible compared to the wire and earth resistances, it must be the proximity of the wire segment of the wire-post-earth loop to the EM38 that interferes with EM38's natural response from just the (low) ground conductivity.

The actual resistance of the post-wire-post-earth loop was measured using a signal generator (Hewlett-Packard Model P33120A, made in U.S.A) to pass a 14.6 kHz sine wave through a reference resistor and the wire-earth loop. The voltage drop across both the reference resistor and the earth loop was measured using a multimeter (Hewlett-Packard Model 34401A, made in U.S.A). Initial measurements yielded a resistance of 720 Ω, which was subsequently reduced to 708 Ω by progressively adding water to the ground via the hollow inside the posts. This is in good agreement with the estimated value of 705 Ω used within the FastHenry modelling to get the amplitude match shown in Figure 4-37 for heavily watered posts.

The electrical resistance between two points (in this instance, grounded posts), can be estimated using the equation for the voltage at a distance, *a,* from a single point source in a homogenous half-space. This equation (Reynolds 1997):

$$V_a = \frac{\rho I}{2\pi a} \qquad \text{Equation 4-5}$$

can then be used to estimate the resistance between two distant points:

$$R_a = \frac{\rho}{2\pi a} = \frac{1}{2\pi a \sigma} \qquad \text{Equation 4-6}$$

Applying this equation to the value of resistance estimated above at 705 Ω implies an apparent conductivity of approximately 0.15 mS $m^{-1}$. This very low value is consistent with the very low values measured by the EM38 at that test site; 2.0 mS $m^{-1}$ to -2.5 mS $m^{-1}$. The results are therefore considered feasible given that the low values are beyond the limit of the instrument's accuracy (approximately ±1.5 mS $m^{-1}$, Section 2.10). Given these limitations, the validity of the resistance value is feasible.

## 4.10 EM38 Response from a Multi-Grounded Wire

To investigate the effect of a multi-grounded wire simulating a steel trellis, a second test area was selected with higher, more typical, ground conductivity values, on the basis that it would provide more realistic ground path effects.

### 4.10.1 Materials and Methods: Multi-Grounded Wire

Before the Gripfast posts were inserted into this new test site, a detailed line of background conductivities was measured with the EM38 along the proposed line of the posts. The area selected had conductivities between 26 and 36 mS $m^{-1}$ as shown in the background conductivity profile of Figure 4-38.

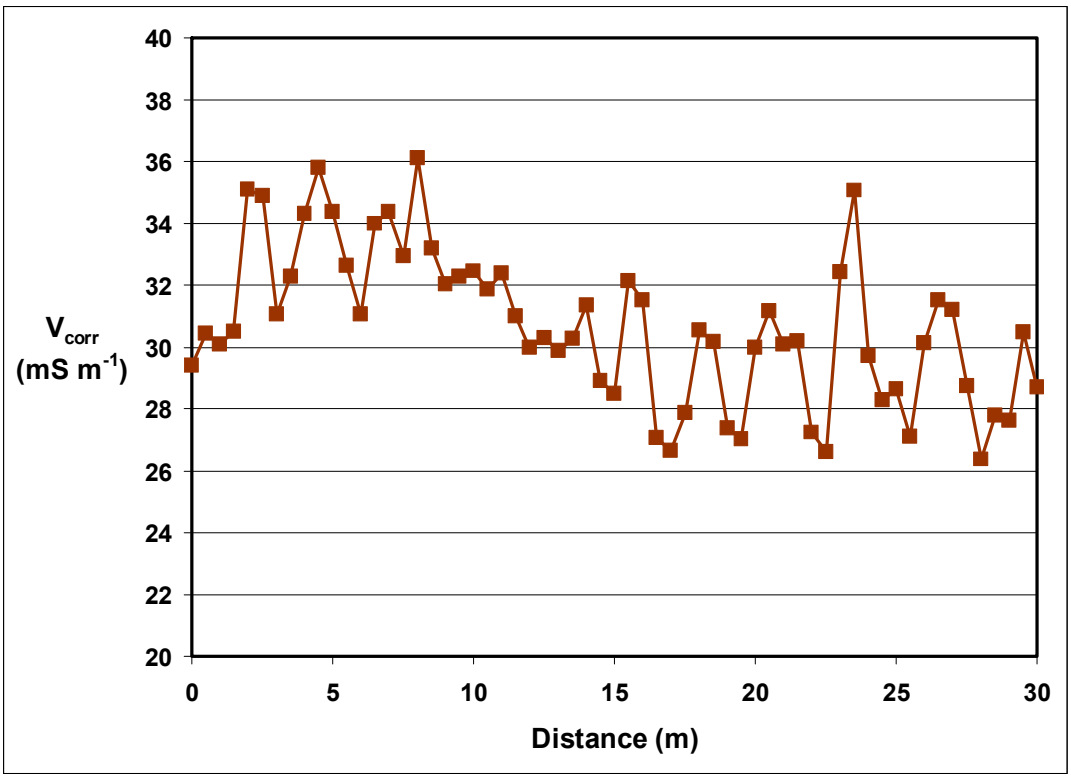


**Figure 4-38. Background EM38 conductivity (vertical dipole) readings along a linear transect, at the multi-grounded wire test site, before the emplacement of any posts or wire. Drift was corrected by subtraction of reference point values after each recording.**

To estimate the responses from the grounding of the wire only, the EM38 measurements were taken directly beneath the wire and midway between the 6 m spaced posts. The measurements were taken in this location because that placed the EM38 dipoles parallel to, and within, the plane of the wire-post loop. In this position and orientation there would be negligible loop coupling. In addition, at this measurement position, the effect from the posts was expected to be negligible due to their minimum 2.5 m separation from the EM38 Tx and Rx coils (Section 4.2). The wire height of 0.56 m limited the wire-only effect to less than 3 mS $m^{-1}$. Instrument drift was corrected by taking a measurement at a reference point after each primary measurement and subtracting the resulting calculated temporal variation from the primary value.

Equation 4-6 was used to estimate the resistance of the ground between posts from the measured apparent conductivity. By assuming that the trellis posts have negligible resistance compared to the wire and the earth, they are, therefore, practically an electrical short. As a result, the resistance of the wire and the ground between the posts, due to the apparent conductivity of the earth, is all that remains

to be considered. Substituting a value of 32 mS $m^{-1}$ (the average of the background EM38 conductivity values graphed in Figure 4-38) and a post separation of 6 m into Equation 4-6 gives a calculated resistance of 0.83 Ω. This value has a similar order of magnitude to the wire resistance (calculated by multiplying the resistance per metre determined for this type of wire of 34.12 mΩ $m^{-1}$ in Section 4.3 by its 6 m length) of 0.205 Ω. To investigate the importance of the post-earth interface, measurements were taken both before post watering and after post watering. The posts were watered by simply pouring fresh water (5 litres/post) down the inside of the Gripfast posts.

Figure 4-39 shows the multi-earthed, single-wire experimental configuration. To investigate the multi-earthed wire effect, the EM38 measurements were taken at the midpoint of Posts 2 and 3, again directly below the single wire, so that the loop coupling was negligible. The wire-to-post connections were shorted to overcome uncontrolled variations in the wire-post contact resistance.

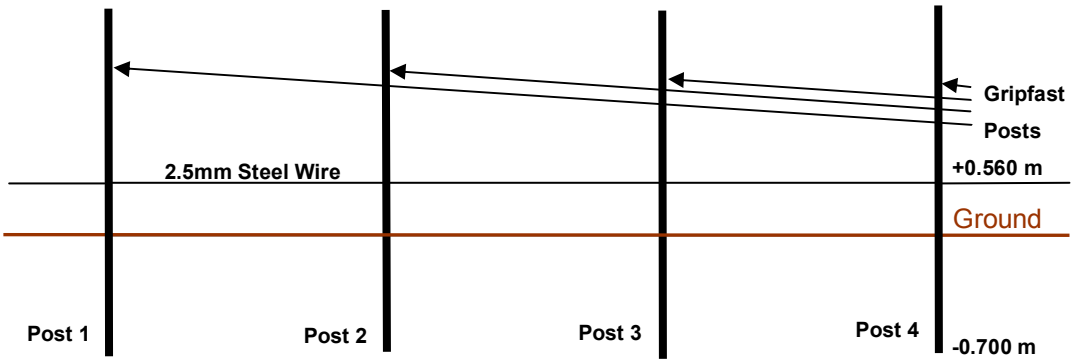


**Figure 4-39. Schematic of the multi-earthed, single-wire experimental configuration.**

### *4.10.2 Results and Discussion: Multi-Grounded Trellis*

As the EM38 instrument was placed below the wire, there was negligible coupling with the posts and wire part of the loop. However, Figure 4-40 shows that connecting the wire to ground (via the posts) increased the EM38 conductivity readings from the background value of 32 (labelled 'None') to 43 mS $m^{-1}$ (labelled '2-3'). This confirms that the trellis wire is increasing the apparent conductivity of the earth-wire system as measured by the EM38. Since the EM38 is not coupling with the trellis, the increased apparent conductivity must be due to the EM38's induced eddy currents in the ground finding an additional electrical path through the trellis posts and wires. This network, therefore, has less resistance

than would have been encountered in the earth-only system due to current path parallelism.

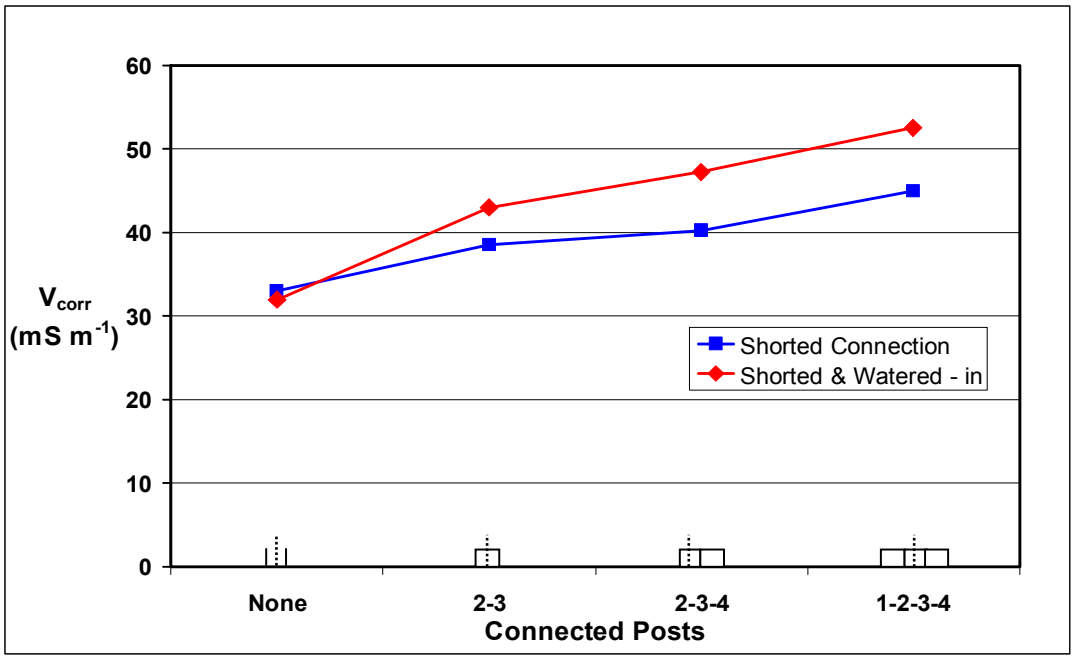


**Figure 4-40. Result of the multi-earthed, single-wire experiment. The posts were 6 m apart and the wire was 0.56 m above the ground. The EM38 measurements (vertical dipole) were taken directly below the wire at the midpoint between Post 2 and 3 (at the location of the dotted line along the graph's abscissa). Drift was corrected by subtracting the measured variation at the reference point.**

If the wire resistance was considered to be in parallel (electrically) with a resistor representing the earth, then the combined resistance would reduce by 25 % (i.e. a reduction from 0.83 Ω to:

$$\left( \frac{1}{\frac{1}{0.83} + \frac{1}{0.205}} \right) = 0.62\ \Omega,$$

where the values 0.83 and 0.205 Ω were calculated in Sub-section 4.10.1) which is comparable to the measured increase in apparent conductivity of 34 %. Whilst this is an overly simplistic view of what may actually be occurring to the current in the earth-wire network, it does, however, mean that the concept is feasible in terms of the observed increase in apparent conductivity.

This is an important aspect of the trellis effect on EM38 measurements because it may invalidate many of the assumptions used to derive the depth functions (Section 2.7) for a vertical dipole survey in the presence of a trellis; in particular,

the assumption that all the eddy currents are horizontal (in a homogenous or horizontally layered earth). If the eddy currents in the ground are being channelled upwards into the trellis posts, then they will no longer be horizontal. This may reduce the usefulness of any attempts to correct a trellis effect by simple subtraction of fixed corrections based on the trellis geometry and wire diameters, as the assumptions about the current flow through the earth may be too variable for correction.

If a single pair of connected posts can increase the EM38 response, then it is possible that the connection of more grounded posts will have a greater effect on the apparent conductivity. An increase in the apparent conductivity due to a multi-grounded wire is supported by Equation 4-6, which shows that the resistance between two posts is inversely proportional to the distance between the posts (for a homogeneous half-space). In addition, it can be postulated that, for a multi-post system, there will be even more parallel current paths (between the ground and the wire) that will further reduce the overall resistance of the earth-trellis system. Countering this effect will be the increasing resistance of the trellis wire (proportional to length).

Testing this postulation revealed that the addition of more connected grounding posts does increase the apparent conductivity (as shown graphically in Figure 4-40), where the result labelled '2-3-4' refers to connection of two adjacent panels (i.e. three grounding points). Furthermore, the response labelled '1-2-3-4' (i.e. four grounding points), is for the situation with three panels (i.e. a panel connected to either side of the central panel) and demonstrates an even greater increase in measured apparent conductivity. Clearly then, connecting more grounded posts into the system significantly increases the measured apparent conductivity (at least up to four connected posts).

Using the same experimental set-sup it was also found that the apparent conductivity was also significantly increased by simply watering the posts. However, with the wire disconnected, the EM38 did not detect an increase in the background reading, indicating that this watering had no significant effect on the apparent ground conductivity of the bulk earth. Hence, this increased response from the watering must be due to a reduction in the earth-post contact resistance. In fact, the addition of grounding posts significantly increased the measured

apparent conductivity, with the connection of four grounded posts (two either side of the of the measurement point) increasing the EM38 response by approximately a third. Furthermore, watering the posts increased the four-post EM38 response (over the background) by approximately two-thirds.

The significance of this result was confirmed by repeating the experiment in the low-conductivity ground (< 2 mS $m^{-1}$) used in an earlier test in Section 4.5. The results from the current experiment are shown in Figure 4-41. This result is for 3 m panels, which will have half the wire resistance, approximately half the earth-half-space resistance, and less mutual inductance coupling with the EM38 (compared to the 6 m panels). However, despite the resistive ground, the experiment still shows a significant increase in the response as more adjacent panels are connected. While the net effect shown in the results graph is over 12 mS $m^{-1}$, it effectively 'plateaus' at three (or more) connected panels and the increase is not practically significant for four, five, or six panels. Bearing in mind that the energising field will be near vertical, and therefore will have minimal coupling with the wire-post part of the loop indicates that the increased response must be due to ground eddy currents finding an easier parallel electrical path through the trellis. Furthermore, the fact that connecting adjacent panels significantly increase the response, even in resistive ground, supports the concept that the assumptions about the horizontal eddy currents may be invalid in proximity to a trellis, and that the EM38 values may not be obeying the well-published vertical dipole depth responses, in the presence of a trellis.

Supporting the above assertions, the '1, 2 & 5, 6' connected post response indicates that the relatively distant grounded posts can increase the EM38 apparent conductivity response from the ground. That is, with the connecting wires far beyond the influence of the EM38, the $EC_a$ has still been increased from 0 m $Sm^{-1}$ to ~9 m $Sm^{-1}$. This also highlights the complexity of the introduction of the grounded wires.

Consequently, it can now be concluded that the introduction of the grounded wires (as would be present in a real trellis scenario) interferes with the EM38's ability to sense the earth's true $EC_a$ via a combination of two interacting factors. Firstly, the trellis modifies the eddy currents in the ground by providing additional current

paths. Secondly, for the trellis eddy currents generated by direct coupling, the earth provides additional current paths.

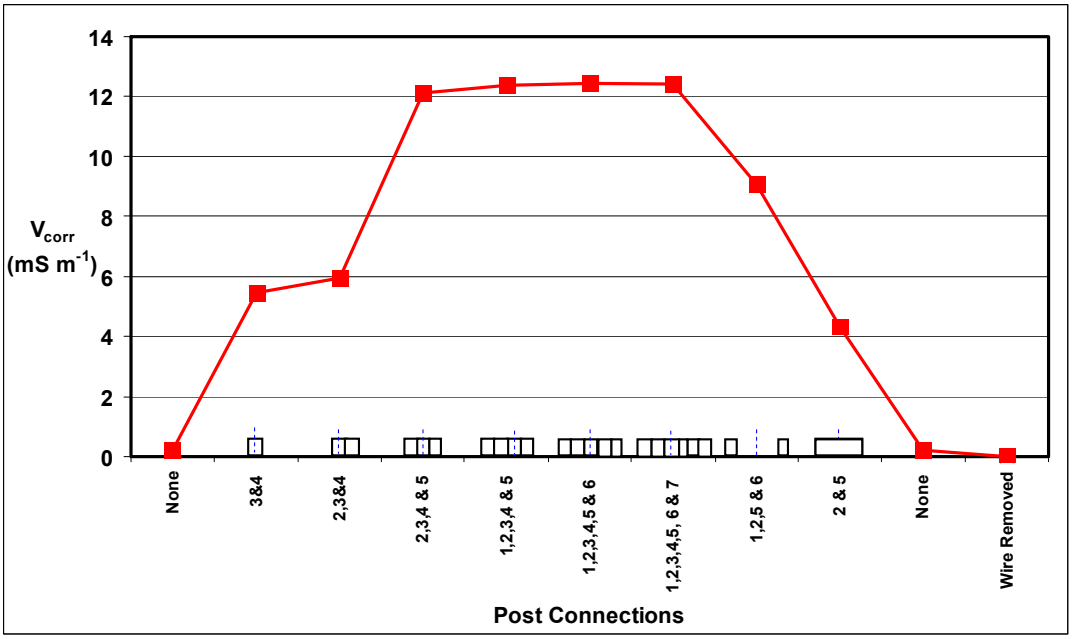


**Figure 4-41. Result of the multi-earthed, single-wire experiment, in resistive ground (~<3 mS $m^{-1}$). The posts were 3 m apart and the wire was 0.30 m above the ground. The EM38 measurements (vertical dipole) were 1.5 m laterally away from the mid-point between Posts 3 and 4 (with the EM38 parallel to the trellis). The posts were watered by pouring fresh water down the inside of the Gripfast posts. The wire/post connections were not shorted but were tensioned with the insulated mechanical tensioners. The blue dashed line along the abscissa indicates the measurement position relative to the numbered posts. (Drift was corrected by taking a measurement at a reference point between each measurement, interpolating the drift, and subtracting it from the primary measurement.)**

## 4.11 Importance of the Post-Earth Resistance

The significance of the earth-post contact resistance is due to the high current density at (and near) the grounding point. At a single current injection point on a homogenous half-space, the current flows radially out equally in all directions within that half-space. The current density, $J$, on a hemisphere of radius, $a$, from the point source is given by

$$J_a = \frac{I}{2\pi a^2}. \qquad \text{Equation 4-7}$$

Consequently, the current density is highest close to the point source. Therefore, the variation in resistance of a small volume of earth close to the point source has a larger affect compared to the same volume of earth at a greater distance. To put

this in perspective, one $cm^3$ of earth, one cm from a point source, has a similar effect to 10 000 $cm^3$, one m from a point source.

In practice, this is a significant fact when interpreting the interference effect of a trellis system on an EM38 survey. A vertical dipole EM38 survey assumes zero contribution from the surface, with most of contribution from a depth of ~0.4 to 1.0 m (Section 2.6). However, the presence of an earthed trellis will not only cause an over-estimation of the earth's apparent conductivity but the magnitude of this effect will significantly depend on the near-surface soil moisture around the posts. That is, from a vineyard surveying perspective, EM38-detected variations conventionally attributed to bulk soil conditions at approximately 0.4 to 1.0 m deep, could, in reality, be dramatically affected by shallow conditions, such as cultivation along the trellis line, mulch application, recent rains and drip irrigation along the trellis.

## 4.12 Conclusions

Experiments with individual Gripfast posts confirmed that their effect on the EM38 (in isolation) is negligible at separation distances greater than 1.0 m. At separations less than this, the post-earth system's response magnitude becomes significant and more complicated, with reductions in EM38 response observed closer than 0.2 m, the magnitude decreasing further with decreased galvanic resistance between the post and the earth.

The effect of a straight, horizontal, isolated 3 m length of2.5 mm steel trellis wire was practically negligible at separations over 0.5 m and this response was further dependent on the relative vertical position of the EM38 and the wire. This confirmed the expected result, enabling the ignorance of this factor from EM38 surveys.

The EM38 response to a large rectangular loop of wire 3 m long by 2 m high (simulating the area and orientation of a trellis panel) was successfully predicted using the analytical formula developed in the previous chapter (although its proportionality constant required refinement for application to the large trellis sized loops tested in this chapter). As part of this prediction process, the FastHenry software was successfully used to estimate the loop's self-inductance, its resistance

and the mutual inductance from the EM38 Tx and Rx to the Target Loop, for substitution into the analytical formula.

Contact resistance between the wire and posts, estimated to be approximately 40 % of the total loop resistance, played a dominant role in the EM38's response magnitude and variability. In fact, it was discovered that the trellis interference on the EM38 was linearly proportional to loop resistance (for low resistances, i.e. excluding the earth). This sensitivity to the loop resistance is important, as both thinner wires and/or increased contact resistances, will significantly increase the trellis interference to the EM38. However, it is the variability of the contact resistance, which will make post-processing corrections for trellis interference more difficult, and corrected results nosier.

Measurements with EM38 suspended 1 m above the ground and moved along the horizontal and vertical axis of symmetry of the 3 m by 2 m vertical loop (i.e. adjacent to its 2-D centre) gave negligible responses at all separations greater than 0.5 m. This was expected due to the 2-D symmetry and the vertical dipole energising field giving a net zero flux through the loop.

Investigating the relative contribution of sub-loops within a real trellis panel revealed that sub-loops containing the lowest Dripper wire made the greatest contribution to the EM38 response. This is understandable as it is the wire closest to the EM38 (i.e. representing an edge of the coupling area close to the EM38). Loops containing both the top (Foliage) and bottom (Dripper) wire gave the strongest responses, consistent with the notion that the response is proportional to the area of the loop and its proximity to the EM38 (provided the geometry allows coupling). Inclusion or omission of wires other than the top (Foliage-2) and the bottom (Dripper) had very little influence on the EM38 interferences.

The effect of the ground on the EM38 response to a trellis was found to be the most variable parameter, and the most difficult to predict (and therefore, to correct). The post-earth interface and the earth within approximately a decimetre of the posts is a critical factor in determining the response.

Modelling a grounded pair of posts gave an adequate response curve match using either a large horizontal conducting layer or a deep single resistor. This indicates

that the earth part of the segment of the post-earth-post-wire loop is contributing to the loop conductance and thereby to the trellis interference on the EM38.

A simple experiment with a grounded pair of posts connected by a steel trellis wire showed that the introduction of such a grounded system increased the measured apparent conductivity. This concept can be understood in terms of the wire providing a parallel current path for the eddy current induced in the earth. Significantly, the connection of a grounded wire into the earth being measured by the EM38 reduces the validity of some of the vertical depth relationships commonly assumed for EM38 surveys in homogenous or horizontal layered earths. Consequently, attempts at correcting for the trellis effect may be limited due to variability of the earth effect and invalidation of assumptions about what part of the earth the EM38 is measuring. The addition of two more grounded posts (to make a total of four) increased the EM38 response of ~30 %. Watering in the posts increased the response from the four, grounded posts by ~70%. This is significant as it is representative of a real trellis row in moderately conductive ground (~32 mS $m^{-1}$). In resistive ground, the effect of the grounded posts was also significant. Importantly, it was argued that, from the high concentration of current density at the grounding point, local, near surface variation in conductivity around the posts could significantly affect EM38 measurements normally attributed to bulk soil conditions between depths of ~0.4 to 1.0 m.

The introduction of distant grounded posts (i.e. >4.5 m) also contributed significantly to the trellis interference by modifying the induced ground eddy currents. However, increasing the number of posts to more than four (i.e. a central panel with a panel either side) did not practically increase the interference effect.

# Chapter 5 The EM38 Response to Multi-Row Trellises

## 5.1 Introduction

Chapter 3 and Chapter 4 investigated the EM38 responses to various components of a steel trellis. Sections 4.2 and 4.3 concluded that the posts and wires (respectively) in isolation have a negligible effect at practical survey distances from the trellis. Section 4.4 presented an analysis of the relative effect of a large trellis-sized rectangular loop of wire, while Section 4.5 covered more realistic trellis loops made up of wires and posts. This was first limited to simple rectangles, and the complexity was then increased with the addition of multiple wires and then multiple panels (Sections 4.6, 4.7 and 4.8). In Section 4.9 the analysis included the ground paths as segments of the coupled loops. The investigation started with a single pair of grounded posts (connected by a wire), with the addition of more posts increasing the response (Section 4.10).

This chapter will complete the next and final step in building the understanding of the influence of a real trellis system, that is, a trellis with multiple rows. However, rather than assembling multi-row trellising from scratch for this investigation, an analysis will be made of data from Lamb, Mitchell and Hyde (2005). This data set had the advantage of containing a bare-earth response before their multi-row test trellis was constructed. In fact, these researchers surveyed the bare-earth, the dripper-wire-only trellis, the all-wire trellis and then the bare-earth again, all in one day. In this way, any significant changes in the ground conductivity were avoided, for example, rain or large temperature variations which can occur when data is collected over different days. For the purposes of this chapter, a brief description of the test site and survey protocols employed by Lamb, Mitchell and Hyde (2005) is firstly given. Following a brief revision of the original experimental methods, the software and procedures specific to this present work are described. The chapter then moves to a discussion of the trellis-induced interference with reference to the findings of the previous two chapters, aiming towards a post-processing interference correction strategy.

### 5.1.1 Kirby Test Site: Survey Procedure and Data Processing

The 'Kirby Farm' test configuration described by Lamb, Mitchell and Hyde (2005) is depicted in Figure 5-1. This map illustrates that each planned trellis row had four Gripfast posts spaced 6 m apart. The configuration comprised three sections, each with different inter-trellis lane spacings. The first section (left-hand third of Figure 5-1) had five inter-trellis lanes spaced 2.5 m apart. The second section (central third of Figure 5-1), contained five lanes at 3.0 m apart, and the final section (eastern third of Figure 5-1), five lanes at 3.5 m apart.

To survey the site, a four-wheel motorcycle was used to tow the EM38 in linear transects between the rows for each stage of the trellis construction (Lamb, Mitchell & Hyde, 2005). Whilst a dGPS was used as part of the continuous data logging apparatus to position the measurements, the transects were navigated along pre-marked painted lines on the ground, to ensure the EM38 sensor was towed (as close as practical) along the same traverse relative to the trellis rows for each survey. For example, Figure 5-2 shows the dGPS track (green-line) for the survey with the dripper-wire only emplaced, while the all-wire track (red-line) is shown closely following that previous track.

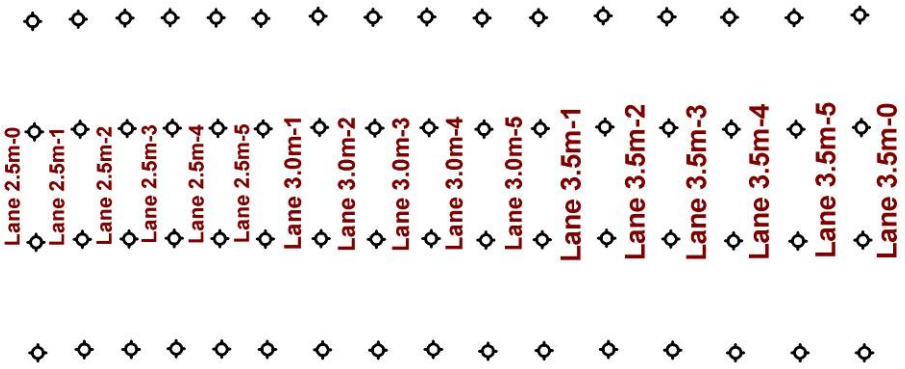


**Figure 5-1. Layout of the Gripfast posts (black symbols). The posts are 6 m apart, north-south (local) and the left hand five inter-trellis lanes are 2.5 m apart. The central five are 3 m apart and the right-hand five are 3.5 m apart. The lanes' labels' prefix indicates the row spacing and a suffix number indicates the lane number (from left-to-right) within that spacing group. Lane 2.5m-0 represents a profile 1.25 m outside the western trellis row. Lane 3.5m-0 represents a profile 1.75 m outside the eastern edge of the trellis area.**

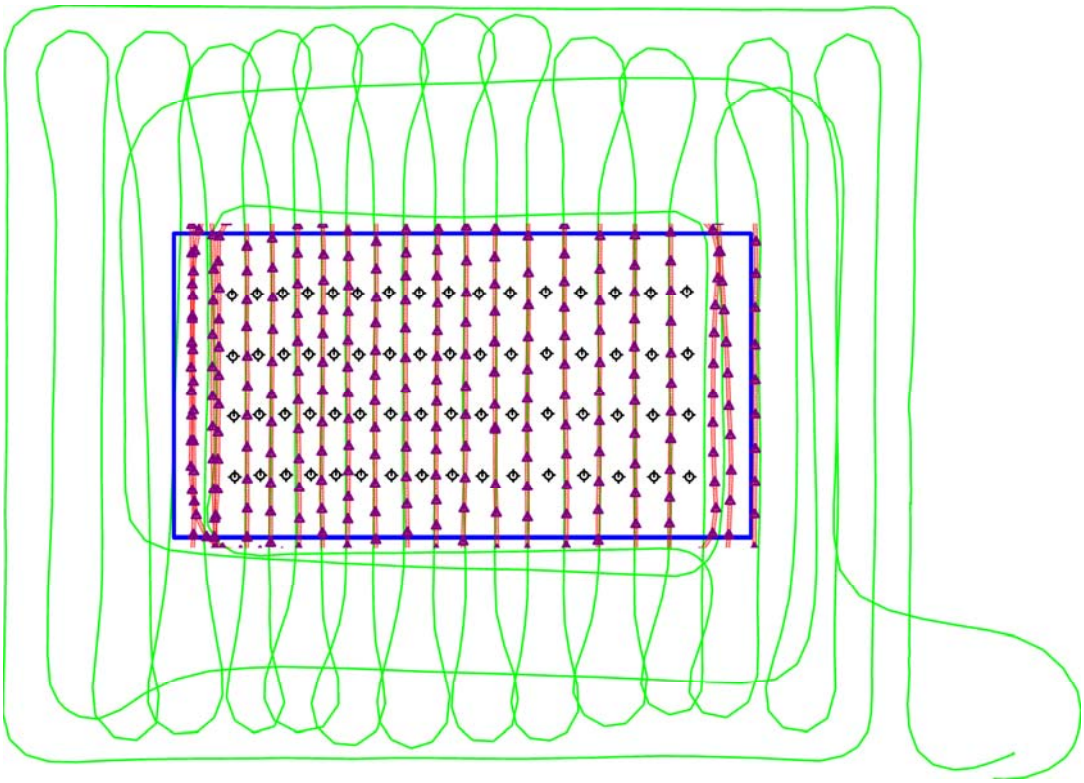

**Figure 5-2. Map of the Kirby Test Site showing survey tracks relative to the Gripfast post locations (black). The GPS track for the dripper-wire survey is the solid continuous line (green). The red GPS track is the all-wires survey (masked so that it is only visible where it passes inside the trellised area). The purple triangles represent the original data points (prior to correction for lag). The rectangle (blue) is the mask area used to exclude data outside the influence of the trellis. The posts are 6 m apart, north-south (local). Local north is at the top of the figure.**

For the purpose of this present analysis, the original georeferenced data (used as a basis for the publication by Lamb, Mitchell & Hyde 2005) was made available by the authors in dbf, Microsoft access format. The dataset, comprising EM38 response (mS $m^{-1}$) and dGPS coordinates collected on a one-second time-base, was imported into Microsoft excel. Analyses of the data were undertaken by utilising the geophysical data processing and presentation software Oasis Montaj (Version 7, Geosoft Inc. USA).

Preliminary corrections were made on the survey equipment (see Figure 1-1a) employed by Lamb, Mitchell and Hyde (2005), for the physical separation between the dGPS antenna and the EM38 unit. The gridded and profiled data set that these preliminary corrections yielded were inspected graphically to determine if, in addition to antenna layback, a time lag in the data with, reference to position, existed. This time lag was determined to be 0.25 s; a value within 11 % of the 0.28 s value found by Sudduth, Drummond and Kitchen (2001). Oasis

Montaj's time lag correction subroutine (lag.gx) was used to reduce the average error to an acceptable level (i.e. the lateral variations matched visually across transects).

Next, the data was refiducialled from its time-base to a distance-base (interpolated and resampled, with linear interpolation, at an along-track distance interval of 0.2 m). This prepared the data for the final correction of the EM38 to GPS antenna layback of +3.1 m. However, the original sparsely sampled data (shown by the location of the raw data positions in Figure 5-2) required interpolation to the relatively fine distance interval of 0.2 m to facilitate accurate time and distance lag corrections. Oasis Montaj's along-track distance offset subroutine (UXlag.gx.) corrected for this layback.

The data was then warped (within Oasis Montaj) from the projected coordinate system to a local grid system. This simplification provided more convenient data presentation. For example, the south-west Gripfast post became localised to 6 mE, 6 mN and the eastern most trellis had an easting of 51 mE (local).

The data set was then gridded to a 0.05 m square mesh using Oasis Montaj's minimum curvature gridding (internal tension: zero; weighting power: 2) and masked (to the rectangle shown in Figure 5-2), to exclude data outside a 6 m buffer around the posts. This data set was presented in coloured map form, adopting a consistent colour assignment throughout the chapter to facilitate comparisons between each set of EM38 responses. For generation of linear (1-D) profiles, inter-trellis profile data was extracted from the gridded data by taking the column of data with the appropriate easting.

## 5.2 Kirby Test Site: EM38 Survey Repeatability Result

Figure 5-2 shows the GPS track for the dripper-wire only survey compared to the survey with all the wires emplaced. The two recorded tracks down the inter-trellis lanes were found to match well, considering the GPS (Trimble Pathfinder PRO XRS DGPS, TSCe controller: Trimble Navigation Limited, Sunnyvale California: www.Trimble.com) with a standard correction service (Omnistar satellite corrections; Omnistar, member of the FUGRO group: www.ominstar.com.au) is quoted as having an accuracy of <1 m. However, even small deviations in recorded track may generate data-artefacts in the created 2-D maps, owing to the map

generation process itself. Therefore, to compare the repeatability of the data collection and processing, a difference grid for the bare-earth data set before the trellis construction, and then the bare-earth data set after dismantling the entire trellis, was calculated. The colour image of this difference grid (Figure 5-3) is a comparison of the first survey and the last survey of the day. Table 5-1 lists the statistics for this difference grid, and shows a mean difference of just 0.4 mS $m^{-1}$, with a standard deviation of 0.7 mS $m^{-1}$. In effect, the two EM38 surveys over the same rectangle of bare earth produced the same maps, well within the quoted accuracy of the EM38.

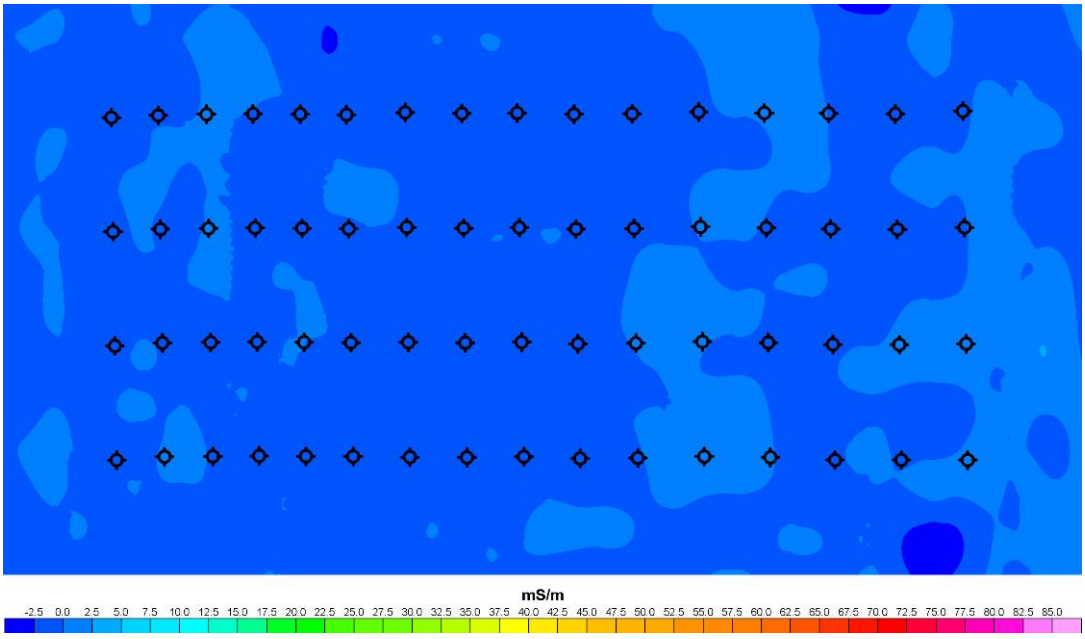


**Figure 5-3. Colour image map of the difference between the EM38 (vertical dipole) survey of the bare earth pre- and post-trellis construction. (Kirby Test Site showing the Gripfast post locations, black symbols, 6 m apart north-south).**

**Table 5-1. Statistics of the difference grid of the bare earth pre-, and post-trellis construction (showing the repeatability of the EM38 surveying).**

| Difference Grid Statistical Variable | Difference Grid Statistic |
|---|---|
| **Number of Grid Points / Point Separation** | 684600 / 0.05 m x 0.05 m |
| **Grid Area** | 1712 $m^2$ |
| **Minimum / Maximum Difference Value** | -4.3 mS $m^{-1}$ / +2.5 mS $m^{-1}$ |
| **Mean Value {Standard Deviation}** | 0.4 mS $m^{-1}$ {0.7 mS $m^{-1}$} |

## 5.3 Kirby Test Site: EM38 Bare Earth and Dripper Wire Survey

Figure 5-4 is the map of the bare-earth (BE) survey result (pre-trellis construction). This test area's apparent conductivity was relatively uniform (standard deviation: 1.8 mS $m^{-1}$) with moderate magnitude (mean apparent conductivity: 38 mS $m^{-1}$).

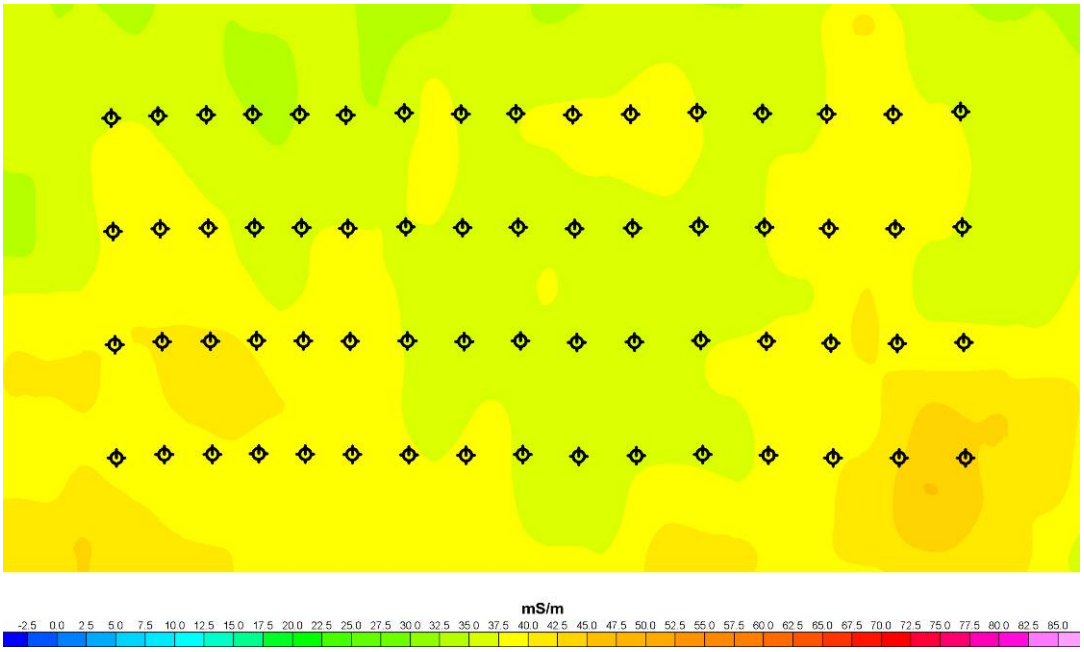


**Figure 5-4. Colour image map of the vertical dipole EM38 survey of the bare-earth before any trellis emplacement. (Kirby Test Site showing the Gripfast post locations, black symbols, 6 m apart north-south).**

Figure 5-5 is a map of the dripper-wire (DW) only grid minus the bare-earth (BE) grid. Figure 5-6 represents this same data (DW-BE) but as a series of profiles down the centre of each inter-trellis lane. In effect, this data is the conductivity change due to a network of grounded wires, enabling an extension of the discussion of multi-grounded wires in Section 4.10. This data set confirms some of the conclusions drawn from the investigations described in Section 4.10, namely:

1. The grounding of the wires (along the trellis rows) significantly increases the EM38 apprent conductivity measurements compared to that of the bare earth;

2. The relative maxima adjacent to the central panel, compared to edge panels (Figure 5-6), confirms that grounding multiple panels increases the EM38 effect compared to just a single panel (for example, compare the responses at 15 mN to 9 mN and 21 mN);

3. The effect on the EM38 survey with the trellis on just one side of the traverse is always less than that along a traverse with a trellis on either side (Figure 5-7); and

4. Closer trellis rows generally produce higher EM38 responses. Figure 5-6 shows that four out of the five 2.5 m spaced trellis-profiles peak at between 46 mS $m^{-1}$ and 51 mS $m^{-1}$, whereas for the 3.0 m spaced trellises, four out of the five profiles peak at between 29 mS $m^{-1}$ and 38 mS $m^{-1}$. For the 3.5 m spaced trellises, four out the five profiles peak at between 22 mS $m^{-1}$ and 26 mS $m^{-1}$.

In addition to reinforcing previous findings about single row EM38 trellis effect, the examination of multiple row trellising revealed furhter patterns in the EM38 interference response. Namely:

1. The further into the trellised area and away from its edge, the stronger the response. For example, Figure 5-5 shows a clear 2-D maxima on the second lane from the left (Lane 2.5m-2). Similarly, there is a 2-D maxima in the fourth lane of the 3.0 m spaced lanes (Lane 3.0m-4). However, there are several exceptions to this pattern. A notable exception is the peak for the 3.5 m spaced trellis lanes occurring in the last lane (Lane 3.5m-5), on the edge of the trellis network; and

2. Whilst Figure 5-5 shows distinct trends, variability in near-post earth resistance, post-earth resistance, and post-wire resistance, most likely play a role in the noise evident in these trends. For example, the profile peak for Lane 2.5m-5 is over 10 mS $m^{-1}$ lower than the peaks of the other four 2.5 m spaced lanes (see profiles in Figure 5-6). This may be due to poor wire-post contact along the entire row (for example, due to an improperly tensioned wire) rather than an isolated, poor post-ground contact. Conversely, the anomalous low in profile Lane 3.5m-3 appears to be associated with a particular post (at 44 mE, 18 mN in Figure 5-5 and Figure 5-8).

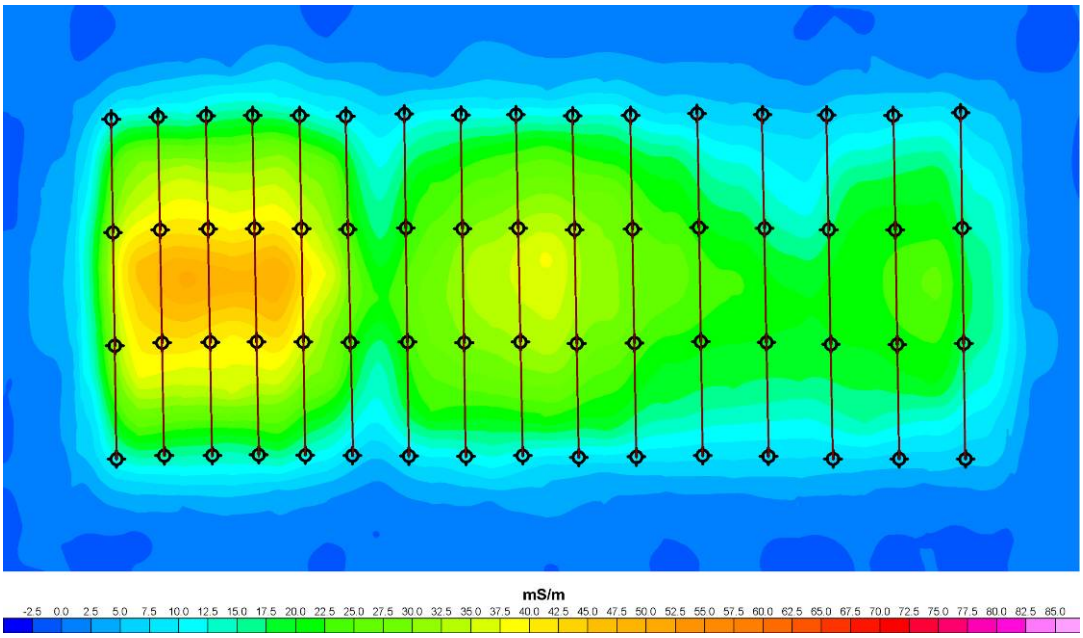


**Figure 5-5. Colour image map of the EM38 (vertical dipole) survey of the dripper-wire only survey minus the bare-earth survey. The brown line represents the wires connecting the grounded posts. (Kirby Test Site showing the Gripfast post locations in black, which are 6 m apart north-south).**

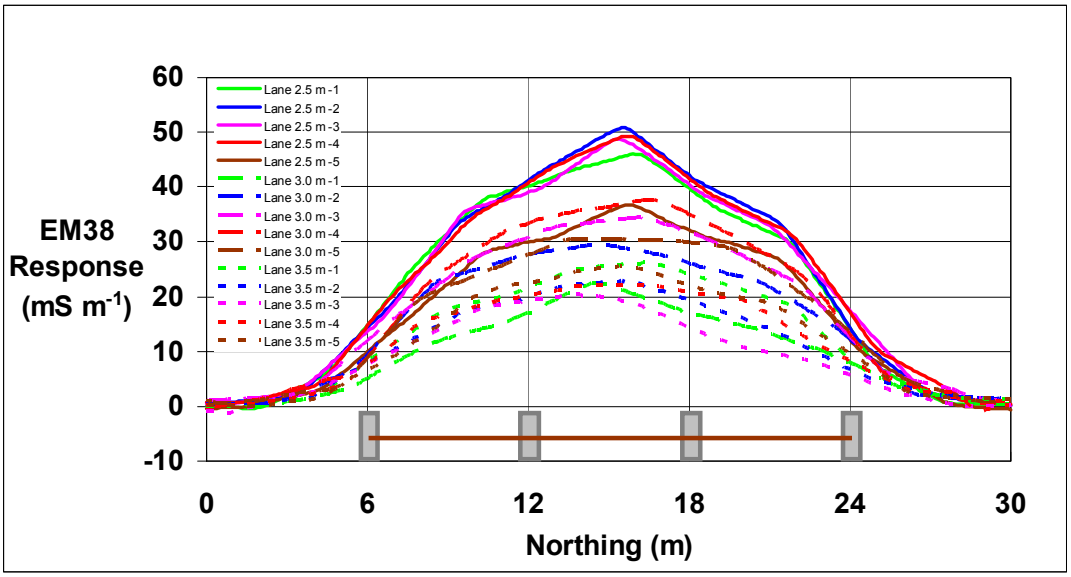


**Figure 5-6. Profiles of the dripper minus bare-earth response for all lanes. The grey rectangles represent the position of the grounded posts and the brown line indicates that they are connected by a single wire.**

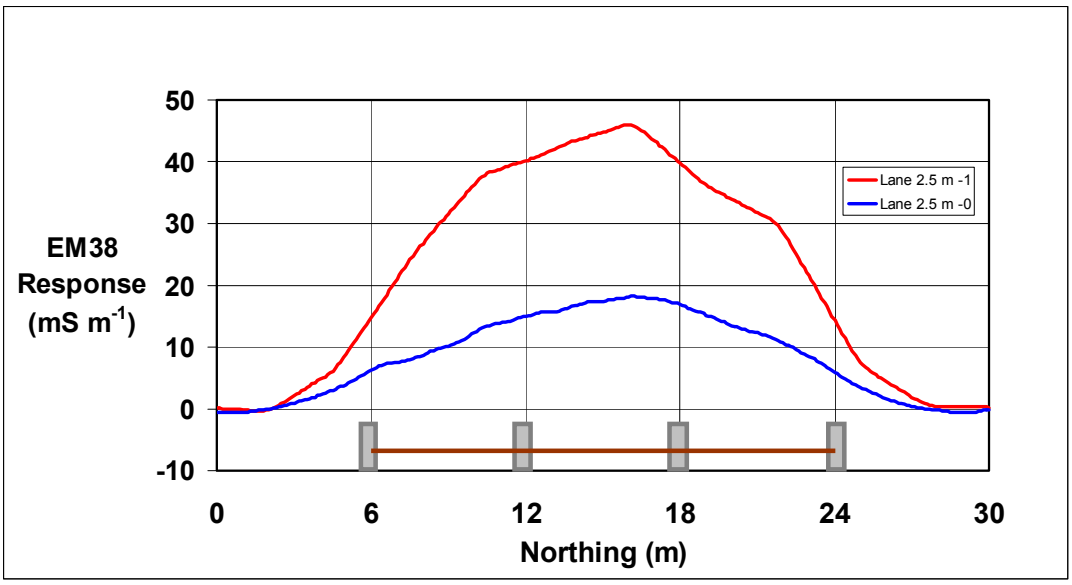


**Figure 5-7. Profiles of the dripper minus bare-earth response for the lane just outside the western edge of the first trellis row (Lane 2.5m-0) and the first lane inside the trellising (Lane 2.5m-1). The grey rectangles represent the position of the grounded posts and the brown line indicates that a single wire connects them.**

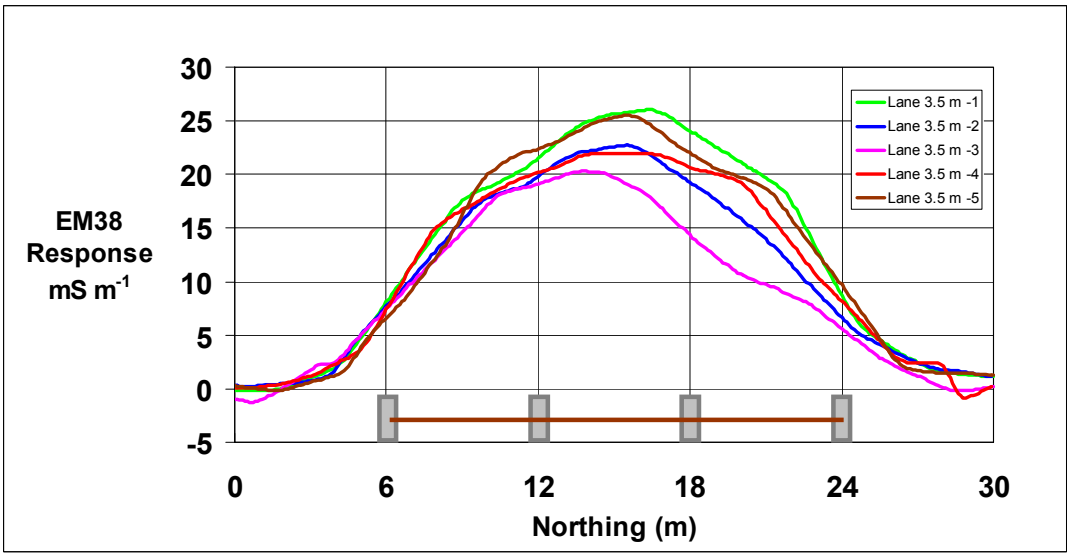


**Figure 5-8. Profiles of the dripper-wire minus bare-earth response for the 3.5 m spaced lanes. The grey rectangles represent the position of the grounded posts and the brown line indicates that a single dripper wire connects them.**

## *5.4 Kirby Test Site: EM38 All Wire Survey*

Figure 5-9 shows the map of the all-wire survey grid minus the dripper wire survey grid (AW-DW). This AW-DW image represents the effect of the all-steel trellis due to the loops made up of the wires and steel posts, and based on the observation of Sub-section 4.10.2, can be considered as having ignored the increase in the grounding effect by the addition of extra wires. Whilst this is a simplistic

separation of the two effects, there are nonetheless several patterns in this map that are consistent with the findings of the previous chapter:

1. The closer spaced trellis rows give significantly higher responses. This is consistent with all previous investigation conclusions that horizontal separation is a major controlling factor of the trellis interference on the EM38;

2. There is no strong evidence that the internal panels of the trellis give stronger responses than those near the edge for the 3.0 and 3.5 m spaced trellis. There is some evidence that there is a stronger response deeper within the 2.5 m spaced trellis. This must be due to earthing effects being enhanced by the additional wires. Therefore, it is possible that the additional wires in the trellis could have increased the grounding effect by providing more conductance due to parallelism. This shows that the initial assumption, that grounding effects can be simply separated from above-ground loop effects, is not completely valid, at least for the 2.5 m spaced trellis case;

3. There are irregularities or anomalies in the pattern of responses. For example, Figure 5-10 shows a strong, single anomaly in Lane 2.5m-2, mid-panel at 9 mN. This anomaly may be due to local post earthing effects combined with earthing of multiple trellis rows (nesting). However, in Figure 5-11, the whole profile of Lane 3.0m-1 is stronger than all other 3.0 m spaced lane profiles. This must be due to the increase in the nested earthing effect provided by the additional wires. This same effect, while not as obvious, appears in the first lane of the 3.5 m spaced lanes (Lane 3.5m-1) compared to the other 3.5 m spaced lanes. This indicates that it is a function of the trellis spacing, combined with the 2-D, nested earthing effect. It also highlights the variability of the earthing and wire-post contacts.

4. There are consistent relative maxima adjacent to the mid-panels compared to adjacent to the posts (see Figure 5-10; Figure 5-11 and Figure 5-12). This confirms the conclusions made in Section 4.8 about the test trellis and the predicted responses.

5. The minima and maxima do not occur precisely opposite the post and mid-panel, respectively. This is most likely attributable to either:

   a. Positioning error associated with the dGPS;

   b. Error in adjusting for timing differences between the EM38 and dGPS; and/or

   c. Surface interpolation artefacts resulting from under sampling. That is, the dGPS sampling interval of one-second, combined with the average survey speed of 10 km $hr^{-1}$ ±2.8 $ms^{-1}$, produces a relatively coarse, on-ground sampling interval of approximately one-half of a panel-length.

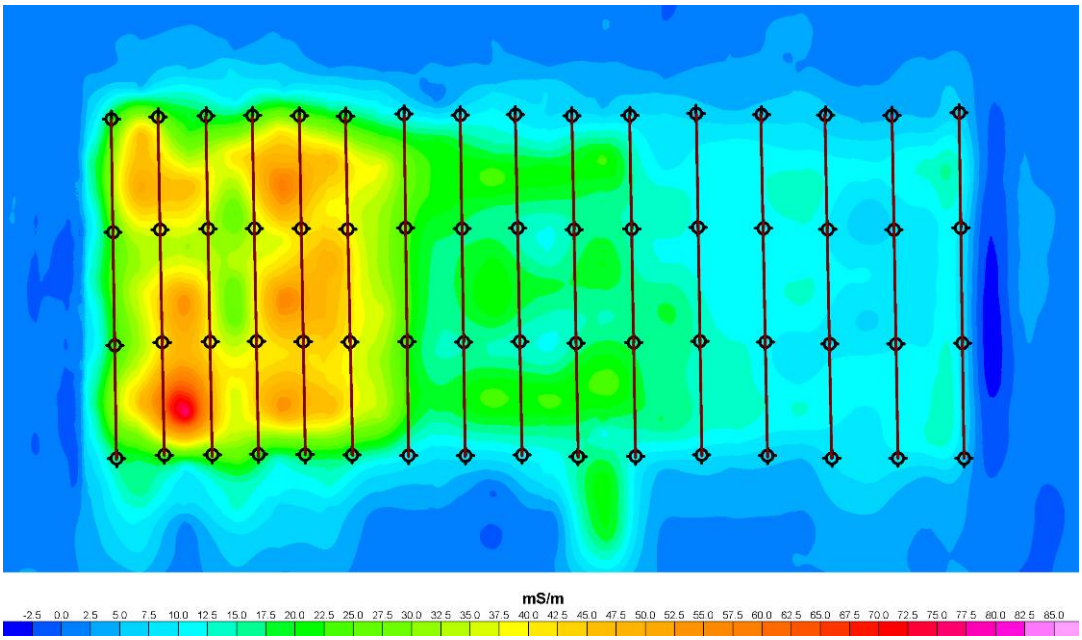


**Figure 5-9. Colour image map of the vertical dipole EM38 survey of the all-wire minus the dripper wire only survey (AW-DW). The brown lines represent the wires connecting the grounded posts. (Kirby Test Site showing the Gripfast post locations in black, 6 m apart north-south).**

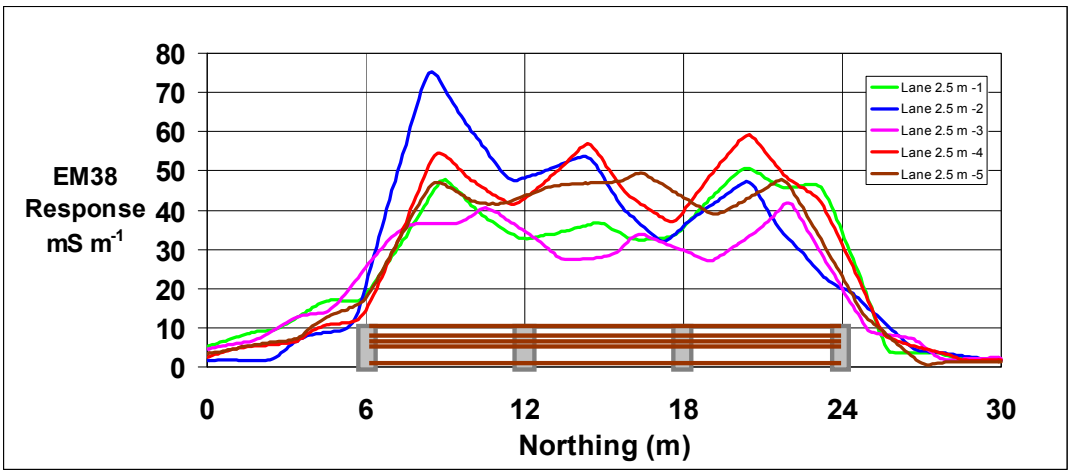


**Figure 5-10. Profiles of the all-wires minus dripper-wires response for the 2.5 m spaced lanes. The grey rectangles represent the position of the grounded posts and the brown lines indicate that all the trellis wires were connected.**

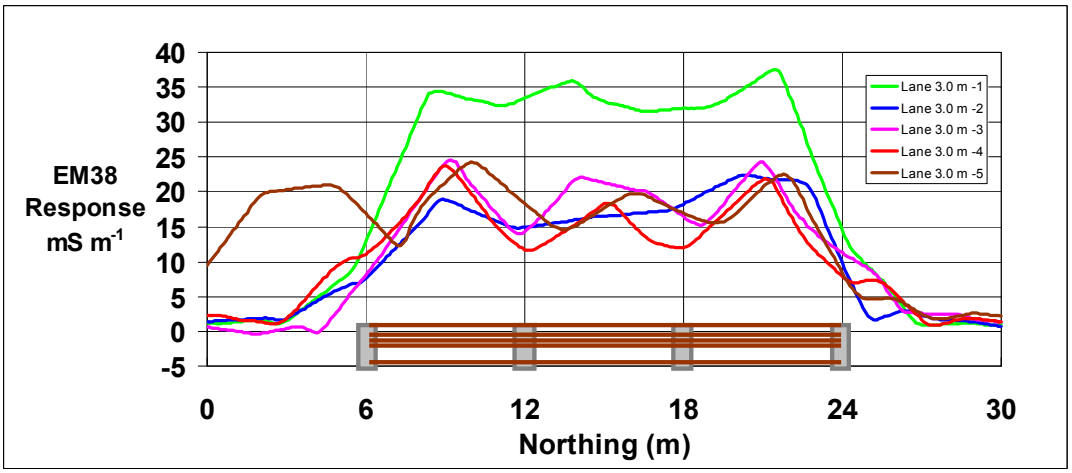


**Figure 5-11. Profiles of the all-wires minus dripper-wires response for the 3.0 m spaced lanes. The grey rectangles represent the position of the grounded posts and the brown lines indicate that all the trellis wires connect them.**

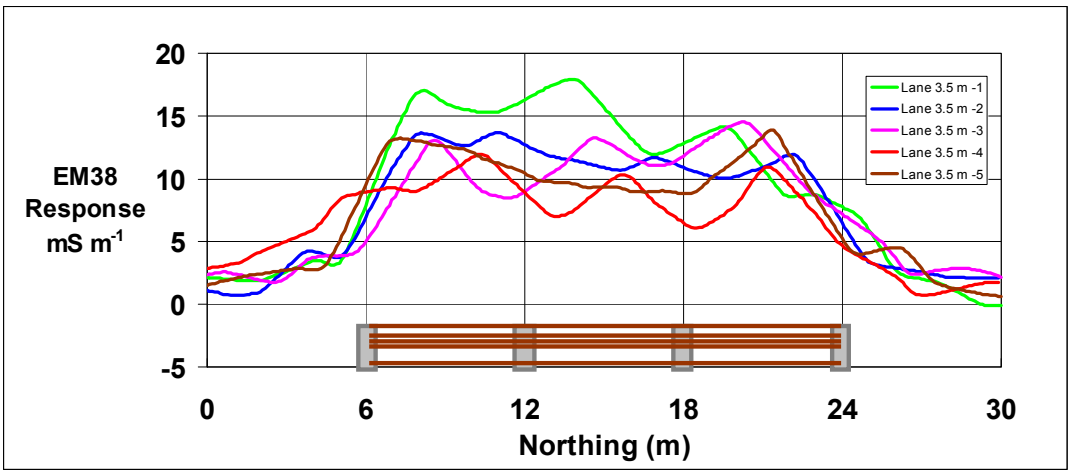


**Figure 5-12. Profiles of the all-wires minus dripper-wires response for the 2.5 m spaced lanes. The grey rectangles represent the position of the grounded posts and the brown lines indicate that all the trellis wires connect them.**

## 5.5 Comparison of the Trellis Minus Ground Loop Data with FastHenry Predictions

Previously, in Section 5.4, the AW-DW grid was found to be an approximate representation of the steel loop part of the trellis interference (especially for row spacings ≥ 3.0 m). The current section investigates whether a FastHenry model of the steel trellis can predict this interference and thereby create a correction matrix for this effect.

### 5.5.1 Materials and Methods: Modelled Response using FastHenry Estimated Parameters

The steel-only part of the trellis was configured in FastHenry, as described previously in Section 2.11, by defining the vertices of the rectangular elements of the experimental trellis, as defined in Lamb, Mitchell and Hyde (2005). The coordinates of the vertices were defined in 3-D, relative to the EM38 Tx and Rx coils positioned at the centre of the inter-row spacing. These vertices were then connected horizontally (with zero assumed contact resistance) with the equivalent of 2.5 mm diameter wire, and vertically with square posts of the same cross-sectional area (and resistivity) as the Gripfast posts. Mid-panel estimates were straightforward and just used a single panel. While adjacent-to-post estimates used just a single panel for edge-posts estimates, this value was doubled to give adjacent-to-internal-post estimates (Section 4.8). Where there was a row either side

of a measuring point (i.e. all the internal lanes) the estimated values were also doubled since, due to symmetry, the contributions from each side are additive.

Figure 5-13 shows a schematic of the adjacent-to-post and adjacent-to-the-mid-panel measuring points, with a simplified eddy current shown in the panels. The adjacent-to-post scenario shows how the eddy currents in the two panels cancel each other out at the post. Extending this symmetry argument, means that the ground eddy currents channelling into the post must also cancel out and hence not contribute to the EM38 response. Therefore, the separation of the DW and AW effect is more complete at the adjacent-to-the post measurement point. In reality, however, the 3-D interaction of the earth and trellis is more complicated than the above description would indicate. For example, there will be other earth eddy currents channelling through the outer posts and finding paths through wires other than the DW which may not cancel. However, these will be weaker due to the larger distances, and, larger resistances and self-inductances.

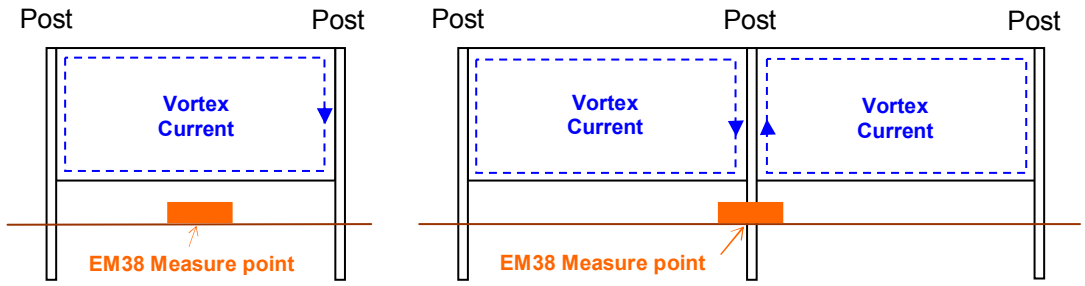


**a)** **b)**

**Figure 5-13. Schematic of the eddy current in a) at the centre of a single trellis panel; b) at the adjacent-to-post measurement point between a joined pair of trellis panels.**

### *5.5.2 Results and Discussion: Modelled Response using FastHenry Estimated Parameters*

Table 5-2 lists the average (and standard deviation) responses as measured at the mid-panel, and the adjacent-to-post position for the 3.0 m and 3.5 m spaced lanes (excluding Lane 3.0m-1 and 3.5m-1, which had residual effects from the adjacent, more closely spaced trellising). In addition, this table has the corresponding FastHenry predicted values and the ratio of the predicted response to the average corresponding measured response. Consistent with the measurements, FastHenry

predicts the mid-panel response to be greater than the response adjacent to the posts, and the adjacent-to-the post response for posts at the row ends to be less than those adjacent to internal posts. However, the average magnitude of the predicted mid-panel response is 72 % above the average measured response (final column in Table 5-2). Unlike the shorted panels created in this current work (Section 4.5), Lamb, Mitchell and Hyde (2005) created trellising without any consideration of wire-post, and post-ground coupling. That is, they did not ensure adequate electrical connection between wire and posts, nor the posts and the earth. The earlier results of Sub-section 4.5.2 and Equation 4-2 demonstrated that the wire-post resistance increased the measured EM38 interference by up to 75 % (for the largest D-F2 3 m long panel configurations). The current mid-panel measurement exceeded the prediction by 72%, which is of the same order as that caused by the wire-post resistance, referenced above.

However, of particular note in Table 5-2 is the fact that the adjacent-to-post predictions closely match those of the measured values, within the standard deviation. Importantly, this implies that the trellis interference adjacent to the post is not sensitive to the post-wire contact resistance.

Table 5-2 also lists some of the average responses for the 3.5 m spaced lanes (excluding Lane 3.5m-1). The magnitudes of the predicted against the actual averaged values show similar over-prediction for the mid-panel responses and reasonable predictions for the adjacent-to-the-posts responses. The adjacent to the edge post responses are a poorer match than for the internal posts. This may be due to the high conductivity gradient in that region exaggerating positional errors or the edge effects invalidating some of the symmetry arguments used above to estimate the adjacent to post predictions.

However, close examination of Figure 5-12 reveals that the maxima and minima are not accurately located mid-panel and adjacent to the posts. Consequently, the average response maxima will be underestimated and the average minima responses over-estimated. Table 5-3 is the same as Table 5-2 except for the manual selection of the actual maxima and minima values near their assumed position (i.e. maxima adjacent to the mid-panels and minima adjacent to the posts). The measured values in this table are closer to the predicted values and the standard deviations are smaller. Furthermore, the under-sampling of the data means that the

actual peaks and troughs have not been sampled, but just their flanks. This, combined with interpolation and minimum curvature gridding, has further 'flattened out' the responses, reducing the accuracy of sampling of the maxima and minima.

**Table 5-2. Average responses of the difference grid of the 3.0 m spaced, all-wire EM38 survey minus the dripper wire only survey (AW-DW). The final column is the ratio of the average predicted response (at each of the three relative locations) to the average measured response. (Lane 3.0 m-1 and 3.5 m-1 have been excluded due to carry over influences from the adjacent, more closely spaced, lanes.)**

| AW – DW Measurement Location: | Average Measured Response ± Std Dev. (mS $m^{-1}$) | FastHenry Predicted Response (mS $m^{-1}$) | Ratio: Predicted Response / Measured Response |
|---|---|---|---|
| ***3.0 m Lanes (excluding Lane 3.0m-1)*** | | | |
| **Mid-panel** | 20.9±2.5 | 35.9 | **1.72** |
| **Internal Posts** | 15.4±2.6 | 16.3 | **1.06** |
| **Edge Posts** | 10.1±3.1 | 8.2 | **0.81** |
| ***3.5 m Lanes (excluding Lane 3.5m-1)*** | | | |
| **Mid-panel** | 11.6±1.6 | 19.1 | **1.65** |
| **Internal Posts** | 10.0±2.0 | 9.1 | **0.91** |
| **Edge Posts** | 6.8±1.8 | 4.5 | **0.66** |

Currently, the 1 Hz sampling rate, at an average survey speed of 10 km $hr^{-1}$, gives a relatively coarse average sample interval of 2.8 m, which is approximately half a panel length. In addition, there is some slippage of the data along the profiles, possibly due to variation in the processing time of the DPGS receiving the EM38 values. Some of these effects would be improved by more accurate real-time kinematic (RTK) DGPS (accuracy <10 cm) systems sampling at a more rapid 10 Hz to take advantage of the EM38's 10 Hz output rate. The introduction of the latest technology GPS with greater processing power should improve this. Improving the sample density by decreasing the survey speed is not practical as it reduces the main benefit of the system, which is efficient mapping.

**Table 5-3. Average responses of the difference grid of the 3.5 m spaced, all-wire EM38 survey minus the dripper wire only survey. Actual maxima and minima were manually selected rather than responses exactly mid-panel or adjacent to posts.**

| AW - DW Measurement Location: | Average Measured Response ± Std Dev. (mS $m^{-1}$) | FastHenry Predicted Response (mS $m^{-1}$) | Ratio: Predicted Response / Measured Response |
|---|---|---|---|
| ***3.5 m Lanes (excluding Lane 3.5m-1)*** | | | |
| **Mid-panel** | 12.3±1.5 | 19.1 | **1.55** |
| **Internal Posts** | 9.0±1.8 | 9.1 | **1.01** |
| **Edge Posts** | 3.9±1.1 | 4.5 | **1.15** |

## 5.6 Correcting the All-Steel Interference of the Trellis

The results of Section 5.5 lead into the development of a correction strategy for trellis-affected EM38 surveys. The first step in such a strategy is to correct for the all-steel part of the trellis because this is more predictable than the grounding component. Table 5-3 shows that the predicted EM38 response (over and above the bare earth value) using FastHenry agrees with the average measured EM38 response of Lamb, Mitchell and Hyde (2005) for positions adjacent to the steel posts. It is therefore proposed that the predicted values in Table 5-3 adjacent to the internal and external posts provide a basis for forming a correction matrix. Table 5-4 shows the values (adjacent to the posts for Lanes 3.0 m-2 to 3.0 m-5) due to the steel-only trellis effect by subtracting the DW survey from the AW survey, [AW-DW]. The correction matrix is made up of both the internal and edge adjacent-to-post predicted values from Table 5-3. The subtraction of the correction grid [$AW_{correction}$] from the [AW] gives the first stage corrected data:

$$[Survey_{AllSteelLoopCorrected}] \sim [AW] - [AW_{correction}]. \qquad \text{Equation 5-1}$$

Using the data of Lamb, Mitchell and Hyde (2005), the difference between the [DW] and the corrected grid, [$Survey_{AllSteelLoopCorrected}$], provides a convenient indication of the success of this approach (i.e. by its closeness to zero):

$$[AW] - [AW_{correction}] - [DW] \sim [0]. \qquad \text{Equation 5-2}$$

Figure 5-14 shows the images of the three data sets, [AW-DW], [$AW_{correction}$], and [AW]-[$AW_{correction}$]-[DW]. Table 5-4 is the actual matrix data used to construct this correction matrix. Ignoring the three large outlier values (at 0, 3 and 6 mN) in Lane 3.0 m-5, the average of the residual column ([AW]-[$AW_{correction}$]-[DW] in Table 5-4) has a low value of just 0.8 mS $m^{-1}$, with a standard deviation of 1.9 mS $m^{-1}$. Inspection of the map of the corrected matrix in Figure 5-14 indicates that the outliers may be caused by a positioning error. The residual map (Figure 5-14c) is a visualisation of the data in the final column of Table 5-4, and while it appears relatively smooth and close to zero, it does show that the mismatches (between the corrected and the target data set) are systematic. This confirms the current research's previous conclusions that the variations relate to physical areas of the trellising, due to post-earth or post-wire electrical connection inconsistencies. However, this result is still a promising indication that this

correction strategy could reduce the effect from the all-steel component of the trellis.

**Table 5-4. Adjacent-to-the-post correction values, AW-DW and correction residual. This is for the 3.0 m spaced data (Lanes 3.0m-2 to 3.0m-5). (Note that the aim is to produce a correction residual value of zero.)**

| Easting (Local-m) | Northing (Local-m) | $AW_{correction}$ (mS $m^{-1}$) | AW - DW (Measured) (mS $m^{-1}$) | Correction Residual: AW – DW – $AW_{correction}$ (mS $m^{-1}$) |
|---|---|---|---|---|
| **Average (excl. 3 outliers) Corrected {Std Dev.}:** | | | | **0.8 {1.9}** |
| ***Lane 3.0m-2*** | | | | |
| **23** | **0** | 0.00 | 1.4 | **1.40** |
| **23** | **3** | 0.01 | 1.86 | **1.85** |
| **23** | **6** | 8.20 | 7.61 | **-0.59** |
| **23** | **12** | 16.30 | 14.91 | **-1.39** |
| **23** | **18** | 16.30 | 18.25 | **1.95** |
| **23** | **24** | 8.20 | 9.88 | **1.68** |
| **23** | **27** | 0.01 | 2.39 | **2.38** |
| **23** | **30** | 0.00 | 0.81 | **0.81** |
| ***Lane 3.0m-3*** | | | | |
| **26** | **0** | 0.00 | 0.61 | **0.61** |
| **26** | **3** | 0.01 | 0.41 | **0.40** |
| **26** | **6** | 8.20 | 8.09 | **-0.11** |
| **26** | **12** | 16.30 | 14.28 | **-2.02** |
| **26** | **18** | 16.30 | 16.45 | **0.15** |
| **26** | **24** | 8.20 | 11.28 | **3.08** |
| **26** | **27** | 0.01 | 2.57 | **2.56** |
| **26** | **30** | 0.00 | 1.4 | **1.40** |
| ***Lane 3.0m-4*** | | | | |
| **29** | **0** | 0.00 | 2.38 | **2.38** |
| **29** | **3** | 0.01 | 1.78 | **1.77** |
| **29** | **6** | 8.20 | 11.03 | **2.83** |
| **29** | **12** | 16.30 | 11.73 | **-4.57** |
| **29** | **18** | 16.30 | 11.96 | **-4.34** |
| **29** | **24** | 8.20 | 7.88 | **-0.32** |
| **29** | **27** | 0.01 | 1.72 | **1.71** |
| **29** | **30** | 0.00 | 1.36 | **1.36** |
| ***Lane 3.0m-5*** | | | | |
| **32** | **0** | 0.00 | 9.41 | **9.41** |
| **32** | **3** | 0.01 | 20.31 | **20.30** |
| **32** | **6** | 8.20 | 16.9 | **8.70** |
| **32** | **12** | 16.30 | 18.36 | **2.06** |
| **32** | **18** | 16.30 | 16.95 | **0.65** |
| **32** | **24** | 8.20 | 8.42 | **0.22** |
| **32** | **27** | 0.01 | 2.52 | **2.51** |
| **32** | **30** | 0.00 | 2.24 | **2.24** |

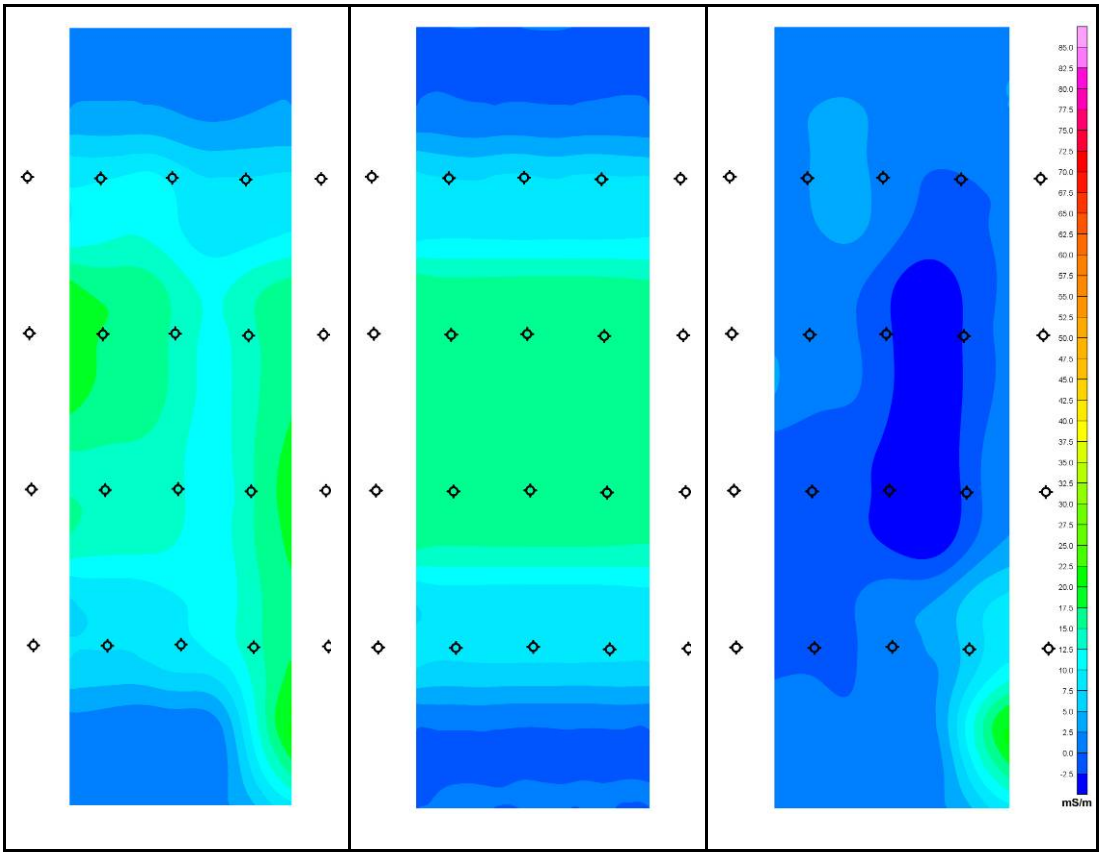


**a) [AW-DW]** **b) [$AW_{correction}$]** **c) [AW-$AW_{correction}$-DW]**

**Figure 5-14. Colour image maps of the EM38 (vertical dipole) survey of the all-wire minus the dripper-wire correction for Lanes 3.0m-2 to 3.0m-5 restricted to adjacent-to-the-post values. a) The [AW-DW] grid; b) The correction grid compiled from predicted values adjacent-to-posts; c) [AW-$AW_{correction}$-DW]. (Kirby Test Site showing the Gripfast post locations in black.)**

## *5.7 Correcting for the Earthing Interference of the Trellis*

In Section 5.5, a feasible correction strategy for reducing the predictable effect of the all-steel part of the trellis was developed. The second (and more challenging) step is to deduce a correction matrix for the earthing effect of the trellis. Section 4.10 has shown that these effects are less predictable due to the variability of the post-earth connection and the interaction between the trellis and the earth.

The estimation of a predicted value for the earthing effect used the FastHenry method with a ground plane (see ground plane description in Section 4.9). This simulation required an assumption about the topsoil thickness and its conductivity (as opposed to a homogenous half-space). The thickness and conductivity were chosen so that Equation 2-12 (the formula for $\sigma_a$ for a two-layer case) gave the same average value, as measured by the bare-earth survey of 37 mS $m^{-1}$, in the

results of Lamb, Mitchell and Hyde (2005). The value for $\sigma_1$ (conductivity of the top layer) and its thickness ($z$) were chosen as 116 mS m$^{-1}$ and 0.5 m so that it was possible to get $\sigma_a$ matching the observed 37 mS m$^{-1}$ with a relatively resistive lower layer . Using Equation 2-12 and the values from the function $R_v(z)$ (Equation 2-10) for a thickness of 0.5m, is 0.716. Substituted into Equation 6-3, this gives $\sigma_2$ (conductivity of the second layer of infinite thickness) as 5.6 mS m$^{-1}$.

Table 5-5 shows the average measured dripper-wire survey values minus the average measured bare-earth values at four types of location, relative to the trellis. That is, adjacent to the internal and edge panels, and adjacent to the internal and edge posts. Similar to the AW analysis (in the previous section), the mid-panel predicted response is over fifty percent too high, whereas the internal post prediction mismatches the measured values by just fifteen percent. The over-predictions are likely related to the fact that the wire-post and post-earth contact resistances have been assumed to be zero, whereas it has been shown previously that they are significant (Section 4.5) and will reduce the measured response where the earth is part of the loop. The prediction for the edge post is a poor match. This may be due, at least in part, to the high $\sigma_a$ gradient at that location (e.g. Figure 5-8 at 6 and 24 mN) combined with the along line positional inaccuracies and breakdown of symmetry arguments used in edge predictions. However, at least the predictions at the internal post locations offer a possible means of deriving a crude correction matrix.

**Table 5-5. Averages of the EM38 difference grid from the 3.0 m spaced, dripper-wire survey minus the bare-earth survey. These differences represent the EM38 interference from the grounded Dripper wire.**

| Dripper Wire - Bare Earth 3.0 m Lanes (exc. 3.0 m-1) Measurement Location: | Average Response (mS m$^{-1}$) | Standard Deviation (mS m$^{-1}$) | Predicted Response (mS m$^{-1}$) | Predicted Response / Average Measured Response |
|---|---|---|---|---|
| **Internal Mid-panel** | 32.5 | 3.2 | 57.7 | **1.78** |
| **Edge Mid-panel** | 24.0 | 1.9 | 40.5 | **1.69** |
| **Internal Posts** | 30.2 | 3.1 | 34.7 | **1.15** |
| **Edge Posts** | 11.4 | 1.9 | 4.1 | **0.36** |

Table 5-6 shows the result of applying the correction matrix based on the adjacent-to-post predicted values from Table 5-5. The average error after correction (the residual matrix [DW-DW$_{correction}$ -BE]) is 1.4 mS m$^{-1}$, with a

standard deviation of 4.9 mS $m^{-1}$. When broken down into internal post and edge posts, residuals of -4.5 ±3.1 and 7.4 ±1.9 mS $m^{-1}$ are obtained, respectively (standard deviation in brackets). Figure 5-15 depicts the colour maps representing this result where the correction residual still retains some systematic trellis earthing effects. This result indicates that while the prediction modelling requires some refinement (and may always be limited) it is still feasible to reduce the trellis grounding effect with this strategy.

Comparison of Figure 5-14b with 5-14c clearly demonstrates the inability to accurately predict the trellis influence at the edges (one-panel length centred on the edge post) of the trellis. From a practical correction perspective, masking of this edge strip of data from the corrected grid may be a necessary step, due to the inaccuracies in predicting the influence around those locations.

**Table 5-6. Measured, correction, and corrected matrix values adjacent-to-posts for the 3.0 m spaced rows. Note that there are two corrected value columns for comparison. The first, [DW-$DW_{correction}$-BE] is the DW survey with the [$DW_{correction}$] applied and the bare-earth subtracted so that an ideal correction would result in a zero residual matrix. The second starts with [AW] survey and has the [$AW_{correction}$], and the [$DW_{correction}$] applied, and then has the [BE] subtracted so that an ideal correction would also produce a zero result. However, the second form contains the residual from the application of two corrections.**

| Easting (Local-m) | Northing (Local-m) | [$DW_{correction}$] (mS $m^{-1}$) | [AW]-[$AW_{correction}$] - [$DW_{correction}$] (mS $m^{-1}$) | [DW] - [$DW_{correction}$] - [BE] (mS $m^{-1}$) | [AW]- [$AW_{correction}$]- [$DW_{correction}$]-[BE] (mS $m^{-1}$) |
|---|---|---|---|---|---|
| **Average (excl. 3 outliers in AW survey) ±Standard Deviation:** | | | | **1.4 ±4.9** | **2.1 ±5.5** |
| **Lane 3.0m-2** | | | | | |
| **23** | **0** | 0.00 | 41.50 | 0.30 | 1.70 |
| **23** | **3** | 0.05 | 41.34 | 1.25 | 3.04 |
| **23** | **6** | 4.05 | 42.35 | 5.55 | 4.95 |
| **23** | **12** | 34.73 | 27.87 | -7.13 | -8.53 |
| **23** | **18** | 34.73 | 30.57 | -8.73 | -6.73 |
| **23** | **24** | 4.05 | 47.55 | 8.15 | 9.85 |
| **23** | **27** | 0.05 | 40.64 | 1.75 | 4.14 |
| **23** | **30** | 0.00 | 36.70 | 1.50 | 2.30 |
| **Lane 3.0m-3** | | | | | |
| **26** | **0** | 0.00 | 41.20 | 0.90 | 1.60 |
| **26** | **3** | 0.05 | 41.24 | 1.75 | 2.14 |
| **26** | **6** | 4.05 | 46.15 | 8.05 | 7.95 |
| **26** | **12** | 34.73 | 30.97 | -3.93 | -6.03 |
| **26** | **18** | 34.73 | 33.17 | -3.03 | -2.83 |
| **26** | **24** | 4.05 | 48.65 | 8.55 | 11.65 |
| **26** | **27** | 0.05 | 42.14 | 3.95 | 6.54 |
| **26** | **30** | 0.00 | 38.50 | 0.70 | 2.10 |
| **Lane 3.0m-4** | | | | | |
| **29** | **0** | 0.00 | 41.00 | -0.30 | 2.10 |
| **29** | **3** | 0.05 | 40.44 | 2.55 | 4.34 |
| **29** | **6** | 4.05 | 44.05 | 4.95 | 7.85 |
| **29** | **12** | 34.73 | 31.07 | -1.53 | -6.03 |
| **29** | **18** | 34.73 | 33.07 | 0.27 | -4.13 |
| **29** | **24** | 4.05 | 46.85 | 9.15 | 8.85 |
| **29** | **27** | 0.05 | 40.44 | 2.75 | 4.44 |
| **29** | **30** | 0.00 | 36.70 | 0.80 | 2.20 |
| **Lane 3.0m-5** | | | | | |
| **32** | **0** | 0.00 | 47.90 | 0.70 | 10.10 |
| **32** | **3** | 0.05 | 58.84 | 2.05 | 22.34 |
| **32** | **6** | 4.05 | 50.15 | 4.85 | 13.55 |
| **32** | **12** | 34.73 | 30.87 | -7.23 | -5.13 |
| **32** | **18** | 34.73 | 32.57 | -4.93 | -4.33 |
| **32** | **24** | 4.05 | 47.75 | 9.55 | 9.75 |
| **32** | **27** | 0.05 | 42.34 | 3.25 | 5.74 |
| **32** | **30** | 0.00 | 37.90 | 0.60 | 2.80 |

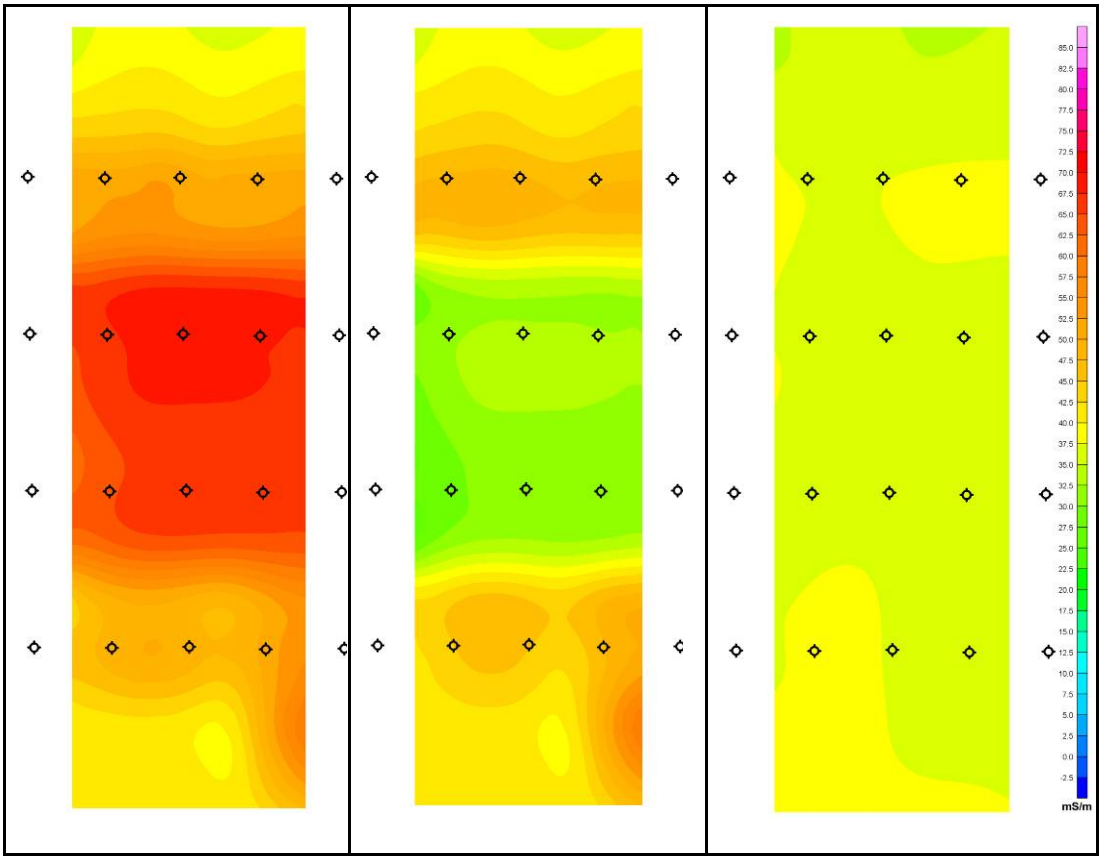


**a) [AW]-[AW$_{correction}$]** **b) [AW]-[AW$_{correction}$]–[DW$_{correction}$]** **c) [BE]**

**Figure 5-15. Colour image map of the EM38 (vertical dipole) survey of the all-wire minus the all-wire correction matrix for Lanes 3.0m-2 to 3.0m-5 compiled from positioned predicted values adjacent-to-posts. a) The [AW-AW$_{correction}$] matrix; b) The [AW-AW$_{correction}$ –DW$_{correction}$ matrix]; c) The [BE] matrix, for comparison (that is, the target response result sought after both AW and DW corrections. (Kirby Test Site showing the Gripfast post locations in black).**

## 5.8 Conclusion

This artificial trellis experiment has confirmed many of the conclusions derived in previous chapters. Moreover, it has demonstrated the potential to produce a correction matrix based on first principles, although there are uncontrollable parameters which require relatively rudimentary model-fitting iterations to achieve optimal results.

In summary, this investigation found that the EM38 response from the all-steel component of the trellis interference (i.e. excluding earthing effects) could be modelled. However, the predicted level of influence more closely matched the measured values when the EM38 sensor was placed mid-lane and adjacent to

internal posts rather than mid-lane and adjacent to the mid-panel sections of the vine rows.

The EM38 response from the combined grounded dripper-wire system was less systematic and predictable, and again the predicted level of influence more closely matched the observed effects when mid-lane EM38 measurements were adjacent to internal posts rather than mid-panel. However, modelling the earthing effect using a single 2-D FastHenry layer to predict the multi-panel, multi-row earthing effect, relies on a knowledge of the two-layer parameters at the site and relies on a horizontal 2-layer model. This, in turn, requires assumptions be made about a highly conductive topsoil layer while still satisfying the two-layer equation and the bare-earth apparent conductivity. Measuring these values using the standard EM38 two-layer technique (i.e. taking measurements at two heights) at various locations just outside the trellis would provide some confidence in such value selection. Care must be taken, however, as an actual vineyard may not have a simple two-layer nature due to along-trellis irrigation, mulching, fertilising and ripping. In addition, the contact between posts and the ground may be different for a test trellis with freshly inserted posts compared to posts that have been in place for years, where corrosion and soil adhesion may have increased electrical contact. Finally, it has been shown that, due to the trellis itself channelling the ground currents, any assumptions about conventional EM38 sampling depths and horizontal current flows may be invalid.

The EM38 influence at the ends of the trellis rows proved the most difficult to predict, owing to the complicated nature of the trellis edge-effects. In the dataset used here, this edge effect extended a single trellis panel length beyond the ends of the rows. A potential solution to this problem is to mask out a strip of the survey data, two panels wide, centred on the trellis edge.

Furthermore, the under-sampling of the data means that the actual peaks and troughs have not been sampled properly, only their flanks. This, combined with interpolation and minimum curvature gridding, has further flattened-out the responses. This could easily be improved with a more accurate, fast sampling (10 Hz) dGPS, which is now available.

This chapter has provided the final step in building the understanding of the influence of a real trellis system, that is, a trellis with multiple rows. After reviewing the data from Lamb, Mitchell and Hyde's research (2005), a brief description of the test site and survey protocols employed by these authors was given, together with details of the software and procedures specific to the present research. Attention then turned to analysing multi-row trellis-induced interference, with reference to the findings of the previous two chapters. The chapter closed by offering a preliminary post-processing interference correction strategy. In the following chapter, these new understandings about the interaction between the EM38 and trellising are applied to an existing, commercial vineyard.

# Chapter 6 Correcting EM38 Survey Data for a Commercial Vineyard

## 6.1 Introduction

Recalling that the goal of this thesis is to develop feasible, practical strategies for the correction of the trellising interference on the EM38 survey data, it now remains to apply the understanding of the interaction between the EM38 and trellising, developed in the previous chapters, to a vineyard of appropriate scale and constructed under industrial conditions; that is an existing, commercial vineyard. The existing vineyard chosen was Peterson's of Armidale, Australia. This is an operating, commercial vineyard.

It should be noted that whilst commercial vineyards may use the same trellis wire material, steel posts (e.g. Gripfast) and even the same configuration of steel and wooden posts (wooden posts are often used as the strain-posts owing to their flexibility and strength); local climatic conditions and the vineyard owner's personal preference will ultimately determine the trellising specifications. For example, heavy wind loads or vine vigour may dictate the use of thicker wire (hence changing the trellis' electrical properties and its EM38 interference).

In the case of Peterson's vineyard, the cool climate (at an elevation of approximately 1000 m) poses a risk of frost damage to crops. One vineyard management strategy to reduce the frost damage is to have the vine cordon (and the therefore the cordon wire) higher than normal, which changes the geometry of the trellis and potentially its interference effect on the EM38. In addition, the top foliage wire is moved down for the start of the growing season (just after pruning) and then incrementally raised throughout the growing season. There are other variations too. For example, a newer portion of vineyard may have a significantly different post-earth contact with the soil, relative to the more established trellis. Consequently, each trellis specification (and vineyard characteristic) will need to be noted and the chosen mitigation strategy calibrated to it. Fortunately, within most commercial vineyards, the trellis posts are set out systemically and consistently (Figure 6-1). This is particularly important as it means that the posts are located on

a precisely rectangular grid pattern as shown in Figure 6-1, which allows for the creation of a correction matrix.


**Figure 6-1. Photograph showing the typical precise alignment of posts across rows (Emerald Hill Vineyard, Stanthorpe, Australia).**

### *6.1.1 Peterson's Commercial Vineyard (Test Site)*

Peterson's Armidale Vineyard, is located in the New England (Australia) winegrowing region (~ 372900 mE, 6619200mN, UTM). The vineyard, comprising 13 Ha under vine, is oriented on a Northeast facing slope. The soils are basalt derived and, during vineyard establishment (1995-7), the vine rows were ripped down to a basalt resistance depth of approximately 0.6 m. A small section of the vineyard, comprising a section of four rows of cultivar Pinot (depicted in the aerial photograph of Figure 6-2), was used for the study. Figure 6-3 is a photograph of the section of the vineyard used for this study and shows the wooden strainer posts (at the row ends), wooden trellis posts, and the first group of four Gripfast steel posts (between the wooden trellis posts). Figure 6-2 comprises photographs across the rows showing the regular alignment of posts and a close-up view illustrating the trellis configuration. Figure 6-4 shows a schematic layout of

the trellis, highlighting the precise rectangular grid layout of the posts. Figure 6-5 depicts the trellises' wire configuration.


**Figure 6-2. Aerial view of Peterson's Vineyard, Armidale (Google Earth Image). The blue outline shows the approximate portion of Rows 35 to 40 (from their northern edge to the 81 m position) used in this research.**


a) b)

**Figure 6-3. a) Photograph of the north end of Row 35 at Peterson's Vineyard. This shows the wooden strainer post, the first of the wooden trellis posts and then a group of four steel Gripfast posts. Note Row 35 is an edge trellis; b) Photograph looking east past Row 35 illustrating the precise, rectangular grid of posts.**

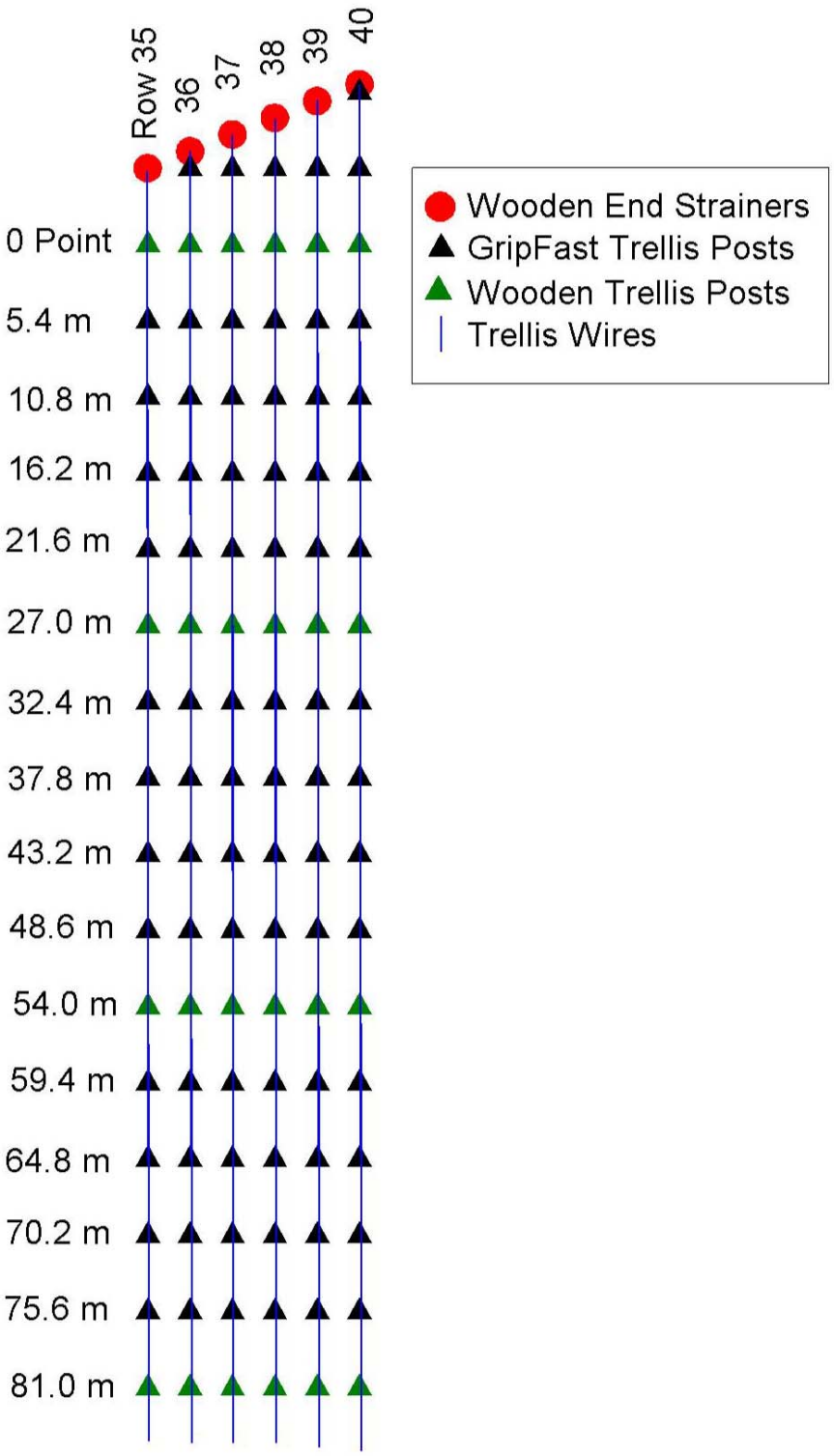


**Figure 6-4. Schematic layout (plan) of posts in a portion of Rows 35 to 40 at Peterson's Vineyard. Black triangles represent metal Gripfast posts, green triangles represent wooden trellis posts and red circles represent wooden strainer posts at the trellis ends. Rows are 3.0 m apart and separated from each other by 5.4 m along each trellis row. The first (northern) wooden trellis post is profile position zero and north is approximately at the top of the map. (The vineyard extends further to the east, south and southeast than shown).**

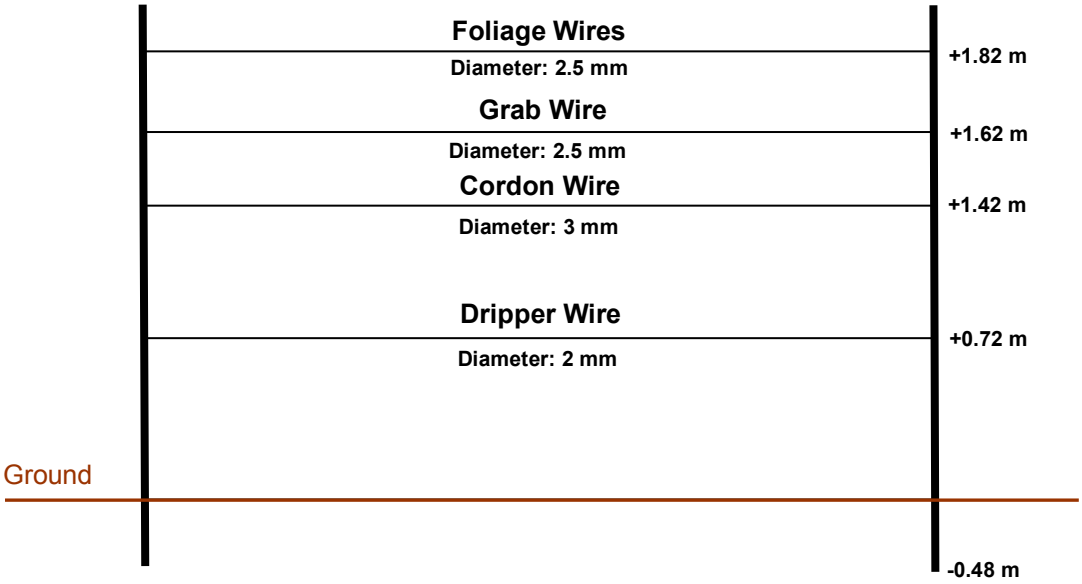


**Figure 6-5. Schematic diagram of a single panel of the Peterson's trellis at the time of the tests.**

## 6.2 EM38 Background Response to an Insulated Trellis

### 6.2.1 Materials and Methods: Background Response to an Insulated Trellis

In accordance with the observations in Chapter 4, individual EM38 measurements (in vertical dipole mode) were taken down the centre of the inter-trellis rows adjacent to the posts, and adjacent to the mid-panel positions, commencing at Position 0 m and ending at 83.7 m (these position designations are indicated in Figure 6-6). Measurements were also conducted along the trellis rows mid-panel, directly beneath the dripper wire. Note that Lane 35/- refers to a lane 1.5 m outside the vineyard but adjacent to Row 35 and Lane 35/36 refers to the mid-row lane between Rows 35 and 36. Those metal posts that had a significant influence (i.e. up to two posts along the trellis according to Figure 4-41) on the profile measurements were insulated from the supported wires as labelled in Figure 6-6, following the insulation procedure described in Section 4.5. To this end, rubber sheets were wrapped around the wires that were then re-inserted into the Gripfast post slots. The selection of posts to insulate was based upon trial-and-error, by monitoring detectable EM38 response changes when insulating the posts. With the trellis insulated, the EM38 response was measured. This data set represented the

actual true bare-earth response and the aim of the correction strategies was to reproduce this target result.

The positions for the measurements down the inter-trellis lanes and along the rows (both adjacent to the posts and mid-panel) were located on the ground with tape measures and marked with spray paint. The EM38 was then manually placed on the ground (and supported on uneven surfaces) in the vertical dipole mode. Along the trellis, placement of the instrument was directly beneath the dripper wire, and the vines themselves caused little need to offset that position. (This may be more of an issue in mature vineyards).

It has been shown previously that when both the wire (Section 4.2) and the posts (Section 4.3) are insulated from each other, they have negligible interference with the EM38 at the separations relevant here.

A bare-earth reference point, free of trellis and metallic litter interference, was marked and an EM38 calibration response was measured before and after recording each profile of data. A linear interpolation of the reference data (over the measurement time) was used to provide a drift correction for each profile measurement. (Instrument drift was found to be linear over the time intervals between re-sampling at the reference point).


**Figure 6-6. Schematic insulation diagram of posts in Rows 34 to 40. (Rows are 3.0 m apart and separated by 5.4 m along the rows.)**

### 6.2.2 Results and Discussion: Background Response to an Insulated Trellis

Figure 6-7 is a background graph of the EM38 response from the insulated trellis, both along the trellis rows and the inter-trellis lanes associated with Rows 35 to 38. Two distinct features are revealed from these trellis-excluded measurements. Firstly, there is a conductivity maximum in the vicinity of Position 55 m. Secondly, the conductivity is significantly lower (20 to 40%) along the trellis rows compared to the inter-trellis lanes.

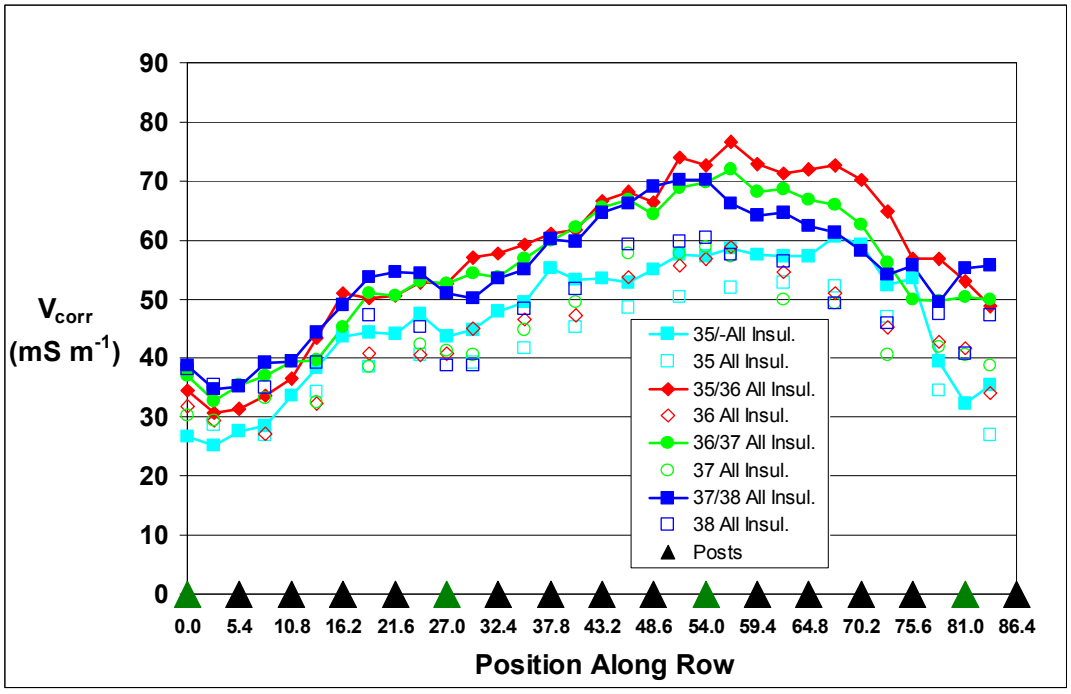


**Figure 6-7. EM38 (vertical dipole) result with the trellis wires insulated from the posts (according to the insulation pattern shown in Figure 6-6). The green triangles along the abscissa represent the location of the wooden trellis posts. Along the trellis rows, measurements were taken mid-panel only. The measurements were drift corrected.**

The methods of Section 4.5 have established that electrically insulating the trellis wires from the posts removes the interference from the trellising on the EM38 measurements of the bare earth. Thus, the maxima in conductivity observed in the linear surveys in Figure 6-7 and Figure 6-8 are actual bare-earth phenomenon and not associated with the trellis. Likewise, the difference between the along-the-trellis and the along-the-lane measurements is not related to the trellis structure itself. Rather, it is due to the soil along the trellis rows:

1. Being cultivated;

2. Regularly subjected to drip irrigation (but not fertigation) which is acknowledged as a mechanism of leaching salts from the soil;
3. Not being subjected to the same compaction as the inter-trellis lanes due to the regular passage of machinery e.g. foliar sprayers, harvesters and mowers; and
4. Having its moisture content reduced by the vines themselves.

Lane 35/- is an exception to the trend, but this can be attributed to the fact that it is outside the vineyard (Row 35 is on the edge of the vineyard). This significant apparent conductivity variation between the rows and the lanes is, in itself, an important finding relevant to the general interpretation of EM38 surveys data in vineyards.

This physical difference in soil attributes between inter-trellis lanes and the rows needs to be considered when evaluating possible EM38 correction strategies, as this will influence the ground-truthing (i.e. the ground-truth down the lanes cannot simply be interpolated to represent the ground-truth along the rows).

The responses along inter-trellis Lane 35/36 (Figure 6-8), with and without the trellis loops insulated, confirms that the trellis does have a significant effect on the readings, contributing an interference of up to 46 mS $m^{-1}$ or ~ 64 %. Figure 6-9 shows the results of all three lanes.

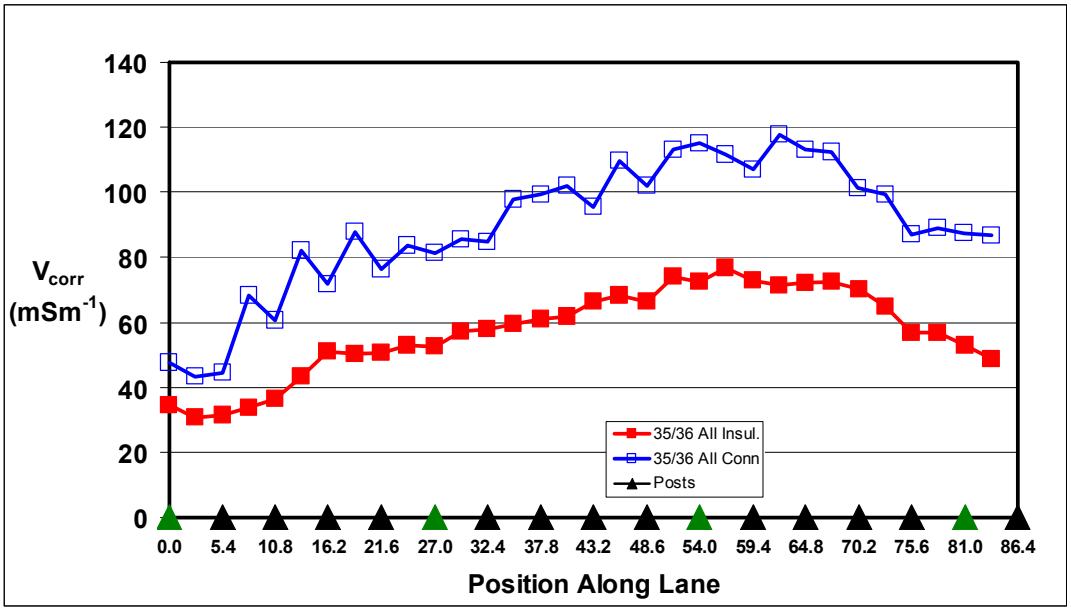


**Figure 6-8. EM38 (vertical dipole) response along inter-trellis Lane 35/36 with the wires connected and the wires all-insulated (according to the insulation pattern shown in Figure 6-6). This includes measurements adjacent to the posts and mid-panel. The results have been drift corrected.**

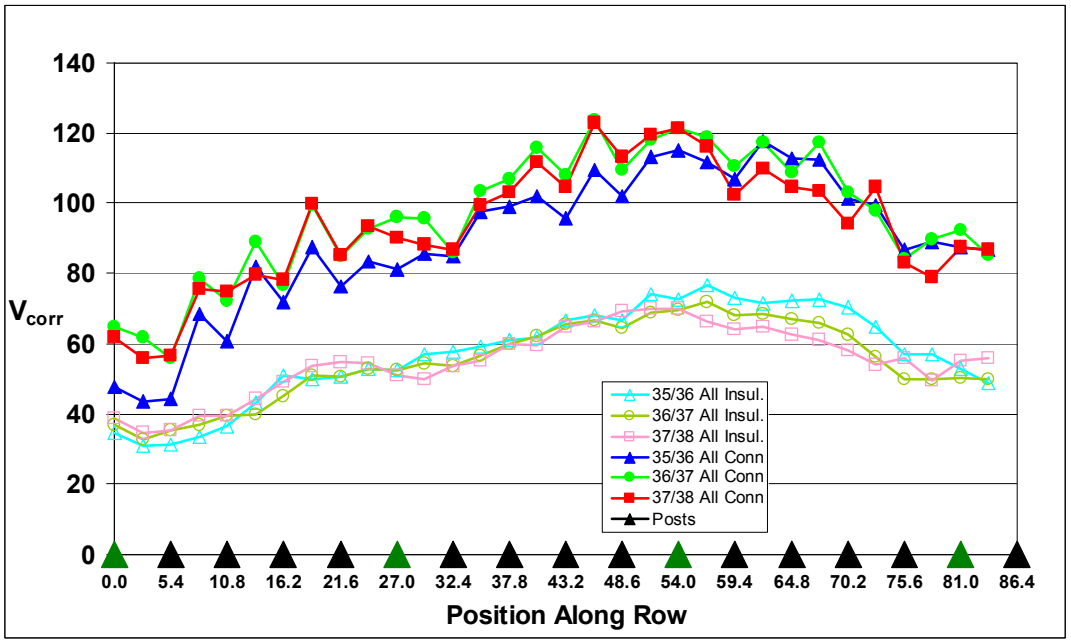


**Figure 6-9. EM38 (vertical dipole) response along inter-trellis Lanes 35/36, 36/37 and 37/38 with the wires connected and the wires insulated (according to the insulation pattern shown in Figure 6-6). The results have been drift corrected.**

An additional feature of Figure 6-8 and Figure 6-9 is that when the wires remain electrically connected to the steel posts, there is a significant modulation between the EM38 results adjacent-to-the-posts compared to mid-panel. This is consistent with the findings in earlier chapters. Figure 6-8 and Figure 6-9, however, also clearly show that the modulation only occurs when there are steel posts involved;

the modulation is absent in panels separated by wooden posts (for example positions 27 m and 54 m in Figure 6-8 and Figure 6-9).

The bare-earth features in the EM38 response (i.e. with the wires insulated) are also reflected when the wires are connected (e.g. the maxima at Position 55 m). The results of Lane 35/36 are influenced by the fact that Row 35 is an edge row and the EM38 trellis interference will be lower than, for example, Lane 36/37, due to deepening of the nesting trellis rows. Nonetheless, the EM38 response to the trellis with the wires connected still reflects the shape of the conductivity profile of the bare-earth.

To investigate further the shape of the bare-earth conductivity profile showing through the trellis interference, the ratio of the insulated result to the wires connected result was graphed for inter-trellis Lane 35/36, in Figure 6-10. While there is some noise, this graph still shows a relatively flat ratio of insulated to connected responses along the lane, with no visible correlation to the actual shape variation in the bare-earth profile (see Figure 6-8). This ratio graph also shows that the adjacent-to-the-post measurements have less noise than those from the adjacent-to-mid-panel location. Importantly, this result leads to a powerful correction strategy. That is, the trellis interference can be corrected by multiplying by a constant factor, at least for adjacent-to-the-post measurements.

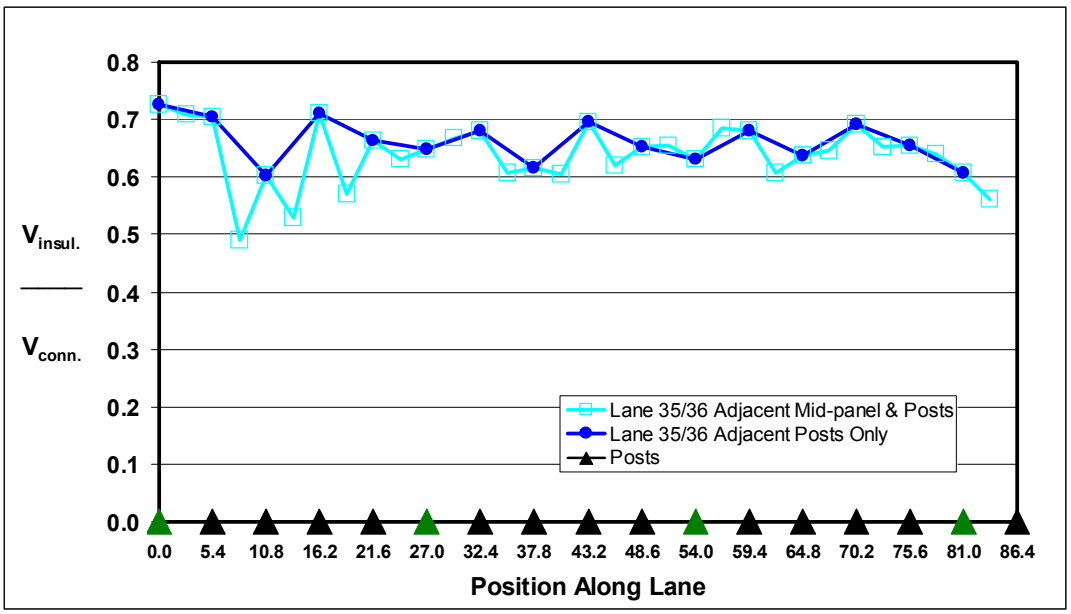


**Figure 6-10. Ratio of EM38 response (vertical dipole) with the wires insulated (according to the insulation pattern shown in Figure 6-6) to that with the wires connected. This ratio is for inter-trellis Lane 35/36. The results have been drift corrected.**

To check this assertion further, the ratio was plotted together with that for the next two lanes (Lanes 36/27 and 37/38) in Figure 6-11. These ratio plots are also flat, with no visible correlation with the underlying bare-earth response. However, these two lanes have a different ratio to that for Lane 35/36. This is because Lane 35/36 is an edge lane. Nonetheless, this confirms that the existence of this constant multiplication factor is the key to a simple correction strategy.

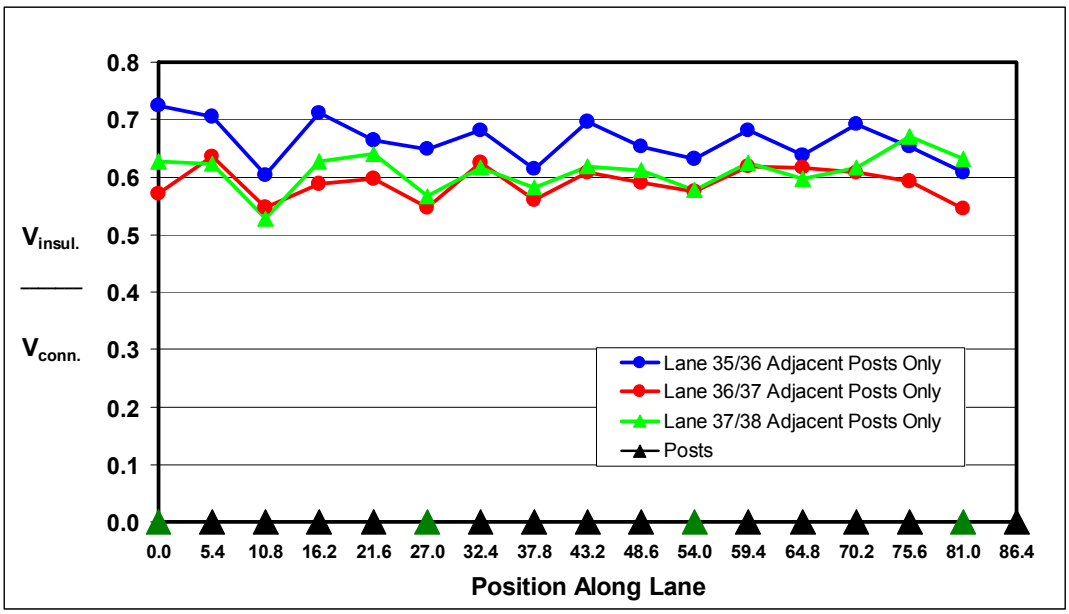


**Figure 6-11. Ratio of EM38 response (vertical dipole) with the wires insulated (according to the insulation pattern shown in Figure 6-6) to that with the wires connected. These ratio are for inter-trellis Lanes 35/36, 36/37 and 37/38. The results have been drift corrected.**

The ratios of the insulated to the connected responses are listed in Table 6-1. The ratio for the internal lane is 0.599, while for the edge lane it is 0.663. The standard deviations for these two factors are just 0.038 and 0.032, respectively. This indicates that a correction strategy is to take measurements along lanes, opposite the posts, and multiply them by an empirically determined correction factor (in this case 0.599 for internal lanes and 0.663 for edge lanes).

One additional complicating factor is that Lane 35/36 is an edge lane only as far as Position 75.6 m, where the first metal post of Row 34 is located (shown in Figure 6-6). This explains the response for Lane 35/36 in Figure 6-9, where it is lower than the internal response up to approximately Position 60 and thereafter is consistent with the internal responses. This is also evident in Figure 6-11 where the ratio for Lane 35/36 (past Position 60) becomes more like that of an internal lane, as would be expected given that it has effectively become one.

This outcome also means that if the absolute values are less important than the relative variations within a vineyard, then a correction may not be entirely necessary within the constraints of the following qualifications:

1. Measurements are located adjacent to the posts;
2. Edge lanes and lane end-effects are taken into consideration;

3. Variations in trellis geometry (e.g. if there is change within the vineyard) are taken into account; and
4. Modifications by the trellis to the depth of investigation have been considered. That is, the response may, in fact, be partially from the shallow ground along the trellis rows (especially around the metal posts) rather than from the depth conventionally attributed to an EM38 survey.

**Table 6-1. Ratios of EM38 wires-insulated response, to wire-connected response. The averages and standard deviations are for each of the three inter-trellis lanes. The final column is an average for the combined internal lanes.**

| Position | Posts | Lane 35/36 Insulated / Connected | Lane 36/37 Insulated / Connected | Lane 37/38 Insulated / Connected | Combined Lanes 36/37 & 37/38 |
|---|---|---|---|---|---|
| **0.0** | **Wood** | 0.73 | 0.57 | 0.63 | |
| **5.4** | **Steel** | 0.70 | 0.64 | 0.62 | |
| **10.8** | **Steel** | 0.60 | 0.55 | 0.53 | |
| **16.2** | **Steel** | 0.71 | 0.59 | 0.63 | |
| **21.6** | **steel** | 0.66 | 0.60 | 0.64 | |
| **27.0** | **wood** | 0.65 | 0.55 | 0.57 | |
| **32.4** | **steel** | 0.68 | 0.62 | 0.62 | |
| **37.8** | **steel** | 0.62 | 0.56 | 0.58 | |
| **43.2** | **steel** | 0.70 | 0.61 | 0.62 | |
| **48.6** | **steel** | 0.65 | 0.59 | 0.61 | |
| **54.0** | **wood** | 0.63 | 0.58 | 0.58 | |
| **59.4** | **steel** | 0.68 | 0.62 | 0.63 | |
| **64.8** | **steel** | 0.64 | 0.62 | 0.60 | |
| **70.2** | **steel** | 0.69 | 0.61 | 0.62 | |
| **75.6** | **steel** | 0.65 | 0.59 | 0.67 | |
| **81.0** | **wood** | 0.61 | 0.54 | 0.63 | |
| **Average:** | | **0.663** | **0.589** | **0.610** | **0.599** |
| **Std Dev.** | | **0.038** | **0.029** | **0.033** | **0.032** |

A similar strategy using just the mid-panel responses gives an internal correction factor of 0.539± 0.038 and edge factor of 0.592±0.053. These values used just panels that had a steel post either side of them because those panels with a wooden post gave a different result. However, as has been shown in previous chapters, the adjacent to the mid-panel effect is stronger than that adjacent-to-the-posts. As a result, all the variability within trellis, which affects the interference (e.g. wire-post resistance, post-earth resistance) will also be amplified. Hence, the adjacent-to-the-post location is the preferred one down the lanes. Intuitively, the adjacent-to-the-wooden-post location may be preferred, because inspection of Figure 6-9 shows that the response around the wooden posts is less variable than around the steel posts. This could be an advantage during towed surveys as it

makes the along line synchronisation errors between the EM38 and the DGPS less critical (see Section 5.4) than when trying to extract precise adjacent-to-post measurements. This strategy gives an internal correction factor of 0.580±0.033 and 0.653±0.051. However, not all vineyards have wooden trellis posts interspersed between the steel posts (see example vineyard in Figure 6-12).


**Figure 6-12. Photograph down inter-trellis showing trellis rows supported entirely on steel Gripfast posts (Emerald Hill Vineyard, Stanthorpe).**

In Section 4.10, measurements were taken directly beneath a grounded wire where the coupling with the large conducting loops of the trellis were negligible. However, in this position, connecting the wires to the steel posts increased the EM38 response, indicating that the grounding of the wire still had an influence on the EM38. The connection of more grounded posts onto the wire increased the response even further (see Section 4.10). In addition, because Figure 6-7 shows that the ground has a different conductivity along rows compared to the lanes, it may still be a desirable option to conduct a survey at mid-panel location along the actual trellis row and then correct for the trellis interference. That is, it may be an advantage, when monitoring vineyards with an EM38 conductivity survey, to measure the response along the rows, and then correct it, even though this would require manual measurements (as opposed to quad-cycle towed measurements). This advantage is two-fold. Firstly, the total interference is significantly reduced and, secondly, the survey would be located directly over the vines' root zone.

Figure 6-13 is the result for the edge row (Row 35). The mid-panel response with all the wires connected is similar to the actual (insulated) apparent conductivity. Again, this presents a possible correction strategy. However, because this is an edge row it has a nested grounding effect from only one adjacent row (Row 36). The effect from an internal row (with adjacent rows either side) Row 36, is shown in Figure 6-14. This shows that the mid-panel response is offset from the target value by approximately double the amount for Row 35. This result is consistent with the other internal rows (Row 37 and Row 38) as shown in the comparison graph, Figure 6-15.

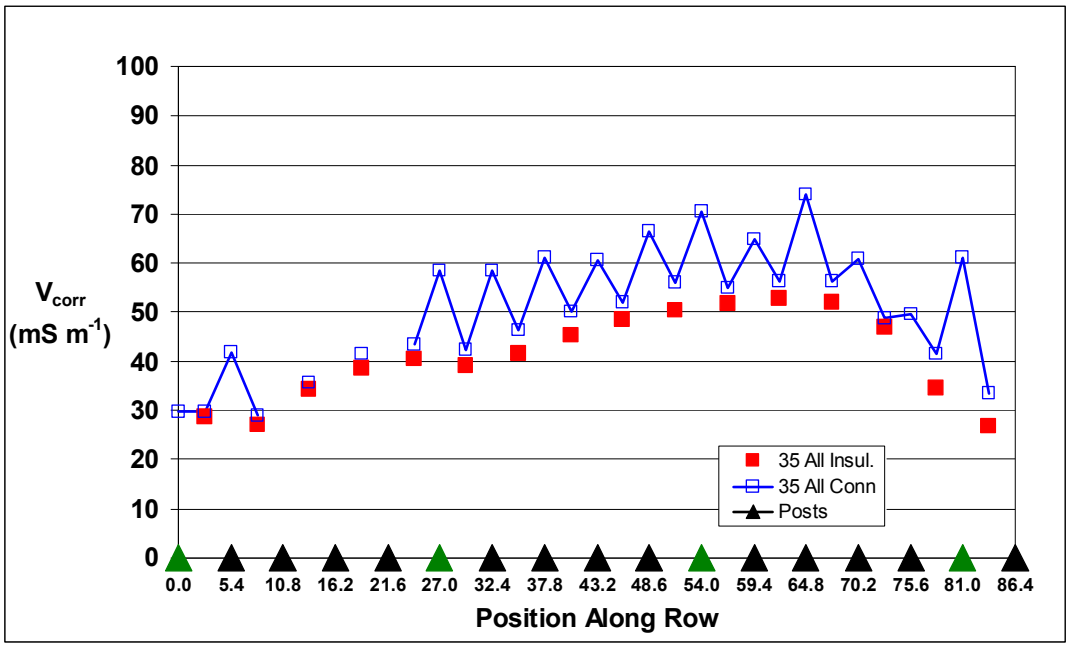


**Figure 6-13. EM38 (vertical dipole) response along trellis Row 35 with the wires connected and the wires all-insulated (according to the insulation pattern shown in Figure 6-6). This includes measurements adjacent to the posts and mid-panel. The results have been drift corrected.**

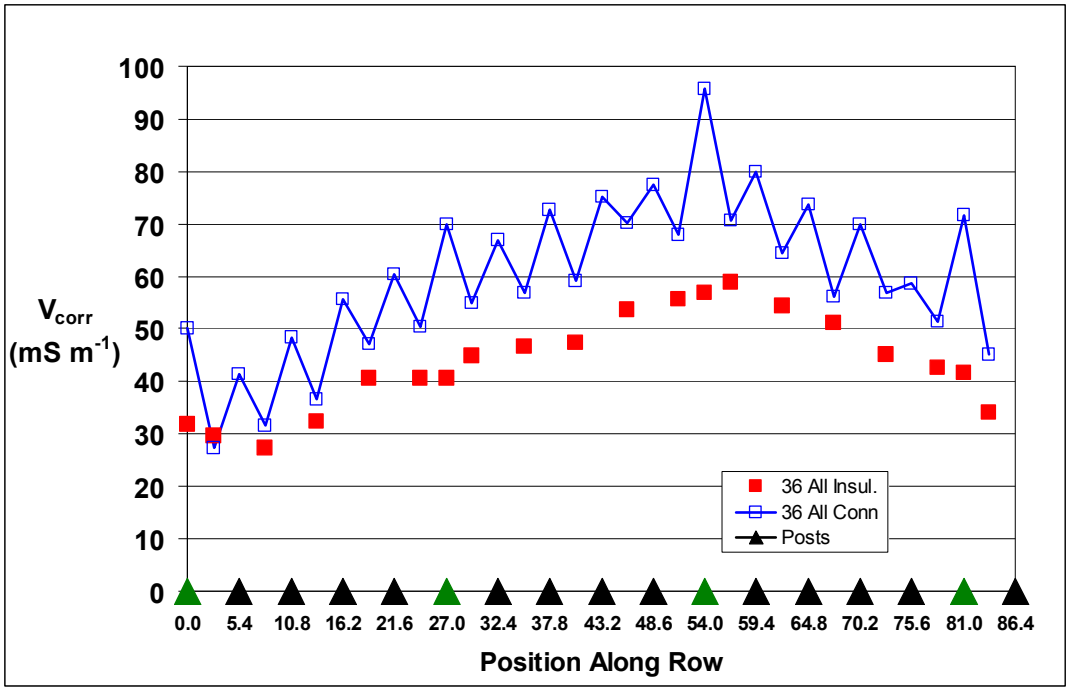


**Figure 6-14. EM38 (vertical dipole) response along trellis Row 36 with the wires connected and the wires all-insulated (according to the insulation pattern shown in Figure 6-6). This includes measurements adjacent to the posts and mid-panel. The results have been drift corrected.**

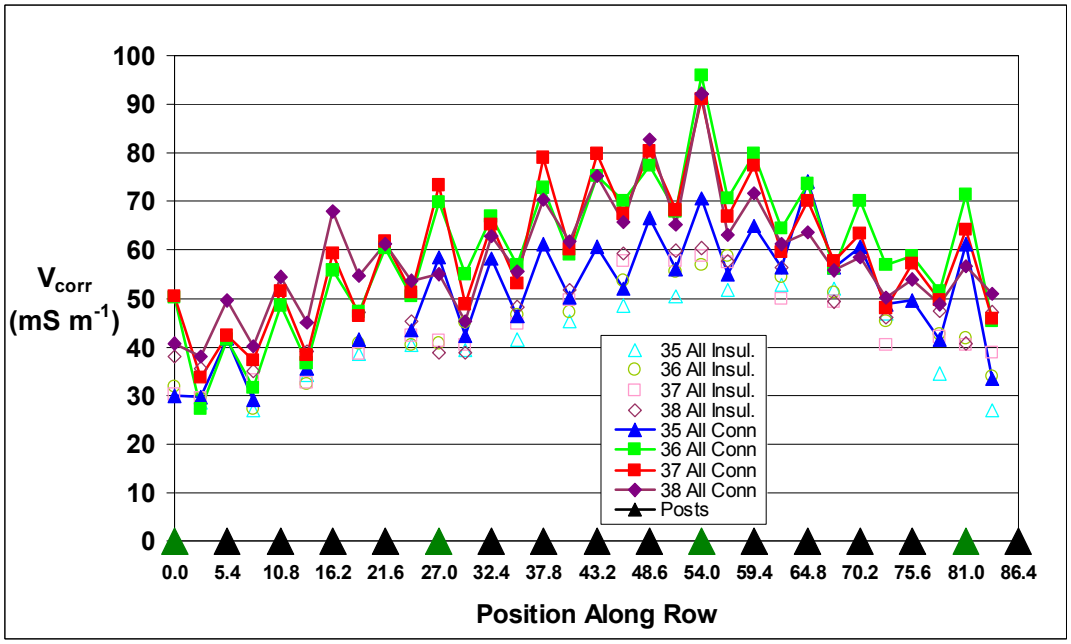


**Figure 6-15. EM38 (vertical dipole) response along trellis Rows 35, 36, 37 and 38 with the wires connected and the wires all-insulated (according to the insulation pattern shown in Figure 6-6). This includes measurements adjacent to the posts and mid-panel. The results have been drift corrected.**

The mid-panel ratios of the response with the wires insulated to that with wires connected along the three rows (Rows 35, 36 and 37) are listed in Table 6-2. The

calculated averages give an internal correction factor of 0.845±0.054 and an edge factor of 0.918±0.045. As expected, these factors are higher than for the inter-trellis corrections because, in this position, there is no coupling with the large trellis loops, just grounding effects.

**Table 6-2. Ratios of wires-insulated to wires-connected EM38 responses along three trellis rows. Average ratios and standard deviation for each lane and for the combined internal lanes (Rows 36 and 37) are also given.**

| Position (m) | Post @ start | Post @ end | Row 35 Insulated / Connected | Row 36 Insulated / Connected | Row 37 Insulated / Connected | Combined Internal Rows 36 & 37 |
|---|---|---|---|---|---|---|
| **2.70** | **wood** | **steel** | 0.96 | 1.08 | 0.87 | |
| **8.10** | **steel** | **steel** | 0.93 | 0.86 | 0.89 | |
| **13.50** | **steel** | **steel** | 0.96 | 0.88 | 0.85 | |
| **18.90** | **steel** | **steel** | 0.93 | 0.86 | 0.83 | |
| **24.30** | **steel** | **wood** | 0.94 | 0.80 | 0.83 | |
| **29.70** | **wood** | **steel** | 0.93 | 0.82 | 0.83 | |
| **35.10** | **steel** | **steel** | 0.90 | 0.82 | 0.84 | |
| **40.50** | **steel** | **steel** | 0.90 | 0.80 | 0.82 | |
| **45.90** | **steel** | **steel** | 0.93 | 0.77 | 0.86 | |
| **51.30** | **steel** | **wood** | 0.90 | 0.82 | 0.85 | |
| **56.70** | **wood** | **steel** | 0.94 | 0.83 | 0.86 | |
| **62.10** | **steel** | **steel** | 0.94 | 0.85 | 0.84 | |
| **67.50** | **steel** | **steel** | 0.93 | 0.91 | 0.85 | |
| **72.90** | **steel** | **steel** | 0.97 | 0.79 | 0.84 | |
| **78.30** | **steel** | **wood** | 0.83 | 0.83 | 0.84 | |
| **83.70** | **wood** | **steel** | 0.80 | 0.75 | 0.84 | |
| **Average** | | | **0.918** | **0.842** | **0.847** | **0.845** |
| **Std Dev.** | | | **0.045** | **0.076** | **0.017** | **0.054** |

Applying these correction factors back onto the data gives the images in Figure 5-15. This shows that the correction restores the data to an approximation of the real (insulated wire) response. The standard deviation of the difference between the real values and the corrected values is 2.0 mS $m^{-1}$. This is comparable to the stated accuracy of the EM38, ±5 % of the average response. The average response with the wires connected here is 50 mS $m^{-1}$, giving an accuracy estimate of ±2.5 mS $m^{-1}$.

Future investigations could look at how critical each of these strategies is to trellis geometry. It may turn out that a universal set of corrections could be determined just from the number and thickness of wires and post / row spacings.

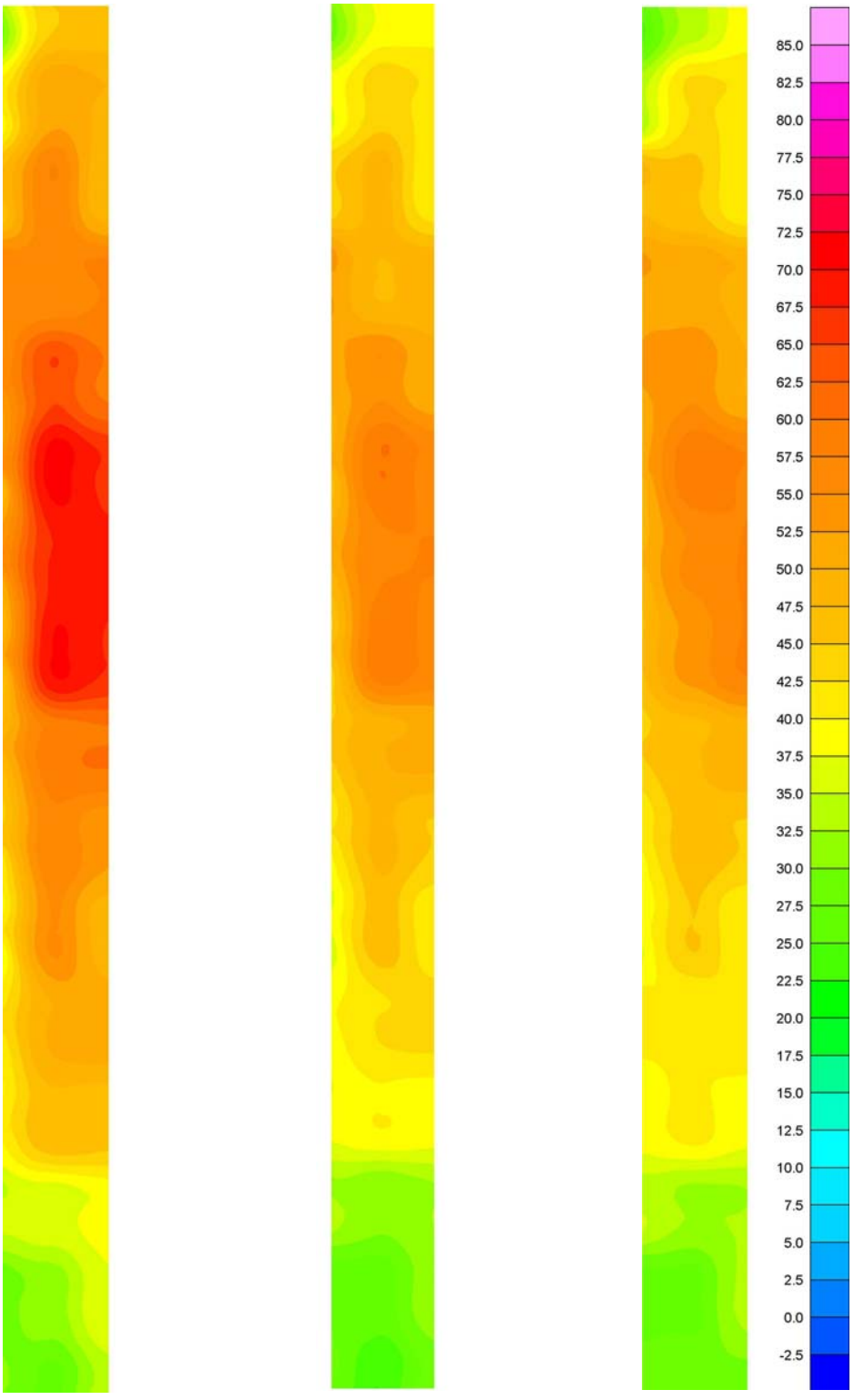


**a) Connected** **b) Insulated** **c) Corrected**

**Figure 6-16. Colour image map of the EM38 (vertical dipole) survey of the along row correction process for Rows 35, 36 and 37. These are mid-panel responses along the rows (drift corrected). The same colour zones apply to the three images and the strips are 81 m long; a) The original response (i.e. with the trellis wires connected; b) The target result with the wires insulated according to Figure 6-6; c) The corrected response with the colour display legend.**

# Chapter 7 Project Review, Conclusion and Recommendations

## 7.1 Project Review

The EM38 is an above-ground electromagnetic induction soil-survey tool that is ubiquitous to precision viticulture. The goal of understanding the physics behind the interference from the steel vineyard trellising on the EM38's soil measurements has been met. A combination of component and whole trellis assembly trials confirmed that the interference was separable into two signification components, the steel trellis, and the trellis-earth system. While these two effects theoretically interact, the contributions of each were found to be conceptually separable in terms of EM38 response, and importantly, in terms of possible mitigation or post-data acquisition correction strategies.

An analytical expression was initially developed to predict the interference from steel conducting loops in terms of the mutual inductance from both the transmit and receive coils of the instrument to the Target Loop, the loop's self-inductance, and its electrical resistance. This formula (and its supporting experiments on simple loops) subsequently confirmed an inverse-sixth-power sensitivity of the EM38 to the proximity of the trellis loops. That is, the trellis interference is approximately inversely proportional to the sixth power of the separation distance.

Not surprisingly, increasing the complexity of the loops to reflect real trellis geometries necessitated the use of a numerical analysis program (FastHenry) to calculate the parameters of loop resistance, self-, and mutual-inductance, for substitution into the analytical expression.

Key drivers of trellis interference on EM38 surveys were subsequently identified:

1. Trellis interference from the trellis loops was found to increase with increasing electrical contact resistance between the posts and the wires. This is a significant result in the context of using a post-acquisition interference correction procedure because there are many points of electrical contact resistance in a commercial trellis (e.g. seven per trellis panel) and the actual resistances are expected to be highly variable (according to trellis age, environmental conditions, corrosion, topography and vine loads).

2. Conducting loops containing the bottom (Dripper) wire made the greatest contribution to the observed interference, and the largest vertically dimensioned loops (for example comprising the top Foliage and bottom Dripper wire) gave the strongest interference. In contrast, connecting the intermediate trellis wires (for example, the Gripper or Cordon wires) made little practical difference to the interference compared to a loop comprising just the bottom Dripper- and top Foliage-wire.
3. A significant component of the EM38 interference arises from the earth part of the trellis system. This effect is due to the grounded post-wire system providing an alternate path for the eddy currents in the earth. This was supported by the interference increasing (both in resistive and moderately conductive soils) when additional earthed posts (along a row) were connected into the post-wire-earth system but where direct coupling with the wire-post loop was negligible.
4. Related to Point 3, experiments verified the critical importance of the post-earth interface and the fact that the near-surface earth conductivity needs to be considered when choosing a mitigation strategy. This is because current channeling from earth eddy currents upwards into the posts violates the horizontal current flow assumptions central to conventional depth response functions used when interpreting EM38 data.
5. The trellis interference on the EM38 is lower when the EM38 is placed adjacent to the posts (i.e. aligned with the panel-edge) compared to locations adjacent to the trellis' mid-panel. In addition, the EM38 interference from the trellising was more predictable adjacent to the posts than adjacent to the mid-panel. Both these revealed aspects of the interference led this investigation towards a correction strategy using data taken from just the adjacent-to-the-posts position.
6. Insulating all the wires from the posts near an EM38 survey removed all the trellis interference, and consequently revealed the sought after bare-earth apparent conductivity. Whilst simplistic, this approach to the complete removal of the trellis interference is the most effective (and reliable) method of revealing the absolute values of the interference-free bare-earth apparent conductivity.

While it was confirmed that the mid-panel interference effects are stronger than adjacent-to-the-post effects, mobile data collection, involving a dGPS and data logger, does not necessarily mean individual EM38 measurements are exactly aligned either with posts or mid-panels. This will pose challenges in applying location-specific correction templates. However, this limitation can be overcome by the employment of readily available faster sampling, lower lag, and more accurate dGPS systems.

Lamb, Mitchell and Hyde (2005) suspected that any lateral movement (i.e. across the inter-trellis lane) of the EM38 unit during surveying would result in data artefacts because of the distance sensitivity of the trellis interference. This effect was confirmed along a track, half a row spacing outside the edge of the vineyard (i.e. with a trellis on just one-side of the survey track) where the EM38 interference's lateral sensitivity was found to be $\sim 10$ mS $m^{-1}$ per decimetre. However, along internal vineyard rows (because there was a trellis either side) the sensitivity of the EM38 lateral displacement was practically negligible (less than 5 mS $m^{-1}$) for an 80 cm deviation either side of the row's centre line.

Extension of the investigation into trellis interference on EM38 measurements to a commercial vineyard, before and after insulating the wires, yielded some additional conclusions:

1. When the vineyard trellis posts and wires were electrically insulated from each other to reveal the bare earth conductivity, the soil conductivity was significantly higher down the inter-trellis lanes compared to along the trellis rows. This will need to be considered when ground-truthing correction strategies, as the ground-truth cannot be just interpolated between the rows and the lanes. However, in a broader sense, this highlighted, for the first time, the measureable impact (via the EM38) of cultural practices on the soil in the inter-row lane compared to the soil immediately below the vine trellising;
2. The interference from the trellis is significant, increasing the EM38 response by approximately 61 % in the inter-row lane adjacent to the posts and 86 % adjacent to the mid-panel;

3. Immediately adjacent to the trellising (i.e. with the EM38 below the trellis wires) the along row mid-panel interference was observed to increase the EM38 response by just 18 %. Importantly, this is less than a third of the mid-panel inter-trellis row interference;
4. The edge lane had an interference of only ~51 % (compared to the internal lanes' interference of ~61 %). This indicated that the along-lane interference has a contribution not only from the adjacent rows, but also from the next rows across (due to the nested earthing effect);
5. There are significant edge effects, with interference along an outside row being only 9 % (standard deviation 4.5 %) compared to the 18 % along internal rows (Point 3 above). This, in itself, is a significant finding, relevant to the general interpretation of EM38 surveys data in vineyards; and
6. Importantly, it was discovered that the proportional interference effect is relatively consistent (i.e. it had standard deviation of just 4.6 % down the lanes, opposite the posts, and 3.8 %, mid-panel). Similarly, the along-row (i.e. directly below the wires) mid-panel response had a relatively low standard deviation of 5.4 %.

## 7.2 Mitigation and Correction Strategies

The observed, relatively consistent patterns summarised above, in Section 7.1, led to several possible mitigation strategies. This group of strategies is based on the observed proportional effect of the trellis interference on the underlying true apparent conductivity. It has the advantage of bypassing the complexity and variability in determining the parameters associated with the trellis-earth system in order to calculate analytical prediction values to form a correction template. This empirical approach is feasible but may require the measuring of a calibration zone within the vineyard, first with the wires connected, and then with them insulated.

### 7.2.1 Strategy: Insulate the Trellis

Insulating the entire trellis would be completely effective but somewhat impractical. As part of this study, all the wires in the small investigation area, within a small section of a commercial vineyard were insulated to obtain the

ground-truth data. This simple operation involved sliding small, square rubber sheets along the wire into the Gripfast post slots. However, there was a finite amount of time involved, with approximately seven wires per panel. In addition, the insulation was not permanent because the wire movement against the sharp edge of the post slot eventually cut through the insulation material. To insulate an entire vineyard would be a major effort. For example, allowing two minutes per post, and in the vineyard tested here, where there was one post every ~20 $m^2$ (i.e. 500 posts per Ha or 6 000 in the 12 Ha site), would require 12 000 minutes (~27 man-days) to complete the insulation process. However, different zones of the vineyard could be insulated (after surveying) to calibrate the correction factors required, as described in the next sections.

### *7.2.2 Strategy: Manual Measurement along the Trellis Rows*

Manually placing the instrument in the mid-panel plane (below the wires) of the trellis decouples the instrument from that trellis loop. Hence, the only effect is the interference from the trellis earthing effect. In the commercial vineyard investigated here, the trellis interference was only 18 % (the smallest interference amount observed in this study). This earthing effect will have a contribution not only from the earthed trellis above the measuring point but also a small earthing contribution from the immediately adjacent trellises. While manual placement means that the problems of accurately positioning the instrument are overcome, the efficient dGPS positioned vehicle towed system cannot be used. In addition, it can be imagined that mature plant trunks may necessitate a small position shift along the trellis to maintain the negligible direct trellis coupling.

The mid-panel, along-row (i.e. in the plane of the trellis) strategy could be corrected by the determination of multiplication factors from calibration zones of insulated trellis. These calibration zones would need to be three rows wide and at least six posts long. In practice, the calibration zones' dimensions could be determined empirically by insulating additional posts until no significant reduction in interference was detectable. In addition, the edge effects would need to be accounted for (or simply omitted from the data set). Due to the effect of the moist soil around the posts, the EM38 survey would ideally not be performed after rain or recent irrigation. In addition, areas of different trellising arrangements would

require separate calibrations zones. This strategy would have the advantage of measuring more directly in the vines' root zone because, as mentioned in Section 7.1, the inter-trellis lanes were found to have a significant and consistently higher apparent conductivity than along the trellis rows.

Taking the measurements at the steel posts is not a viable option. The experimental evidence shows that the eddy current mechanism in close proximity to a grounded post presented challenging complexities. There would also be the problems of misalignment with the post due to orientation sensitivity from the proximity to such a long piece of highly conductive metal.

### 7.2.3 Strategy: Measurement along the Inter-trellis Lanes (with Calibration)

Vehicle towed EM38 surveying down the lanes is undoubtedly the most efficient method of data collection. Therefore, the application of a correction factor for measurements adjacent to the post is probably the most practical and reliable way of reducing the trellis interference. Ideally, a fast-sampling dGPS, with precise corrections for data lag from the instrument, would improve the registration of the data to the adjacent-to-the-post locations. These values could then be confidently multiplied by the correction factor calibrated for that trellis zone. For the vineyard zone studied here, the correction factor was determined to be 0.60 internal and 0.66 along an edge. Ideally, these factors would be re-calibrated (temporally and spatially), based on a geo-statistical regime in order to characterise the vineyard zones. This zone characterisation would, in fact, be part of an overall precision viticulture approach.

A possible (inferior) alternative to precisely registering the data opposite the posts, would be to apply a smoothing algorithm down the rows to remove the modulation due to post / mid-panel interference variation, and a different calibration factor determined for that approach. Unfortunately, this approach would include the effect of the highly variable post-wire resistances.

An alterative to the insulation of certain calibration portions of the vineyard for determining the correction factor would be to use the ground just outside the influence of the trellis. Observations at the commercial vineyard and the artificial

vineyard suggest that a position as little as one panel-length from the end of the lanes or two row widths off to the side of an edge row could be used to determine the calibration factor. This has the advantage of supplying a large amount calibration data without the need for insulating the wires. However, caution would still need to be applied as it was also discovered that different parts of the vineyard do have different conductivities, due to anthropogenic activities such as soil compaction (e.g. due to more traffic on access roads just outside the trellising, less traffic from mechanical vineyard activity, differential irrigation and fertiliser inputs to the ground outside the vineyard). However, just one post length outside the vineyard along an inter-trellis lane, the soil compaction could be expected to be similar to a lane internal to the trellised area. In this approach, the trellised edge effect would need to be carefully excluded.

### *7.2.4 Strategy: Measurement along the Inter-trellis Lanes (without Calibration)*

The 'do nothing' strategy, based on the discovery (during this investigation) that the trellis interference is linearly proportional to the underlying true soil apparent conductivity (provided the mid-panel /adjacent to the post modulation effect is accounted for) is the most convenient approach. Ironically, it is the development of the understanding of the complicated interference of the trellis on the EM38 soil conductivity map that allows anomalies in the uncorrected data to be interpreted with confidence, albeit qualitatively. In fact, the trellis interference is actually amplifying the apparent conductivity of the soil. The qualifications to this approach are that:

1. The edge effects will need to be excluded;
2. A moving average will need to be applied to smooth out the interference modulation between the adjacent-to–the-post and the mid-panel locations; and
3. There will be a superimposition of shallow soil conductivity effects (due to the current channeling into the grounded posts) over the values conventionally attributed to come from deeper in the root zone.

## 7.3 Scope for Further Work

The achievement of the goal of understanding the physics behind the interference effect of the trellis on the EM38 has provided the context for developing some mitigation and correction strategies (Section 7.2). During the development of this contextual background, the variability and complexity of the real-world trellis scenario has shown that the formulation of an analytical correction template is not practical. Therefore, there is no advantage to be gained from the further development or refinement of a global analytical prediction methodology, but rather the effort should be on the development of robust empirical, site-specific correction templates, based on the multiplicative correction factor approach discovered here. The mitigation strategies should also then be assessed for their relative effectiveness in developing global empirical correction templates for providing first estimates of the true bare-earth apparent conductivity.

Not withstanding these conclusions, there is still scope for improving the understanding of the trellis interference, but at an empirical/statistical level:

1. Develop (over a range of vineyard soil conditions and geometries) a robust limit on the distance that adjacent trellis rows and panels can contribute to the interference. This would be valuable when insulating calibrating portions of a vineyard in order to get the true apparent conductivity;
2. In order to further understand the effect of ground eddy currents being channeled upwards into the trellis, a simple set of experiments could be performed by adding grounding posts in various numbers and spacing. These spacings patterns should simulate adjacent rows and increasing panel numbers but instead of connections with steel trellis wire, the use of thick (low resistance) insulated copper wire could be made via routes remote to the location of the EM38;
3. An EM38 survey could be performed at a height of 1 m above the ground, effectively eliminating the coupling with the trellis, to evaluate whether or not it is an effective mitigation strategy; and

4. Further investigation into the contribution of the shallow soil conditions in the immediate vicinity of the grounded posts would be of benefit in maximising the value of the collected and/or corrected EM38 data.

The most productive area for further work is to develop and assess the practical, efficient correction strategies identified in Section 7.2. This would be performed on a wider scale across a number of different real-world vineyard/trellis scenarios, while referring back to the fundamental underlying physics and patterns identified in this investigation.

# References


Allred, B.J., Daniels, J.J. & Ehsani, M.R. 2008, *Handbook of Agricultural Geophysics*, CRC Press-Taylor & Francis Group, Boca Raton Florida.

Bramley, R.G.V., 2003, 'Smarter thinking on soil survey', *Australian and New Zealand Wine Industry Journal*, vol. 18, pp. 88-94.

Bramley, R.G.V. 2001a, 'Vineyard sampling for more precise, targeted management', *In Proc. National Conference on Geospatial Information & Agriculture, Incorporating Precision Agriculture in Australasia*, CD-ROM, 5th Annual Symposium, Sydney, (Causal Productions: Sydney), pp. 417-27.

Bramley, R.G.V., 2001b, 'Progress in the development of Precision Viticulture – Variation in Yield, Quality and Soil Properties in Contrasting Australian Vineyards', *Precision tools for improving land management*. Occasional Report 14 (Fertiliser and Lime Research Centre, Massey University, Palmerston North, NZ, pp. 25-43.

Bramley, R.G.V. & Lanyon, D.M., 2002, 'Evidence in support of the view that vineyards are leaky – Indirect evidence and food for thought from precision viticulture research', Vineyard "leakiness"'. *Proceedings of workshop held at Waite Campus, Adelaide, January 24-25, 2002 to scope potential threat to the sustainability of Australian viticulture through excessive drainage below the root zone, Final Report on GWRDC Project No. GWR01/04,* CSIRO Land and Water /Grape and Wine Research and Development Corporation, Adelaide.

Bramley, R.G.V., Pearse, B. & Chamberlain, P. 2003, 'Being profitable precisely – A case study of precious viticulture from Margaret River', *Australian and New Zealand Grapegrower and Winemaker,* vol. 461 no. a, pp. 84-87.

Brevik, E.C., Fenton, T.E. & Lazari, A. 2006, 'Soil electrical conductivity as a function of soil water content and implications for soil mapping'. *Precision Agriculture,* vol. 7, pp. 393-404.

Chirlian, P.M. 1969, *Basic Network Theory*, Mcgraw Hill Book Company, New York.

Corwin, D.L. & Lesch, S.M. 2001, 'Apparent soil electrical conductivity measurements in agriculture', *Computers and Electronics in Agriculture*, vol. 46, no. 11, pp. 11-43.

Corwin, D.L. & Lesch, S.M. 2003, 'Application of Soil Electrical Conductivity to Precision Agriculture: Theory, Principles, and Guidelines', *Agronomy Journal*, vol. 95, no. 3, pp. 455-471.

Corwin, D.L., Lesch, S.M., Shouse, P.J., Soppe, R. & Ayars, J.E. 2003, 'Identifying soil properties that influence cotton yield using soil sampling directed by apparent soil conductivity', *Agronomy Journal,* vol. 95, pp. 352-364.

Corwin, D.L. & Plant, R.E. 2005, 'Applications of apparent soil electrical conductivity in precision agriculture', *Computer and Electronics in Agriculture,* vol. 46, pp. 1-10.

Dabas, M. & Tabbagh, A. 2003, 'A comparison of EMI and DC methods used in soil mapping – theoretical considerations for precision agriculture', *Precision Agriculture: Papers from the 4th European Conference on Precision Agriculture*, Berlin, Germany, 15-19 June 2003.

Geonics Limited 1992, (updated 2006) 'Geonics EM-38 Soil Conductivity Meter Operating Manual'.

Geonics 2005, 'Product Catalogue', Geonics Limited, Canada. Retrieved 5 October 2008 from www.geonics.com/ html/em38.html

Geonics 2008, Geonics Limited, *EM38Mk2 Brochure*. Retrieved 12 March 2009 from http://www.geonics.com/html/em38.html

Grover, F.W. 2004, *Inductance Calculations*, Dover Phoenix Editions, New York.

Hazell, P. 'Application of radiometrics for land capability assessment', *Environmental Research and Information Consortium Pty Ltd (ERIC*), Retrieved 28 November 2008 from http://www.regional.org.au/au/gia/06/185hazell.htm?print=1

Howatson, A.M., Lund, P.G. & Todd, J.D. 1972, *Engineering Tables and Data*, Chapman and Hall, London.

Hubbard S., Chen J., Williams K. Peterson J., & Rubin Y., *Environmental and Agricultural Applications of GPR,* Berkely National Laboratory, Retrieved 12 arch 2009 from http://esd.lbl.gov/susanhubbard/pubs/hubbard_gprag_env.pdf

Jackson, R.S. 2008, *Wine Science: Principles and Applications*, Academic Press.

Kamon, M., Tsuk M.J. & White J. 1994, 'FASTHENRY:A Multipole-Accelerated 3-D Inductance Extraction Program', *IEEE Transactions on Microwave Theory and Techniques*, vol. 42, no. 9.

Kamon, M., Smithhisler, C. & White, J. 1996, *Fast Henry USER'S GUIDE version 3.0*, Dept Electrical Engineering and Computer Science, Massachusetts Institute of Technology, Cambridge.

Kaufmann, A.A. & Eaton, P.A. 2001, *The Theory of Inductive Prospecting*, Elsevier, Amsterdam.

Keller, G.V. & Frischknecht, F.C. 1966*, Electrical Methods in Geophysical Prospecting*, Pergamon Press.

Kip, A.F. 1962, *Fundamentals of Electricity and Magnetism*. McGraw Hill, Kogakusha Ltd. Tokyo.

Kunetz, G. 1966, 'Principles of Direct Current Resistivity Prospecting', *Geoexploration. Monographs,* Series 1 – 1*,* Gebrüder Borntraeger, Berlin.

Kuphaldt, T.R. 2007, *Fundamentals of Electrical Engineering and Electronics*, Virtual Institute of Applied Science, eBook Retrieved 5 0ctober 2005 from www.vias.org/feee/conduct_07.html.

Lamb, D.W., Mitchell, A. & Hyde, G. 2005, 'Vineyard Trellising with Steel Posts Distorts Data from EM Soil Surveys', *Australian Journal of Grape and Wine Research,* vol. 11, pp. 24-32.

Lowenberg-DeBoer, J. & Erickson, K. 2000, *Precision Farming Profitability*. Purdue University, West Lafayette, IN.

MATWEB 2008, Material Property Data, *Overview of materials for AISI 1000 Series Steel,* Retrieved 5 October 2008 from http://www.matweb.com/search/DataSheet.aspx?MatGUID=81a26031d1b44cbb911f70ab863281f5

Lorrain, P. & Corson, D.R. 1962, *Electromagnetic Fields and Waves,* W.H. Freeman and Company, San Francisco.

McCorkle, W.H. 1931, 'Determination of soil moisture by the method of multiple electrodes'. *Texas Agricultural Experiment Station Bulletin,* p. 426.

McNeill, J.D. 1980, 'Geonics Technical Note 6: Electromagnetic Terrain Conductivity at Low Induction Numbers', *Geonics Technical Notes*, Geonics Limited, Canada. Retrieved 5 October 2008 from http://www.geonics.com/pdfs/technicalnotes/tn6.pdf

McNeill, J.D. 1986, 'Geonics Technical Note 18: Rapid, accurate mapping of soil salinity using electromagnetic ground conductivity meters*'. Geonics Technical Notes*, Geonics Limited, Ontario, Canada.

McNeill, J.D. 1992, 'Rapid, accurate mapping of soil salinity by electromagnetic ground conductivity meters,' In: advances in Measurement of Soil Physical Properties: Bringing Theory into Practice. Spec. Publ. 30 SSSA, Madison WI, pp. 209-229.

McNeill, J.D. 1996, 'Geonics Technical Note 30: Why doesn't Geonics Limited build a multi-frequency EM31 or EM38 ?' *Geonics Technical Notes*, Geonics Limited, Canada. Retrieved 5 October 2008 from http://www.geonics.com/pdfs/technicalnotes/tn30.pdf

Proffitt, T., Bramley, R., Lamb D. & Winter E. 2006, *Precision Viticulture-A new era in vineyard management and wine production*. Winetitles Pty Ltd, Ashford, SA, Australia.

Reedy, R.C. & Scanlon, B.B. 2003, 'Soil Water Content monitoring using electromagnetic induction', *Journal of Geotechnical and Geoenvironmental Engineering*, vol. 129, pp. 1028-1039.

Reynolds, J.M. 1997, *An Introduction to Applied and Environmental Geophysics*, John Wiley and Sons Ltd, England.

Rhoades, J.D. & Corwin, D.L. 1981, 'Determining Soil Electrical Conductivity-Depth Relations Using an Inductive Electromagnetic Soil Conductivity Meter', *Soil Science Society of America Journal*, vol. 45, pp. 255-260.

Rhoades, J.D. & Ingvalson, R.D. 1981, 'Determining salinity in field soils with soil resistance measurements'. *Soil Science Society of America Proc.* vol. 35, pp. 137-141.

Rhoades J.D., Lesch S.M., LeMert, R.D. & Alves, W.J. 2006, 'Assessment of Salinity and Irrigation/Drainage Practices', *Agricultural Research Service - Water Reuse and Remediation,* United States Department of Agriculture. Retrieved 5 October 2008 from www.ars.usda.gov/Research/docs.htm?docid=10323

Rhoades, J.D, Waggoner, B.L., Shouse, P.J. & Alves, W.J., 1989a, 'Determining Soil Salinity from Soil and Soil-Paste electrical Conductivities: Sensitivity Analysis of Models', *Soil Science Society of America Journal,* vol. 53, pp. 1368-1374.

Rhoades, J.D, Waggoner, B.L. Shouse, P.J. & Alves, W.J. 1989b, 'Soil electrical conductivity and soil salinity: New formulations and calibrations', *Soil Science Society of America Journal,* vol 53, pp. 433-439.

Robinson, D.A., Robinson, I.L., Lesch S.M. & Shouse, P. 2004, 'Minimizing Drift in Electrical Conductivity Measurements in High Temperature Environments using the EM-38', *Soil Science Society of America Journal*, vol. 68, no. 2, pp. 339-345.

Sharma, P.V. 1976, *Geophysical Methods in Geology*, Elsevier Scientific Publishing Company, Amsterdam.

Sudduth, K.A., Drummond, S.T. & Kitchen, N.R. 2001, 'Accuracy issues in electromagnetic induction sensing of soil electrical conductivity for precision agriculture', *Computers and Electronics in Agriculture,* vol. 31, pp. 239-264.

Sudduth, K.A., Kitchen, N.R., Bollero, G.A., Bullock, D.G. & Wiebold, W. J. 2003, 'Comparison of Electromagnetic Induction and Direct Sensing of Soil Electrical Conductivity', *Agronomy Journal*, vol. 95, pp. 472-482.

van Egmond, F.M., Loonstra, E.H. & Limburg J. 'Gamma-ray sensor for topsoil mapping; the Mole', Retrieved 31 October, 2008 from http://www.soilcompany.com/nl/PaperAustralie.pdf

Walker J.P. & Houser P.R., 2002 'Evaluation of the OhmMapper Instrument for Soil Moisture Measurement', *Soil Science Society America Journal*, vol. 66, pp. 728–734.

Wenner, F. 1915, 'A method of measuring earth resistivity'. *United State Department. Commerce Bureau Standards Science Paper,* No. 258.

# Appendix A . The EM38 History and Model Designations

Mineral prospecting was the early motivation for the development of EMI instruments. Geonics Limited (Geonics) developed the EM15 in 1965 (and the EM15-Mk2 in 1972) for mapping the conductivity highs associated with contiguous mineralised veins to a depth of 1.5m (Catalono 2008). This was a very low frequency (VLF) type instrument sensing distortions (due to local conductors) of the transmissions from distant military communication systems. However, the motivation for the original EM38 development in 1980 was agriculture.

In his landmark technical note, McNeill (1980) lists the various engineering, shallow geological, mineral exploration and archaeological applications of two other EM instruments, the EM31 and EM34-3. The two-man portable EM34-3 has a depth range of approximately 7.5 m to 60 m, while the one-man portable EM-31 ranged from 3 to 6 m.

However, while J.D. Rhoades (Rhoades and Corwin, 1981) concluded that inductive techniques had advantages over galvanic techniques, evaluations of the EM15and EM31 instruments showed they were not well suited to agricultural salinity investigations. The EM15 was too sensitive to the magnetic susceptibility of the soil and the EM31 was sensing soil $EC_a$ too deeply (mostly below the root zone). Rhoades and his associate subsequently commissioned Geonics to develop an instrument specifically for agricultural salinity applications, the EM38.

Table A-1 lists the various EM38 models (and their initial year of production), while Figure A-1 contains the photographs of some of the different model configurations. The prototype EM38 was a modified EM31, rather than an EM15.

The original EM38 was an analogue instrument, which required manual reading from a needle-deflection type meter. This was superseded by the digital form with the 10 Hz digital output stream for automatic logging into a hand-held computer and then, later, for interfacing to a GPS for automatic logging of georeferenced data. There is a time-lag involved in the data logging which requires correction (Sudduth, Drummond & Kitchen 2001). The instrument's popularity and usefulness then motivated the evolution of automatic ranging, simultaneous

quadrature and in-phase measurements, and simultaneous vertical and horizontal dipole models. This finally culminated in the latest model which has two receivers enabling simultaneous measurements from two depths, in addition to simultaneous quadrature and in-phase measurements.

However, the basic digital EM38 versions are still widely used in field mapping applications today (including agriculture) due to their simplicity and low-cost. The basic instrument used for this study was an EM38DLM with manual range control.

**Table A-1. EM38 Model designations, initial year of production, approximate number of units produced and their configurations (Geonics, 2006; Catalano 2008, pers. comm.).**

| Model | Year | Approx. No. Units | Specification |
|---|---|---|---|
| **EM15** | 1965 | (unknown) | Analogue EM38 predecessor |
| **EM15-Mk2** | 1972 | (unknown) | Analogue EM38 predecessor (Designed to map mineralisation to a depth of 1.5 m.) |
| **EM38** | 1980 | (unknown) | Analogue Display. No output port. |
| **EM38DLM** | 1986 | 125 | Analogue and then digital display. Analogue output port. |
| **EM38RT** | 1995 | 300 | Digital (RS232), Manual (1000 mS $m^{-1}$,100 mS $m^{-1}$). Automatic ranging (0 to 1000 mS $m^{-1}$) s/n >0034200. Quadrature or in-phase mode. (Analogue or digital output) |
| **EM38B** | 1999 | 125 | Digital (RS232), Simultaneous quadrature and in-phase measurements. |
| **EM38DD** | 1999 | 125 | Digital (RS232), Simultaneous vertical and dipole modes. |
| **EM38-MK2** | 2007 | 40 | Digital, two receiver coils (0.5 m and 1 m separation). Simultaneous quadrature and in-phase measurements. Improved temperature compensation on the 1 m receiver. Automatic calibration. RS232 & Blue tooth wireless data transmission. External Power option. (EM38-Mk2-1 can have the 0.5 m coil retrofitted) |

**a) EM38: Analogue.**

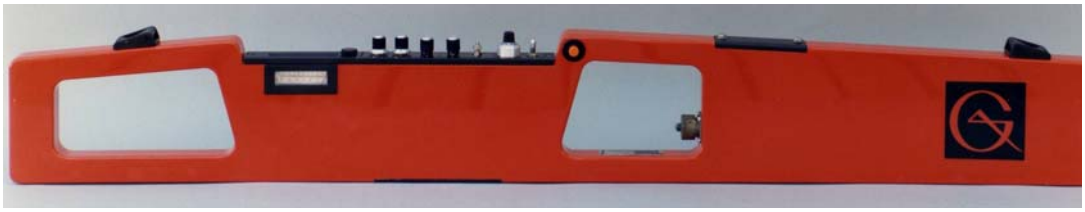

**b) EM38DLM: Analogue moving-needle display and analogue output port.**

**c) EM38DLM Digital Display and Analogue output port**

**d) EM38RT: Digital**

**e) EM38B: In-phase & Quadrature simultaneously.**

**f) EM38DD: Vertical & horizontal simultaneously**

**g) EM38-Mk2: Two coil spacings. Quadrature and In-phase simultaneous.**

**Figure A-1. Photographs of some of the different EM38 models a) EM38 (Geonics 2008a); b) EM38DLM-Analogue (Geonics 2008a); c) EM38DLM-Digital (Geonics 2008a); d) EM38RT; e) EM38B (Geonics 2005); f) EM38DD (Geonics 2005); g) EM38-Mk2.**